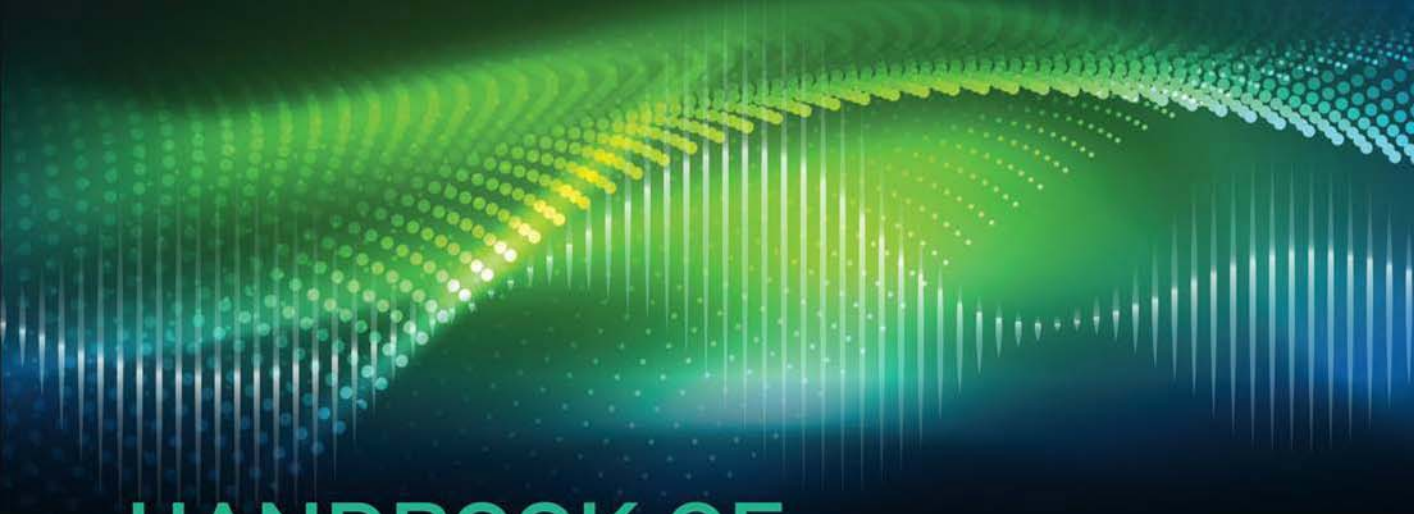

HANDBOOK OF NONDESTRUCTIVE EVALUATION

THIRD EDITION

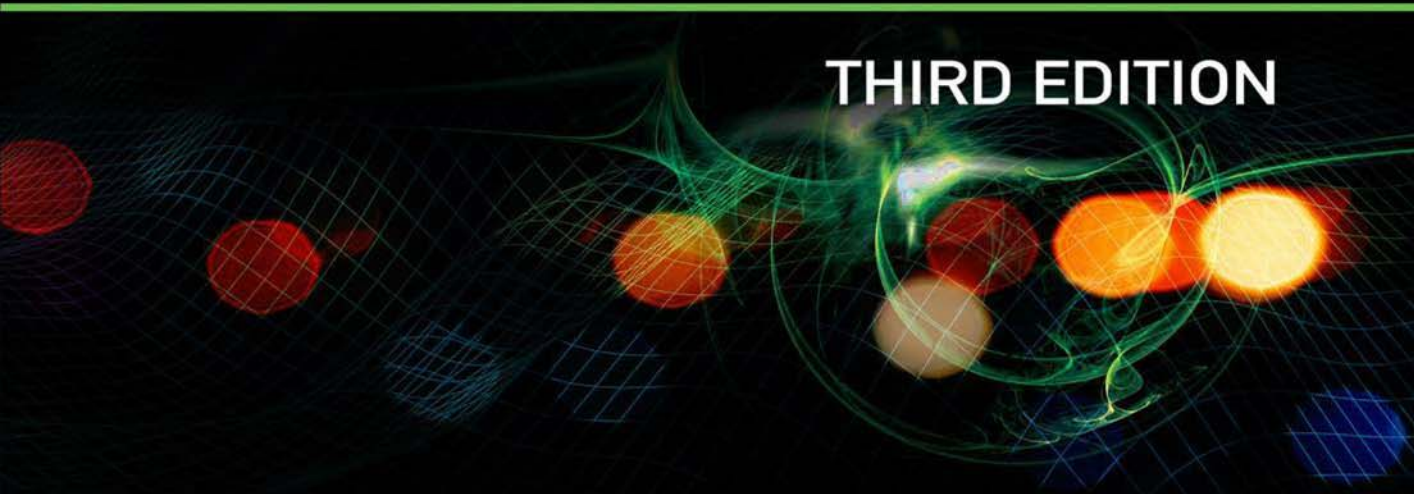

CHARLES J. HELLIER

Mc Graw Hill

13.3.2 Pipe

Ultrasonic guided waves were first introduced in tubing inspection by Rose et al. [1993]. Following the research results of Ditri and Rose [1992], Li and Rose developed an analytical method to simulate the angular profiles in hollow cylinders [2001a]. In 2002, Li and Rose presented the phased array focusing technique for longitudinal guided waves propagating in cylindrical shells. Rose and Mudge [2002] introduced a commercial application of the guided wave focusing technique with a pipeline inspection tool, the Teletest-focus instrument. Sun et al. [2003a] carried out the angular profile calculations and the phased array focusing technique for torsional guided wave propagation in hollow cylinders. If the angular profiles show that ultrasonic energy is naturally concentrated at a circumferential location at a particular propagation distance, this phenomenon, which is called "natural focusing," can be used to improve pipeline inspection. See Sun et al. [2003b]. Real-time phased array technology for pipe was introduced to the world by Rose et al. [2002, 2003].

Circumferential waves were studied by Thompson et al. [1972], who used Lamb waves for steel plate and pipe inspections. Van Velsor et al. [2009] developed enhanced circumferential guided wave coating disbond detection methods with guided wave physically based features.

Defect imaging and synthetic focusing methods were introduced by Hayashi et al. [2005], Mu and Rose [2008a] by focusing and with coatings by Mu et al. [2008b], Davies and Cawley [2009], Mu et al. for synthetic focusing [2010], and Velichko and Wilcox [2009] with post-processing.

Pavlakovic et al. [1997] introduced a commercial software package for dispersion curve calculation: DISPERSE. Demma et al. [2001] studied mode conversion of longitudinal and torsional guided modes due to pipe bends. Ma et al. [2007] studied sludge and blockage detection inside pipes.

SAFEM-efficient computational techniques were introduced for guided wave problems by Hayashi et al. [2002]. Magnetostrictive methods were pioneered by Kwun et al. [1998] covering guided wave inspection of pipe using magnetostrictive sensors. Kim et al. [2005] used magnetostrictive transducers with ferromagnetic strips 45 degrees from the axis of a pipe.

13.3.3 Rail

Grewal [1996] used Rayleigh waves in rail. Hayashi et al. [2003] computed guided wave dispersion curves for a bar with an arbitrary cross section with a rod and rail example. Wilcox et al. [2003b] also introduced some interesting aspects of rail inspection. Gunawan and Hirose [2005] used boundary element analysis of guided waves in a bar with an arbitrary cross section. Bartoli et al. (including Lanza di Scalea) [2006] employed modeling aspects of wave propagation in damped waveguides of arbitrary cross section. Lee et al. [2009] used a guided wave approach for defect detection under shelling in rail with wave structure selection examples for sensor design to achieve special effects.

13.3.4 Bonding and Composites

Mal et al. [1988] studied guided wave evaluation of adhesive bonds. Chimenti et al. [1988] made use of guided waves reflection and propagation in fluid-coupled

composite laminates. Datta et al. [1990] studied edge and layering effects of guided waves in a multilayered composite plate. Na [2002] researched ultrasonic guided waves for steel bar concrete interface testing. Hosten and Castaings [2005] employed finite elements method (FEM) for modeling the guided waves propagation in structures with weak interfaces. Puthillath and Rose [2010] introduced higher-order ultrasonic guided wave inspection of a titanium patch that was bonded to an aluminum aircraft skin.

13.3.5 Phased Array for Plates

Li and Rose [2001b] implemented guided wave mode control by use of a phased transducer array. Giurgiutiu et al. [2002] invented a virtual beam steering technique by using PZT transducer arrays. Wilcox [2003c] developed omni-directional guided wave transducer arrays for rapid inspections of large areas in plates. Yan and Rose in 2007 used beam steering in composites and in 2009 with a phased array time delay comb. Salas and Cesnik [2010] presented guided wave structural health monitoring (SHM) by using composite long-range variable-length emitting radar (CLoVER) transducers in composite materials. Senesi et al. [2010] developed guided wave frequency-steerable arrays for SHM.

13.3.6 Guided Wave Imaging and Tomography

Hinders et al. [1999] studied Lamb wave tomographic scanning and Gao et al. [2005] introduced guided wave mode and frequency selection for tomography for aircraft structures. Breon et al. [2007] did guided wave damage detection tomography for SHM in pipeline elbows, and Van Velsor et al. [2007] studied pipe defects by employing guided wave tomography technique. Yan et al. [2010b] also used ultrasonic guided wave imaging techniques in SHM.

Some research has been carried out to improve the guided wave imaging techniques. Ruzzene [2007] employed frequency wave number domain filtering for improved damage visualization. Hall and Michaels [2011] studied computational efficiency of ultrasonic guided wave imaging algorithms.

13.3.7 Ultrasonic Vibration

Rose et al. [2010b] introduced an ultrasonic guided wave modal analysis technique (UMAT) for defect detection, followed by work by Yan and Rose [2010c].

13.3.8 Deicing

Venna et al. [2007], Zhu et al. [2008], and Gao et al. [2009] utilized ultrasonic guided waves for deicing experiments.

13.3.9 SHM

Michaels et al. [2004] used feature-based classifiers for ultrasonic SHM. Raghavan and Cesnik [2004] modeled use of piezoelectric-based Lamb wave generation and sensing for SHM. Many other investigators are also using guided waves in SHM.

13.3.10 Nonlinear

Nonlinear methods are now finding applications in ultrasonic guided wave analysis. See Cantrell et al. [2001], Kim et al. [2006], and Pruell et al. [2009].

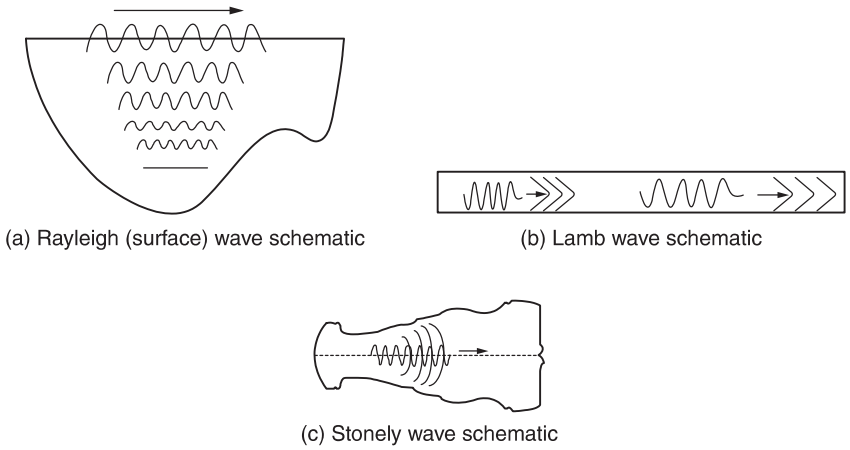

Figure 13-1 Guided wave possibilities.

13.4 Fundamentals

Compared to ultrasonic bulk waves that travel in infinite media with no boundary influence, guided waves require a structural boundary for propagation. As an example, some guided wave possibilities are illustrated in Fig. 13-1 for a Rayleigh surface wave, a Lamb wave, and a Stonely wave at an interface between two materials.

There are many other guided wave possibilities, of course, beyond that presented in Fig. 13-1, as long as a boundary on either one or two sides of the wave is considered. Let's look further into a variety of different natural waveguides as outlined in Table 13-1.

When you think about it, most structures are really natural waveguides provided the wavelengths are large enough with respect to some of the key dimensions in the waveguide. If the wavelengths are very small, then bulk wave propagation can be considered, those waves that were used traditionally for many years in ultrasonic nondestructive pulse echo and through transmission testing. One very interesting difference, of many, associated with guided waves, is that many different wave velocity values can be obtained as a function of frequency, whereas for most practical bulk

- Plates (aircraft skin)
- Rods (cylindrical, square, rail, etc.)
- Hollow cylinder (pipes, tubing)
- Multilayer structures
- Curved or flat surfaces on a half-space
- Layer or multiple layers on a half-space
- An interface

Table 13-1 List of Natural Waveguides

wave propagation purposes, the wave velocity is independent of frequency. In fact, tables of wave velocities are available from most manufacturers of ultrasonic equipment that are applicable to bulk wave propagation in materials, showing just a single wave velocity value for longitudinal waves and one additional value for shear waves.

A comparison of bulk wave and guided wave ultrasonic inspection is illustrated in Fig. 13-2. Note the coverage volume increases as a result of guided wave inspection.

To get some idea of how guided waves are developed in a waveguide, just imagine a bunch of bulk waves bouncing back and forth inside a waveguide with mode conversions between longitudinal and shear constantly taking place at each boundary. The resulting superimposed wave form traveling along the waveguide is just a sum of all of these waves including amplitude and phase information. You can visualize the outcome being strongly dependent on frequency and impinging wave angles of propagation inside the structure. The strongly superimposed results are actually points that end up on the phase velocity dispersion curve for the structure. Elsewhere there is strong cancellation. To solve for the points on the dispersion curve either you could consider a partial wave summation process accounting for all reflections and mode conversions or you could solve an appropriate boundary value problem in wave propagation.

Information on ultrasonic guided waves can be found in many excellent textbooks, see for example, Graff [1975], Rose [1999], Achenbach [1973], Auld [1990], Datta [2008], and Achenbach [2003]. A very reasonable up-to-date state-of-the-art literature review and evaluation of ultrasonic guided waves can be easily found in the literature.

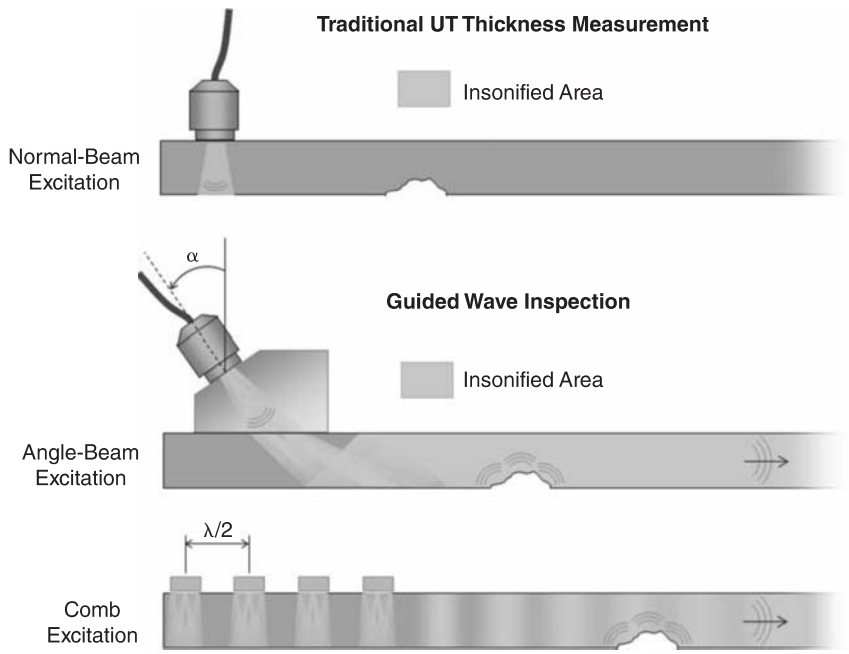

Figure 13-2 Comparison of bulk wave and guided wave inspection methods.

- 100 percent coverage.
- Inspection over long distances from a single probe position.
- Ability to inspect hidden structures and structures under water, coatings, soil insulations, and concrete.
- Beam focusing capability is possible for improved probability of detection, reduce false alarm rate, penetration power, and inspection confidence.
- Often greater sensitivity than that obtained in other NDT techniques.
- Cost-effectiveness because of inspection simplicity and speed.
- Avoidance of removal/reinstallment of insulation or coating, except at location of transducer tool.
- Excellent overall defect circumferential length in pipe.
- Lateral and depth sizing potential.

Table 13-2 Principal Benefits of Guided Waves

The use of ultrasonic guided waves is increasing tremendously over the past decade because of a variety of different reasons, notably understanding and improved computational efficiency for complex problem solving. The principal benefits of guided waves can be summarized as follows. Inspection over long distances from a single probe position is possible giving complete volumetric coverage of the item to be inspected as presented in Fig. 13-2. There's no need for scanning; all of the data is acquired from the single probe position. Quite often, greater sensitivity than that obtained in standard normal beam ultrasonic inspection or other NDT techniques can be obtained, even with low frequency ultrasonic guided wave inspection techniques. There is also an ability to inspect hidden structures, structures under water, coatings, insulations, and concrete because of the inspection capability from a single probe position via wave structure change and controlled mode sensitivity along with an ability to propagate over long distances. There is also a tremendous cost-effectiveness associated with guided wave propagation and inspection because of the inspection simplicity and speed. See Table 13-2 for a brief summary of the benefits.

13.5 Dispersion

The subject of dispersion and the propagation of either dispersive or nondispersive modes is a very critical one to understand when dealing with ultrasonic guided waves. In Figs. 13-3 and 13-4, for example, you can see an example of dispersive and nondispersive guided wave propagation. For nondispersive wave propagation, the pulse duration remains constant as the wave travels through the structure. On the other hand, for dispersive wave propagation, since wave velocity is a function of frequency, the pulse duration changes from point to point inside the structure. This is because each harmonic of the particular input pulse packet travels at a different wave velocity. There's a decrease in amplitude of the waveform and an increase in pulse duration, but energy is still conserved, unless of course, lossy media is considered.

13.5.1 Dispersion Curves

Let's now consider the development of a phase velocity computation in a waveguide. A particular waveguide such as a plate or pipe can be used as an example. The appropriate

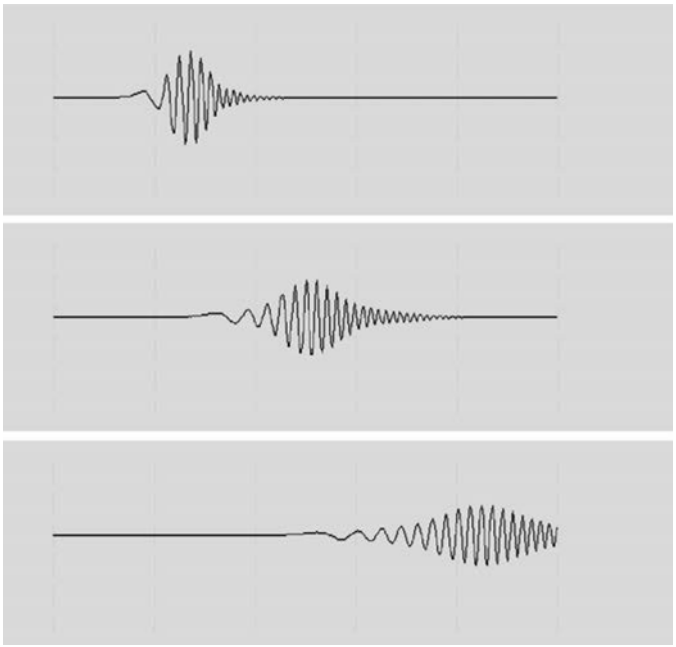

Figure 13-3 Dispersive wave propagation as it travels along a structure.

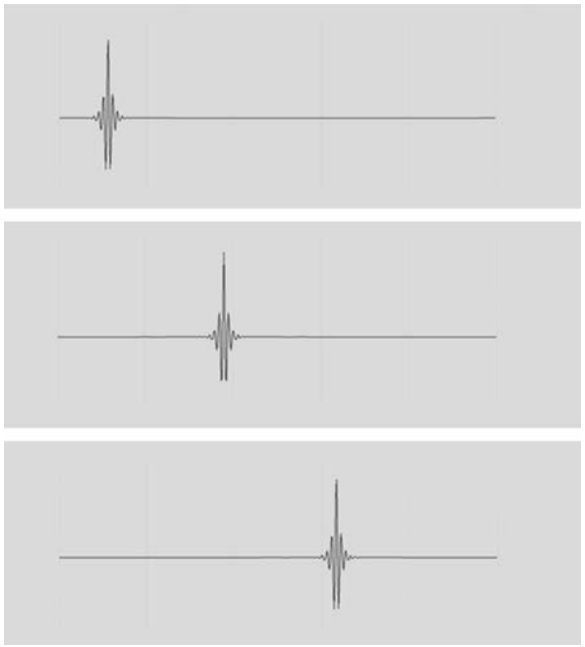

Figure 13-4 Nondispersive wave propagation as it travels along a structure.

boundary conditions in these items call for a traction-free upper and lower surface, or outer and inside surface respectively. If we now consider some form of the governing Navier's wave equation in rectangular or cylindrical coordinates and an assumed harmonic solution for displacement, we can through elasticity theory derive the equations to satisfy the boundary conditions of the problem being studied. This leads to a transcendental equation, or a characteristic equation that most often requires a numerical solution. In extracting the roots from the characteristic equation, usually associated with a system of homogeneous equations, the determinant of the coefficient matrix must be set equal to zero. The resulting characteristic equations for a plate are as follows:

$$\frac{\tan(qh)}{\tan(ph)} = -\frac{4k^2pq}{(q^2-k^2)^2} \quad \text{for symmetric modes} \tag{13-1}$$

$$\frac{\tan(qh)}{\tan(ph)} = -\frac{(q^2-k^2)^2}{4k^2pq} \quad \text{for anti symmetric modes} \tag{13-2}$$

where:

$$p^2 = \left(\frac{\omega}{c_L}\right)^2 - k^2 \quad \text{and} \quad q^2 = \left(\frac{\omega}{c_T}\right)^2 - k^2 \tag{13-3}$$

In this case, the roots extracted determine the phase velocity versus frequency values that can be plotted, as illustrated in Fig. 13-5. In Fig. 13-5 are shown the phase velocity dispersion curves for a particular traction-free steel plate. The modes are labeled as antisymmetric A0, A1, A2, A3, etc. or symmetric as S0, S1, S2, S3, etc. The S0 mode intersects the zero frequency axis at the plate velocity value for the plate. The plate velocity formula is as follows:

$$C_{\text{plate}} = \left[\frac{E}{\rho(1-\upsilon^2)}\right]^{1/2} \tag{13-4}$$

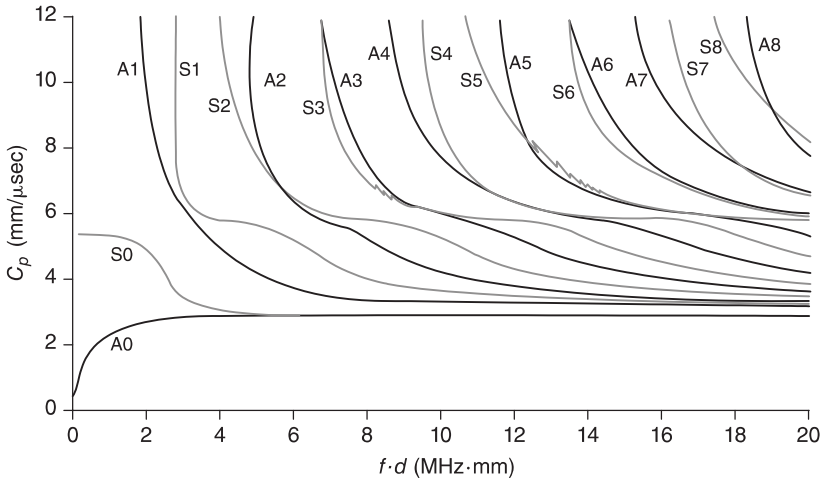

Figure 13-5 Phase velocity dispersion curve for a carbon steel plate.

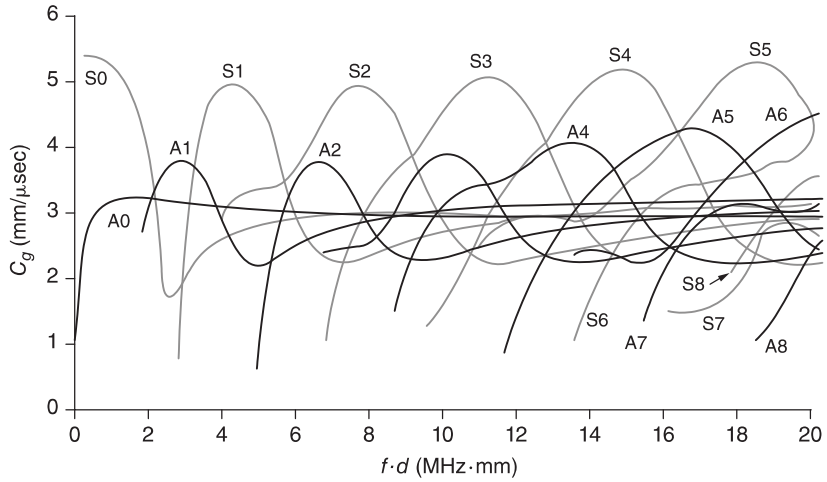

Figure 13-6 Group velocity dispersion curves for a carbon steel plate.

The A0 mode at high frequency approaches the Rayleigh surface wave velocity. All other modes at new high frequency converge to the shear wave velocity for the plate. Notice the cut-off frequencies at high phase velocities C_p. The group velocity curves are derived from the phase velocity curves and represent the velocity of a packet of waves of similar frequency. See Fig. 13-6. The group velocity formula is as follows:

$$C_g = C_p^2 \left[C_p - (fd) \frac{dc_p}{d(fd)} \right]^{-1} \tag{13-5}$$

Note that wave structure across the thickness of a waveguide changes as you move along frequencies for a particular mode. Sample results are shown in Fig. 13-7. Note that for an *fd* valve of .037 the in-plane displacement on the outer surface of the plate is a maximum, whereas for an *fd* valve of .245 the in-plane displacement is maximum on the outer surface. Wave structure considerations and mode and frequency choice have

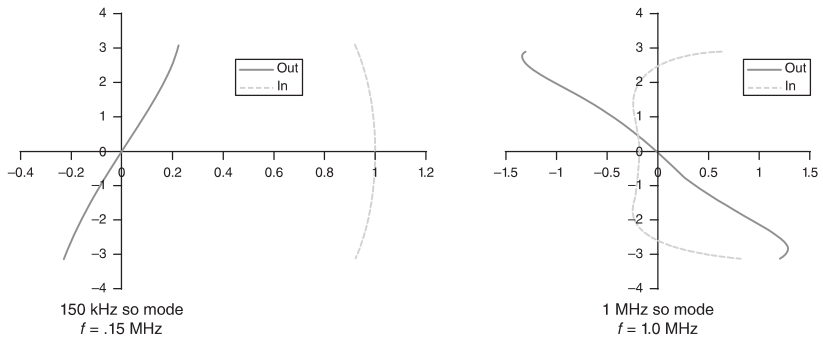

Figure 13-7 Sample normalized wave structures of the S0 mode in a 0.245-in.-thick steel plate. Solid line: Out-of-plane displacement; Dotted line: In-plane displacement.

serious consequences in defect detection sensitivity, penetration power, and influence to water loading situations as an example.

Let us now consider dispersion curves for a pipe and also consider longitudinal and torsional loading. The modes are labeled as L(0,1), L(0,2), L(0,3), etc. or torsional T(0,1), T(0,2), etc. The particular limits in the diagram are surface wave velocity, shear wave velocity, and cut-off frequencies as shown in Fig. 13-8. Group velocity dispersion curves are shown in Fig. 13-9. Details on the development and the nomenclature considered here

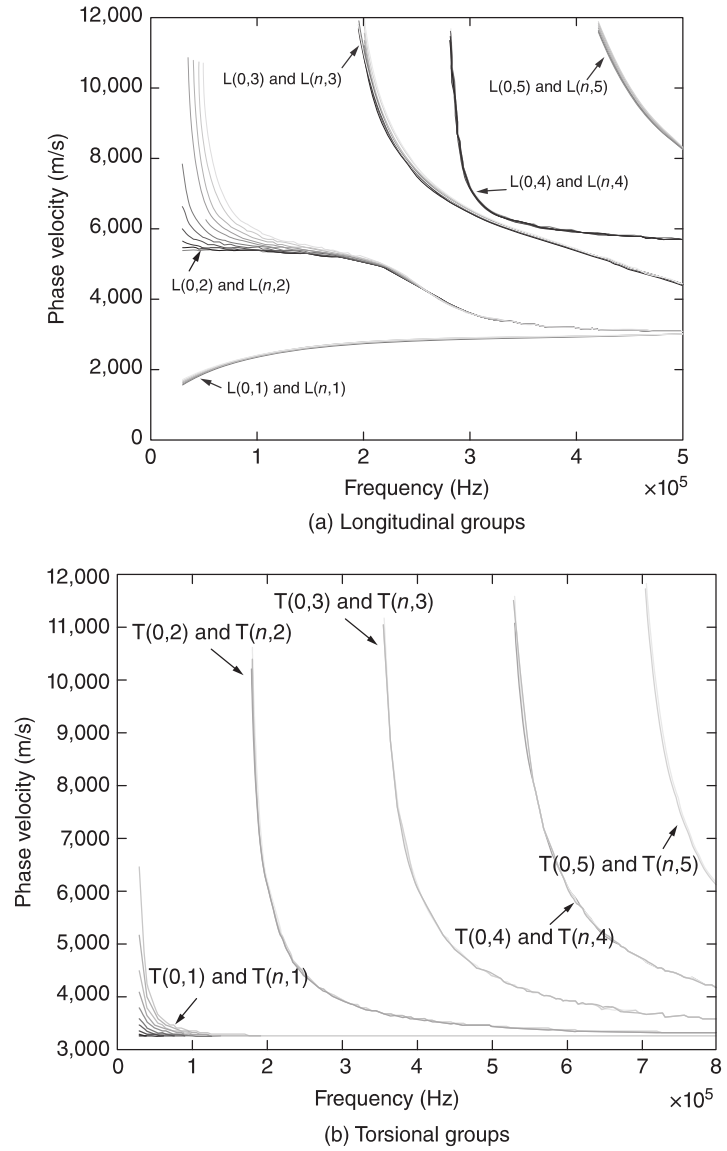

Figure 13-8 Sample PHASE velocity dispersion curves for a 16-in. schedule 30 elastic steel uncoated pipe.

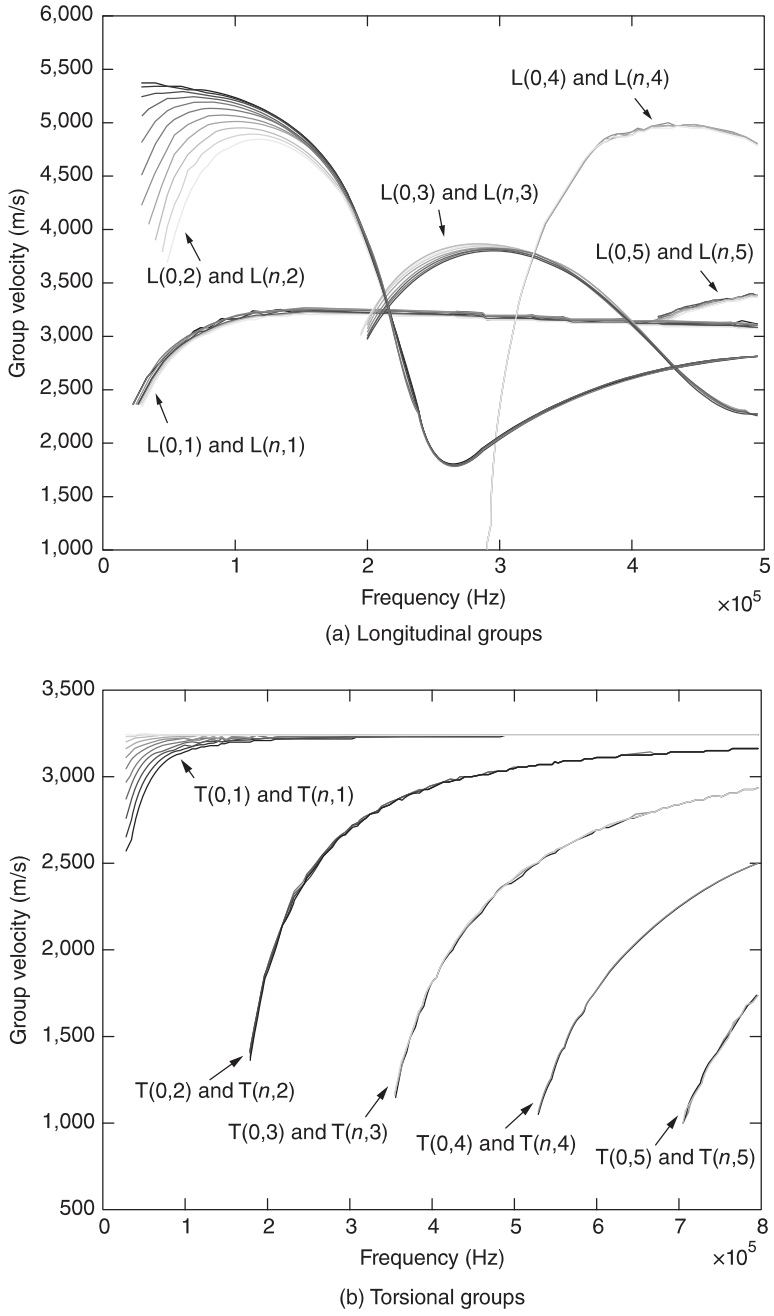

Figure 13-9 Sample GROUP velocity dispersion curves for a 16-in. schedule 30 elastic steel bare pipe.

can be found in such references as Rose [1999]. Flexural modes are shown in Figs. 13-8 and 13-9 as well as the axisymmetric modes. Flexural modes are associated with partial loading around the circumference of a pipe. Derivable from the phase velocity dispersion curves are sets of the group velocity dispersion curves. The values of the group velocity dispersion curves depend on the ordinate and slope values of the phase velocity dispersion curves as indicated in the group velocity formula. The group velocity is what you actually measure in an experiment. See Rose [1999] for details.

If a steel pipe is filled with or is under water, there will be energy leakage as the wave travels along the pipe, because of an out-of-plane displacement component that would load the liquid. The in-plane displacement components would not travel into the liquid media since this would be like shear loading on the fluid. If you solve this wave propagation problem, or as another example the wave propagation associated with bitumen coating on a pipe, there would also be leakage of ultrasonic energy as the wave propagates along the plate. Following the phase and group velocity dispersion curves, the complex roots from the characteristic equation would then lead to a set of attenuation dispersion curves. A sample attenuation dispersion curve is shown in Fig. 13-9.

A pipe sample problem is used here. For the common plate problem in the literature, the modes are labeled as A0, A1, A2, …, S0, S1, S2, … because of symmetric and antisymmetric character. In the case of guided wave in pipes, the axisymmetric longitudinal waves are labeled as L(0,1), L(0,2), L(0,3), … and the axisymmetric torsional waves as T(0,1), T(0,2), T(0,3), …. Flexural modes are also possible due to partial loading around the circumference of a pipe. See Sun et al. [2003a, 2003b] for example for more details on flexural modes. The flexural or antisymmetric modes are shown in Fig. 13-10 whenever $n \neq 0$. Note in Fig. 13-10 that attenuation does not always increase as frequency is increased as in a usual bulk wave problem. Some modes are also attenuated more quickly than others.

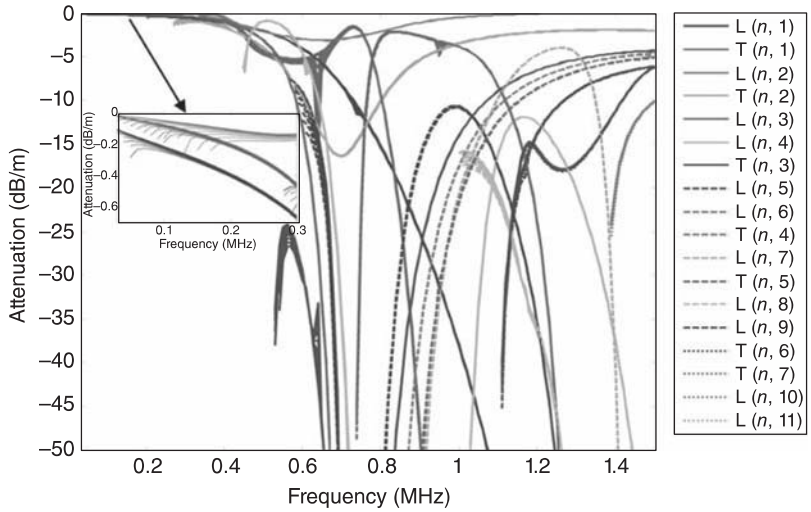

Attenuation dispersion curves for guided wave modes with circumferential order n from 0 to 10. Pipe size: a 4-in. schedule 40 steel hollow cylinder coated with 0.02 in. thick E&C 2057 Cat 9 epoxy.

Figure 13-10 A sample complete solution of guided wave attenuation dispersion curves.

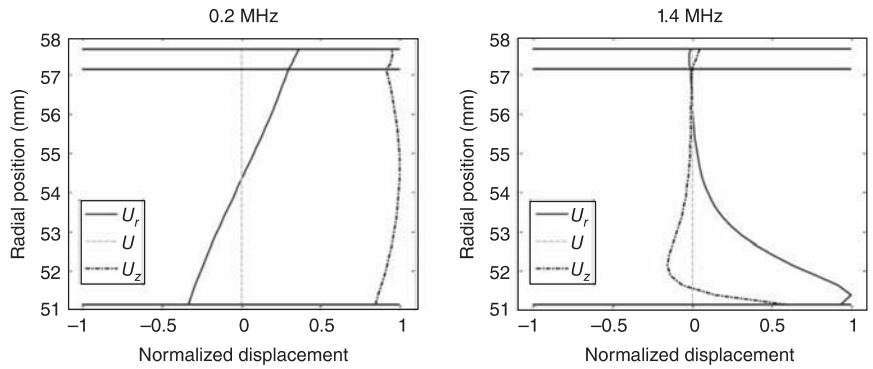

Figure 13-11 Sample wave structures L(*n*, 2). *Note:* The energy is mostly concentrated at the inner surface of the coated pipe at high frequency.

All guided wave problems have associated with them the development of appropriate dispersion curves and corresponding wave structures. Of thousands of points on a dispersion curve, only certain ones lead to a successful inspection, i.e., those with greatest penetration power, maximum displacement on the outer, center, or inner surface, with only in-plane vibration on the surface to avoid leakage into a fluid, or with minimum power at an interface between a pipe and a coating, etc. A sample set of wave structure curves is illustrated in Fig. 13-11 for a pipe. In plane u_z, out-of-plane u_r and shear horizontal u_θ are shown. Notice the in-plane vibration behavior across the thickness compared to the out-of-plane motion. The wave structure changes from point to point along every mode on a dispersion curve. The characteristics of every point on each dispersion curve are different, primarily with respect to wave structure, a critical feature for the development of an efficient test technique for a particular structure. For a particular mode any frequency value, for example, the in-plane displacement could be totally dominant across the thickness with almost no out-of-plane vibration. This mode, as an example, would travel very far even if the pipe were full of water.

In addition to the Lamb-type longitudinal waves illustrated here so for a pipe, there could be torsional, guided wave propagation in the pipe as well, depending on the sensor loading situation. In this case, the shear horizontal-type wave produces an in-plane component that's perpendicular to the wave propagation or wave vector direction but in the circumferential direction of the pipe. For the torsional mode, there is no out-of-plane displacement. The leakage into a nonviscous fluid media from a pipe would be nonexistent as far as wave propagation is concerned. Keep in mind, however, that mode conversion at a defect could create some leaky reflected waves.

Note that dispersion curve examples for other waveguides can be found in Rose [1999]. Of particular interest might be the closed-form solution possibility for shear horizontal waves in a plate.

13.5.2 Bulk versus Guided Waves

Further comparison of bulk and guided waves can be seen in Table 13-3. Key elements of the differences between isotropic and anisotropic media are listed in Table 13-4. Methods of determining characteristic equations for anisotropic waveguides can be found in the literature. See also Rose [1999].

	Bulk	Guided
Phase Velocities	Constant	Function of frequency
Group Velocities	Same as phase velocities	Generally not equal to phase velocity
Pulse Shape	Nondispersive	Generally dispersive

Table 13-3 Ultrasonic Bulk versus Guided Wave Propagation Considerations

	Isotropic	Anisotropic
Wave Velocities	Not function of launch direction	Function of launch direction
Skew Angles	No	Yes

Note: All metals are not isotropic. For example, columnar dendritic centrifugally cast stainless steel is anisotropic. This must be considered in any wave propagation studies.

Table 13-4 Ultrasonic Wave Considerations for Isotropic versus Anisotropic Media

Bulk Wave	Guided Wave
Tedious and time-consuming	Fast
Point by point scan (accurate rectangular grid scan)	Global in nature (approximate line scan)
Unreliable (can miss points)	Reliable (volumetric coverage)
High-level training required for inspection	Minimal training
Fixed distance from reflector required	Any reasonable distance from reflector acceptable
Reflector must be accessible and seen	Reflector can be hidden

Table 13-5 A Comparison of the Currently Used Ultrasonic Bulk Wave Technique and the Proposed Ultrasonic Guided Wave Procedure for Plate and Pipe Inspection

A further practical comparison of the use of bulk and guided waves is presented in Table 13-5, in particular for plate and pipe inspections.

13.5.3 Aspects of NDT and SHM

Major differences between NDT and SHM are highlighted in Table 13-6, the most crucial of which is the requirement of a baseline in SHM. Very complex structures can be studied with SHM that are not even approachable with NDT. Baseline information can

NDT	SHM
Off-line evaluation	On-line evaluation
Time-based maintenance	Condition-based maintenance
Finds existing damage	Determines fitness-for-service and remaining useful life
Baseline generally not available	Starts with baseline on initial data collection

Table 13-6 The Major Differences between NDT and SHM

change, however, and such items as temperature and boundary condition compensation are being studied. Utilization of guided waves in an SHM environment has great potential.

13.5.4 Source Influence

The development of the dispersion curves discussed so far employs a harmonic plane wave excitation in the waveguide. Because of a bounded transducer problem, though, we must study a source influence problem for a particular size sensor. The finite size of a transducer and various vibration characteristics give rise to a phase velocity spectrum. Therefore, in addition to the ordinary frequency spectrum, there is a phase velocity spectrum, and because of these two spectral bandwidths of frequency and phase velocity, it makes it difficult to excite a specific point on a dispersion curve. Some interesting discussion on the source influence problem can be found in Rose [1999], Ditri et al. [1992], and Rose et al. [1994]. Mode separation in the dispersion curve space then becomes useful for single-mode excitation potential.

Guided wave energy can be induced into a waveguide by a variety of different techniques including piezoelectric, magnetostrictive, electromagnetic acoustic means (EMAT), laser, or physically controlled impact. The challenge is to excite a particular mode at a specific frequency. Normal piezoelectric beam probes can be used. Angle beam piezoelectric sensors can also be used to impart beams that lead to desired kinds of guided waves in a pipe or plate. A comb transducer can also be used, either piezoelectric, magnetostrictive, EMAT, etc., that is, considering a number of different elements at a specific spacing, that together pump ultrasonic energy into the plate, hence causing wave propagation of a certain wavelength in the waveguide. The excitation zones in the phase velocity dispersion curve can be evaluated by the source being considered in the problem. Again Rose [1999], Ditri et al. [1992], and Rose et al. [1994] can provide details in this exercise. A comb transducer, as an example, could be wrapped completely around a pipe or laid out as fingers or an interdigital transducer design on a plate. See Figs. 13-12 and 13-13. Activation lines on a dispersion curve are horizontal in the case of Fig. 13-12 in using Snell's law and angled from the origin of a slope to λ, the spacing of the elements shown in Fig. 13-13.

Because of a phase velocity spectrum and a frequency spectrum, the excitation zone is not a single point in the phase velocity dispersion curve; it is a region as illustrated in Figs. 13-14 and 13-15. See Rose [1999] for details.

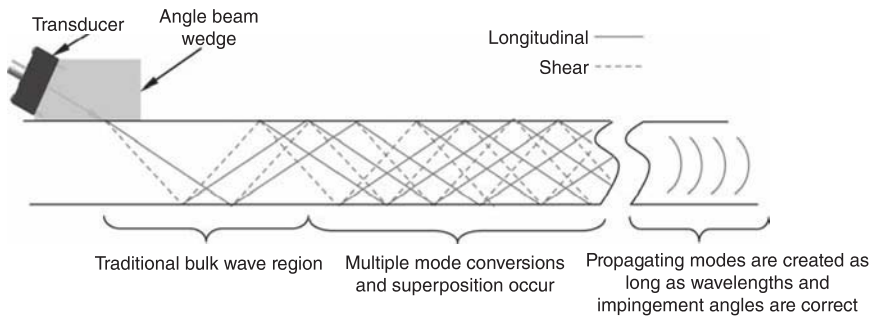

Figure 13-12 Angle beam guided wave generation.

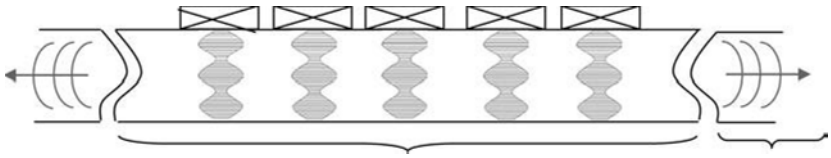

Figure 13-13 Guided wave generation with a comb transducer.

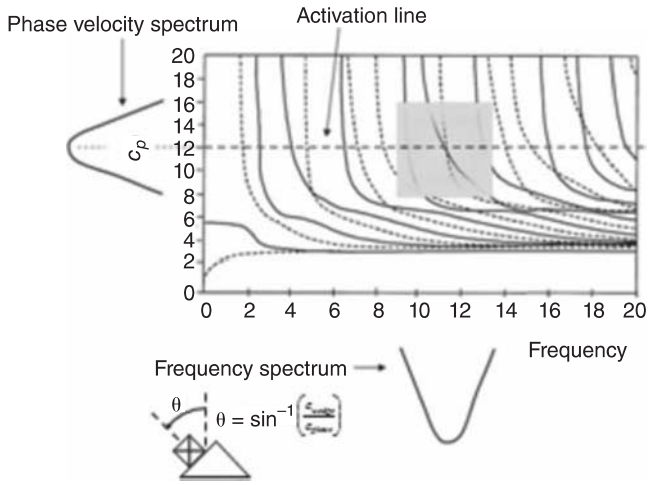

Figure 13-14 Source for a typical angle beam excitation or an ability to generate a specific mode and frequency.

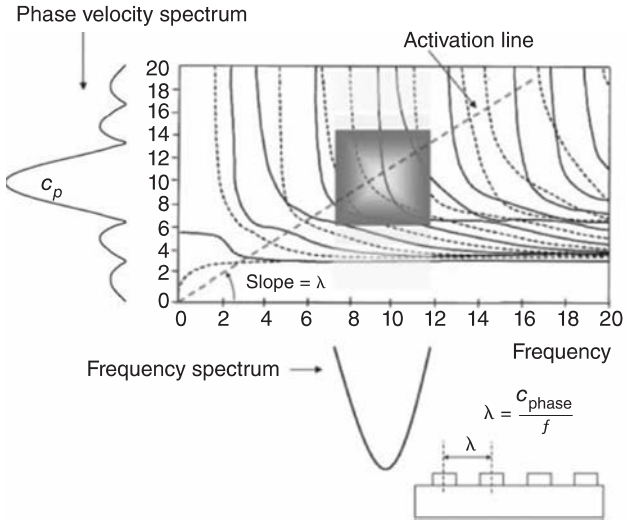

Figure 13-15 Source influence for a typical comb transducer excitation or an ability to generate a specific mode and frequency.

13.6 Hybrid Analytical FEM COMPUTATION

We will now consider the modeling analysis component associated with the understanding of ultrasonic guided waves. The approach makes use of a hybrid analytical FEM computation as exhibited in Fig. 13-16. The FEM computation process is useless unless proper boundary conditions are considered in a simulation of an ultrasonic guided wave inspection. The boundary condition comes from a sensor design that comes from a choice of appropriate wave structure from the phase velocity dispersion curve space, hence an appropriate mode and frequency choice to solve a particular problem in NDE or SHM.

A few sample problems that have been solved using the hybrid analytical FEM computation are listed in Table 13-7 along with appropriate references.

Phased array systems have risen to ecstatic heights in the NDT field for ultrasonic bulk waves because of electronic beam scanning with one transducer array compared to manual scanning with many different angle beam probes. Laid out in Fig. 13-17 is the historical progression of phased array development from the 1970s to current-day developments. Just recently, phased arrays for real time and synthetic focusing in practical pipe inspection applications have been introduced by Rose and Mudge [2002]. Even more recently phased arrays for plate inspection were introduced by Li and Rose [2001b] and Giurgiutiu and Bao [2002].

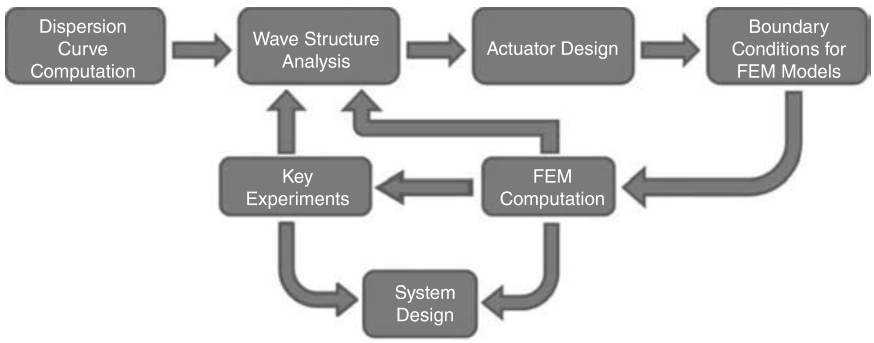

Figure 13-16 The hybrid analytical FEM approach for solving guided wave problems.

- Rail—transverse cracking under shelling, defect in base
- Adhesive bonding—weak interface
- Water-loaded structure—to avoid false alarms
- Gas entrapment—leaky and nonleaky waves
- De-icing—maximum shear stress at the interface
- Piping—flexural mode best selection for focusing

Table 13-7 Examples of the Use of the Hybrid Analytical FEM Approach for Solving Guided Wave Problems

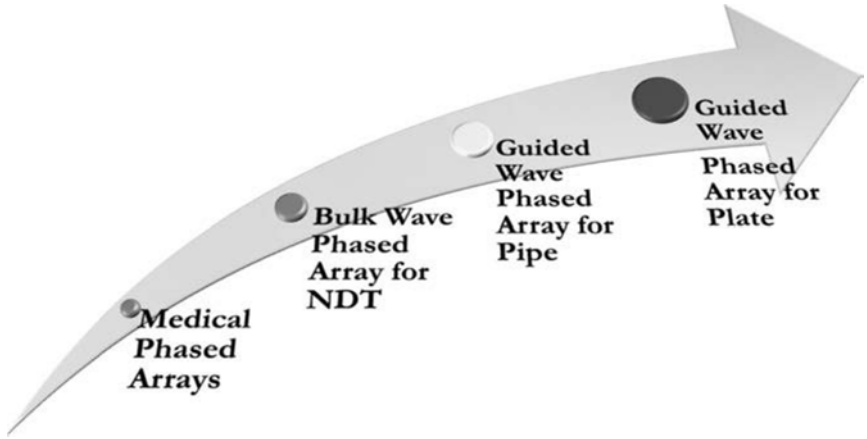

Figure 13-17 Guided wave phased array technologies.

13.6.1 Applications

Pipe

Static shot FEM simulations at different times of axisymmetric guided wave propagation in a pipe are demonstrated in Fig. 13-18. To go beyond the axisymmetric wave to focusing considerations, the methods of focusing are listed in Table 13-8. A static shot example of a real-time phased array result is illustrated in Fig. 13-19. Notice the achievement of the focal spot in the 5th frame. The focal spot can be changed in size by changing the probe and instrument design parameters. The focal spot can then be moved anywhere axially and circumferentially in the pipe. The benefits of focusing are described in Table 13-9.

A sample experiment is presented here in Figs. 13-20 and 13-21 where all three of the defects shown in Fig. 13-20 are found and presented in Fig. 13-21. The upper diagram shows an FFA plot over a frequency range from 20 to 80 kHz showing that defect

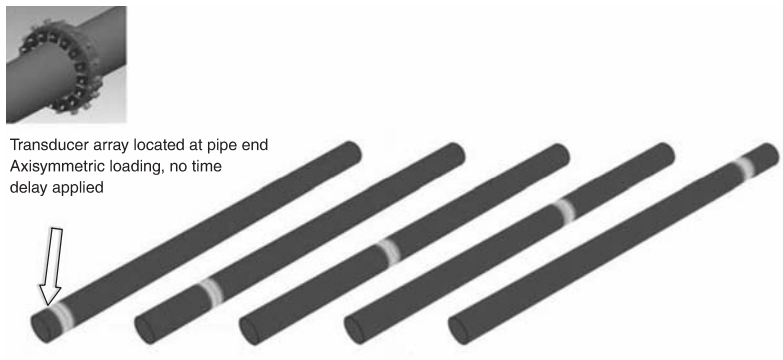

Figure 13-18 Axisymmetric guided wave propagation along the pipe.

- **Frequency tuning**
  Axisymmetric excitation and receiving
- **Natural focusing**
  Partial loading excitation and receiving
- **Phased array focusing**
  Multi-element array excitation and receiving with time delay and amplitude tuning

Table 13-8 Guided Wave Pipe Focusing Techniques

- Improved defect probability of detection (approximately 3 percent CSA, compared to 9 percent for axisymmetric)
- Decreased defect false alarm rate
- Increased inspection confidence
- Improved penetration power for coated pipe
- Excellent defect circumferential location analysis
- Improved SNR compared to axisymmetric
- 6 to infinite dB improvement compared to axisymmetric

Table 13-9 Focused Guided Wave Inspection Benefits

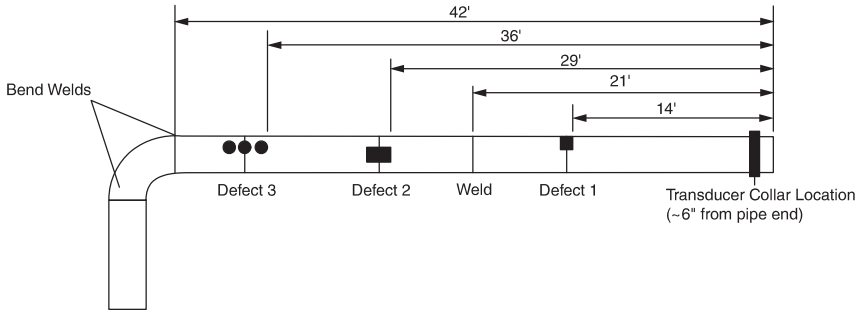

Figure 13-19 Guided wave active focusing in pipe FE simulation results.

Figure 13-20 Details of the pipe section that was studied.

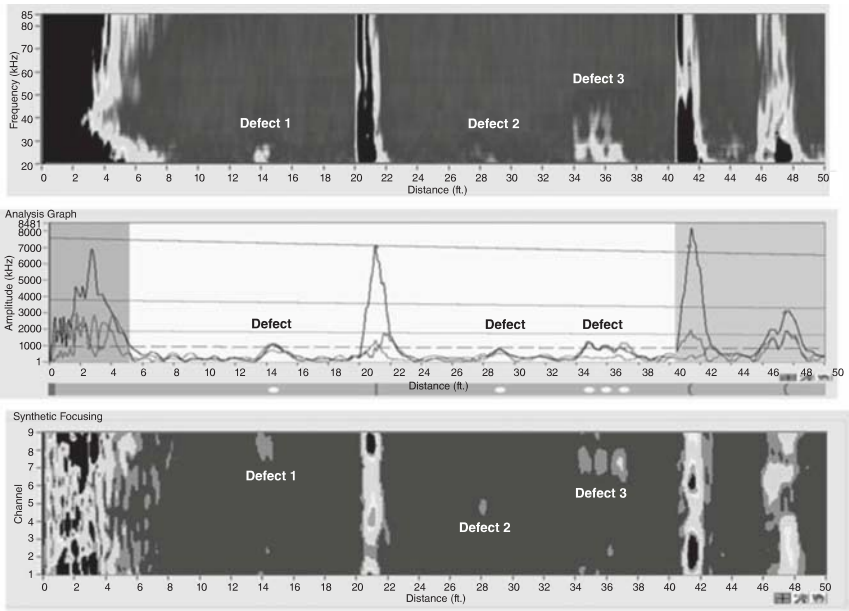

Figure 13-21 Fast frequency analysis [FFA], envelope, and synthetic focusing result after examining the pipe section in Fig. 13-20.

detection sensibility is a function of frequency. The FFA plot shows the best frequency to see each defect. Each defect could have a different preferred frequency in its reflection characteristics. The second trace is a video envelope of the RF waveform clearly showing the defects and welds in the structure. The third trace shows a pipe laid out flat with an image of the defect locations both axially and circumferentially. Excellent results were obtained.

To illustrate the focusing principle in a practical sense, consider the partial loaded field natural focusing result as calculated in Fig. 13-22. The loading transducer is centered at zero degrees. With the pipe laid out flat it can be seen that the natural focal spot in this example occurs at the opposite side of the pipe at 180 degrees at an axial location of around 10 meters. If we were to have an angular profile due to some partial loading around the circumference at some axial position as shown in Fig. 13-23a, and if we were to arrange a series of partial loadings around the circumference and phase them properly, we could end up with a superimposed result at the same axial distance with a strong focal point as plotted in Fig. 13-23b. Two focused experimental results are diagrammed in Fig. 13-24. These profiles provide confidence in a call that a defect is indeed there and its circumferential position can be clearly determined.

Wave propagation into a pipe elbow and beyond can create blind spots at a specific frequency due to mode conversion. Pipe coating and buried pipes can also seriously reduce penetration distances.

Presented in Figs. 13-25 and 13-26 are some interesting aspects of pipe elbow inspection. Frequency tuning can help but a challenge remains to inspect pipelines beyond elbow regions.

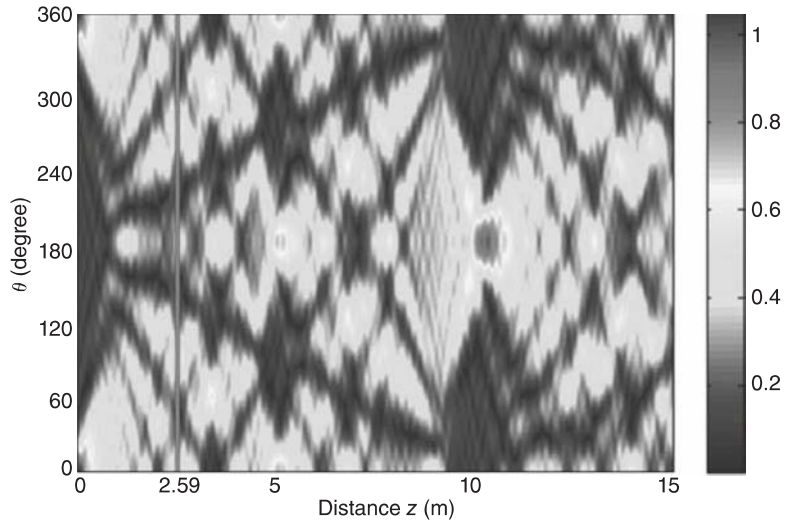

Figure 13-22 Guided wave displacement interference pattern in an 8-in. schedule 40 steel pipe (unwrapped). The waves were generated by a 45° source loading vibrating in the circumferential direction at 80 kHz.

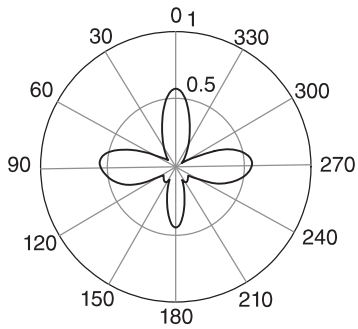

(a) Partial loading angular profile

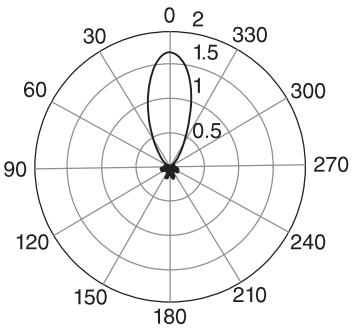

(b) Focused profile

Figure 13-23 Pipe active focusing concept.

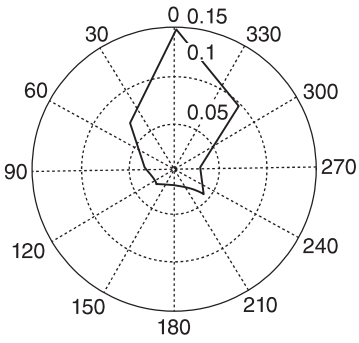

(a) Response from actively focusing around the saw cut distance.

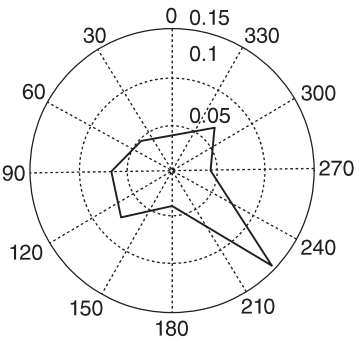

(b) Response from actively focusing around the cluster hole distance.

Figure 13-24 Active focusing results from pipe end at 65 kHz.

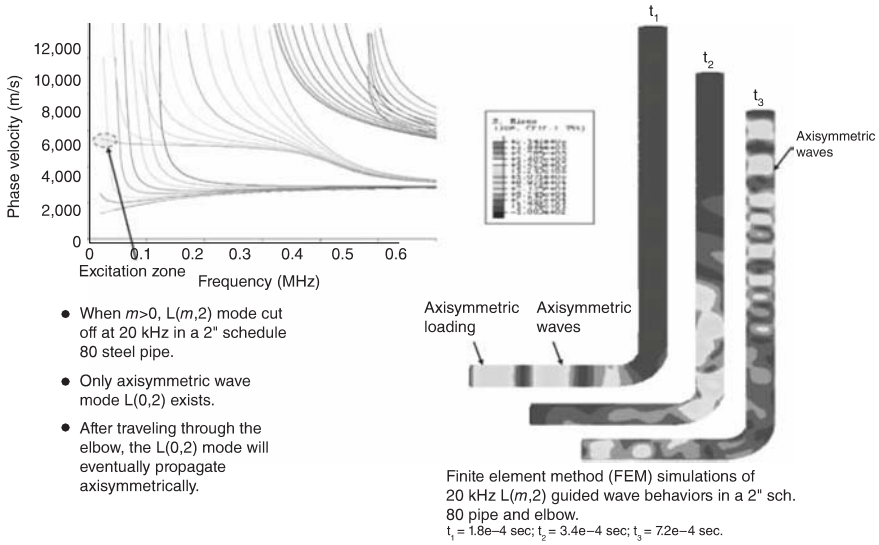

FIGURE 13-25 Inspection beyond some elbow sections is often easy and straightforward. *Note:* Returned axisymmetric behavior beyond elbow.

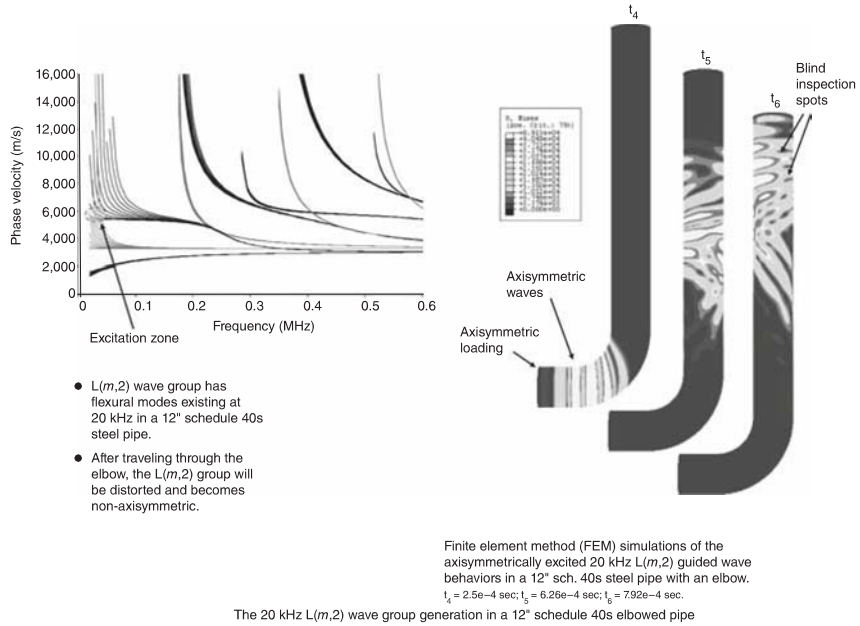

FIGURE 13-26 Inspection beyond some elbow sections is difficult and incomplete. *Note:* Non-axisymmetric behavior beyond elbow.

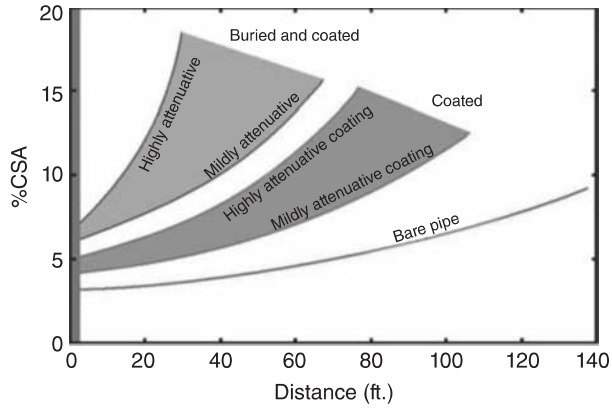

Figure 13-27 Guided wave detection sensitivity concept curves (coated pipe buried in clay) showing penetration power distance reduction due to various coatings and soil influence.

Another challenge is depicted in Fig. 13-27. Unfortunately, coated and buried pipe decreases ultrasonic guided wave penetration power significantly.

Rail

Guided waves are also finding increased use in a variety of different rail inspection applications. See Lee et al. [2009], for an example. We'll consider here the ability to cover various portions of a rail, from head, to web, to base in this brief discussion. The dispersion curves for a rail are close together, and in fact almost cover the entire phase velocity dispersion curve space except for bounds, as an example on the lower end where we only propagate a pseudo-Rayleigh surface wave mode. Despite the complexity, the curves are useful. Wave structure variations occur from one region to another in the dispersion curve space. It becomes possible with the appropriate mode and frequency choice to have energy propagate in the head only, or in the entire rail. See a few static shots in Fig. 13-28. If transverse crack detection under shelling was a goal, the energy in the head-only example would work well. If you were seeking a solution to find a base defect, complete rail coverage would be useful. See Lee [2009] for details.

Bonding and Composites

Mode and frequency selection are also useful when solving inspection problems with bonding situations for composite materials. Let's consider the inspection of a titanium repair patch bonded to an aluminum structure on an aircraft. If we were to find an interface weakness or a kissing bond, guided waves would be useful as we could get a dominant in-plane displacement component into the interface which from earlier work we know would be sensitive to the weak interface. To do this, consider the dispersion curve for the titanium to aluminum bonded structure as calculated in Fig. 13-29.

Superimposed on the curves is the magnitude of the in-plane displacement component. Red areas, for example, point to good portions of the curve to carry out an inspection. Of the possibilities, consider the source influence study depicted in Fig. 13-30. The mode selected is somewhat separated from the others, and can easily

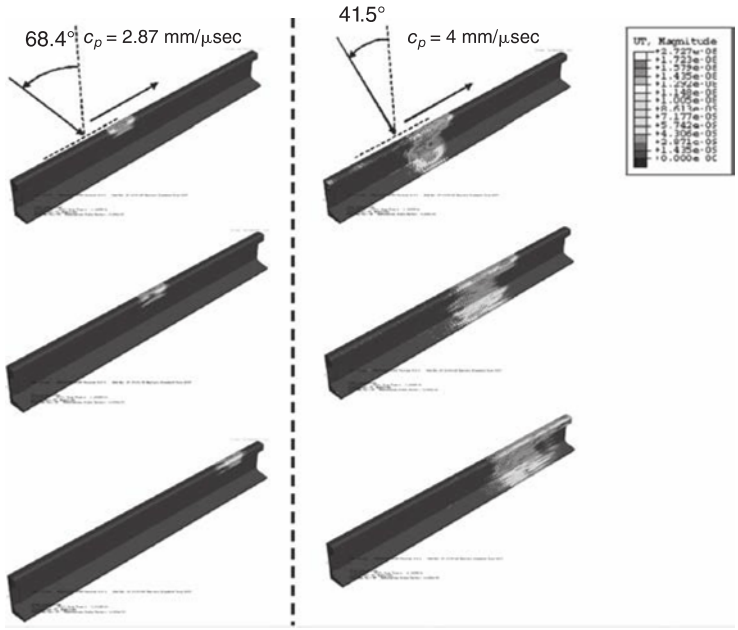

(a) Transverse crack detection under shelling

(b) Defect detection in the base of a rail

Figure 13-28 Rail coverage as a function of mode selection.

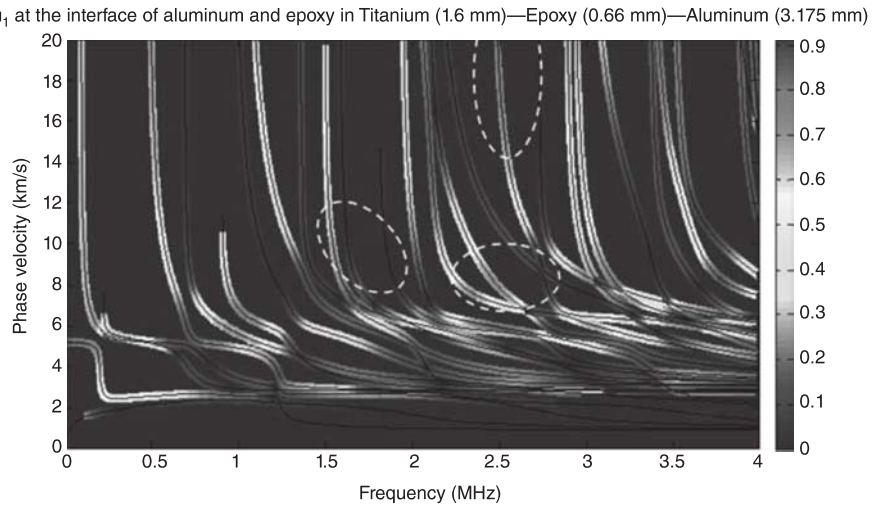

Figure 13-29 Interfacial displacement (in-plane) at Al-epoxy interface in Ti-epoxy-Al specimen.

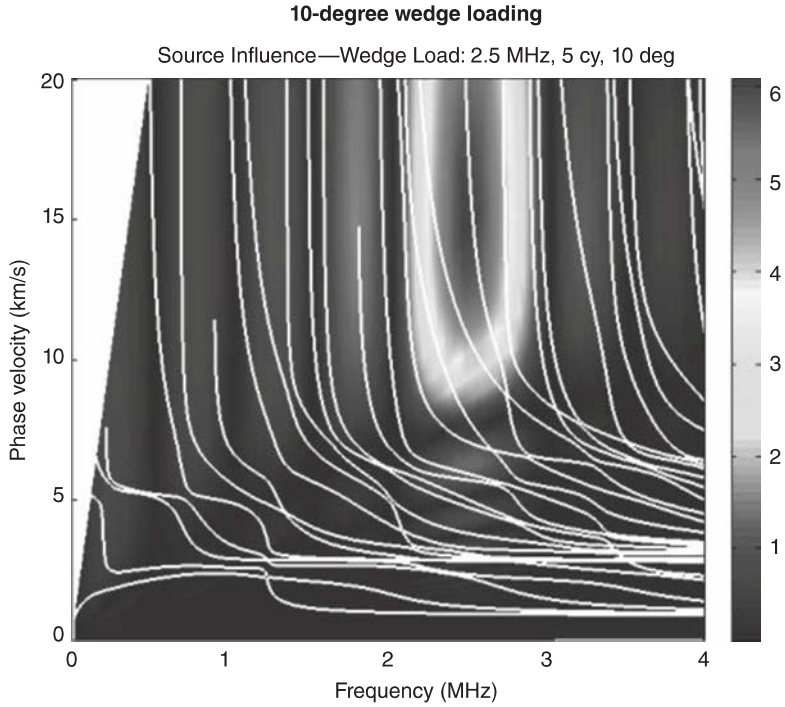

Figure 13-30 Source influence study of guided wave loading sources.

be generated with an actuator having a narrow phase velocity spectrum and frequency spectrum. An angle beam piezoelectric sensor or a comb-type piezoelectric or EMAT activation could be designed for the inspections. See Puthillath et al. [2010] for details.

Imaging and Tomography

Ultrasonic guided wave tomography with a variety of different sensor distributions on a structure can become a valuable tool in SHM. The basic guided wave tomographic image reconstruction process is illustrated in Figs. 13-31 and 13-32. More sensors can produce better images, but sparse array utilization can be very useful. Keep in mind that the data acquisition process should be for a particular guided wave mode, perhaps the mode and frequency most sensitive to the kind of defect that you are looking for. A sample result of corrosion on a pipe elbow is illustrated in Fig. 13-33.

Success depends, however, on using the right actuators. For example, in the plate with a corrosion defect shown in Fig. 13-34, a guided wave tomography experiment was conducted with a set of cylindrically shaped transducers commercially available off the shelf; very poor results were obtained when water was splashed onto the plate. On the other hand, when using a carefully designed set of annular array transducers, excellent results were obtained whether the plate was dry or wet. See Fig. 13-35. This is possible by selecting a point on the phase velocity dispersion curve space with dominant in-plane displacement so that the ultrasonic wave would not leak into the water. The annular array sensor is similar to a comb-type transducer, and its activation line in

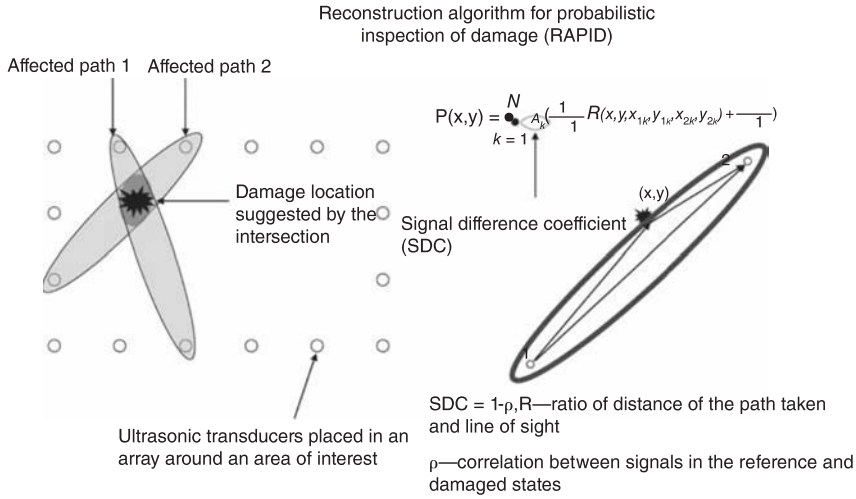

Figure 13-31 The basic tomographic image reconstruction process.

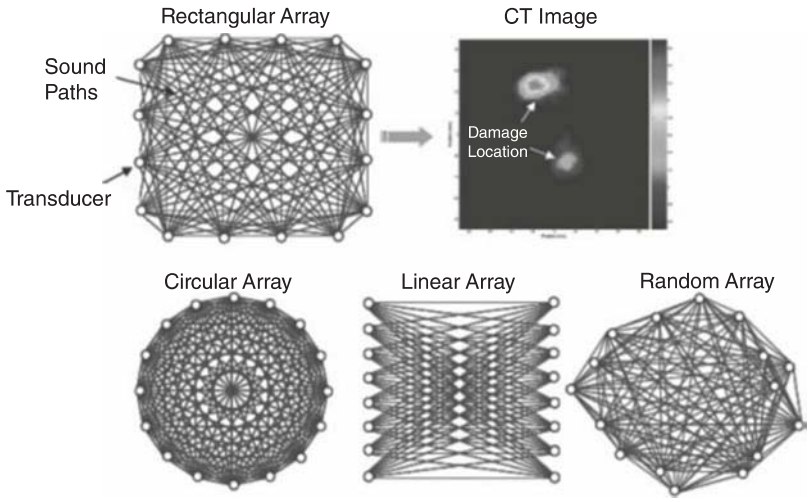

Figure 13-32 Guided wave computed tomography (CT) concept and embedded array possibilities.

the phase velocity dispersion curve space can intersect the optimal test point. The sensor design process is based on selecting an appropriate wave structure as shown in Fig. 13-36. For emphasis on the concept, see Fig. 13-37. The annular array can be designed with different spacing between the elements or application of phasing or the use of time delays from one element to the next.

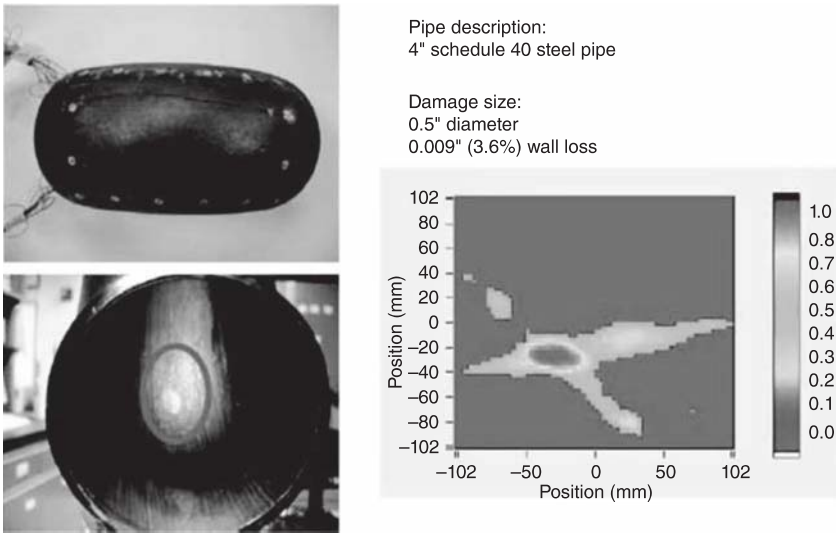

Figure 13-33 Tomographic pipe elbow SHM showing interior erosion simulation via acid etch.

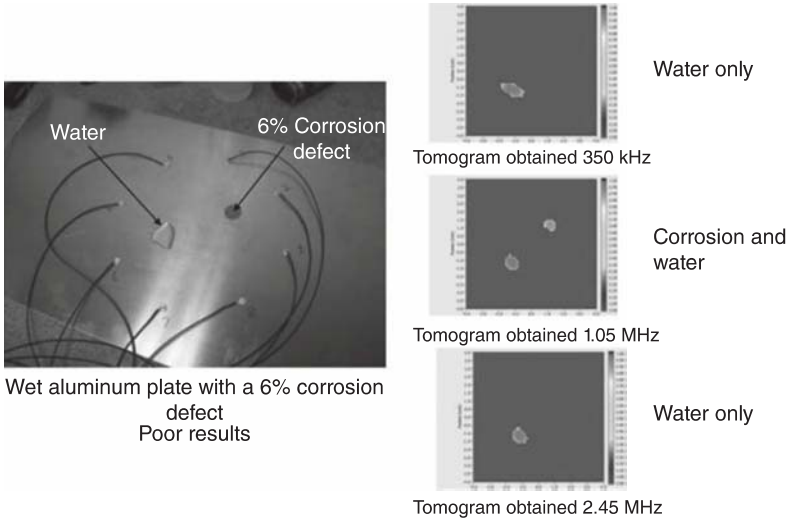

Figure 13-34 The water-loaded plate influence using piezoelectric disk sensors for corrosion detection.

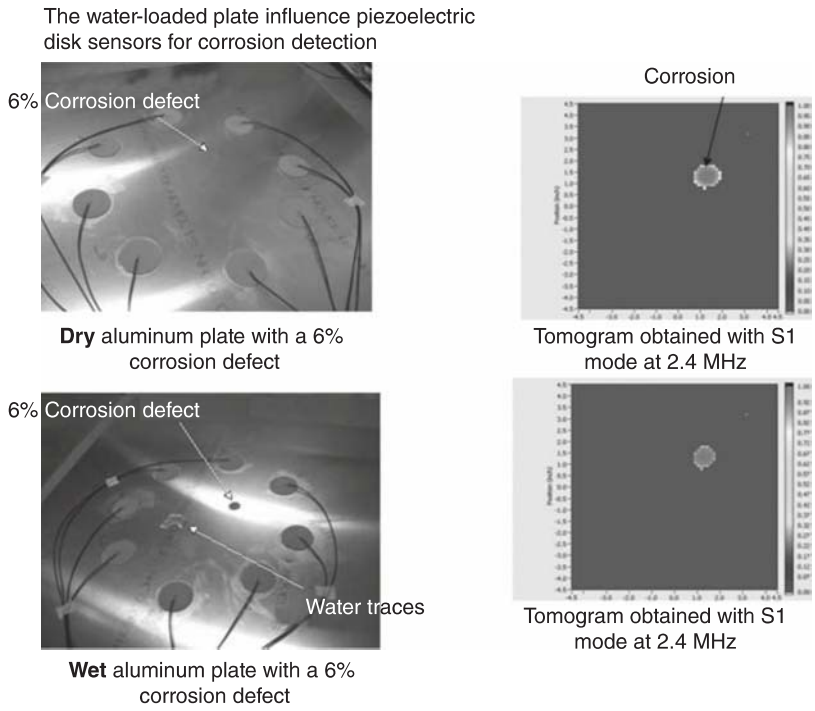

Figure 13-35 Corrosion detection with good annular array sensors.

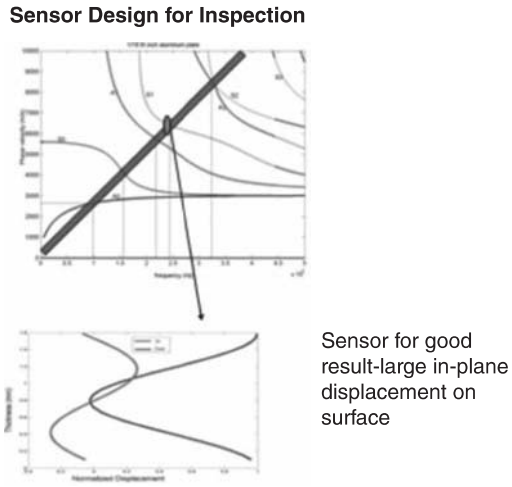

Figure 13-36 Wave structure selection for achieving a document in-plane displacement component to avoid water influence.

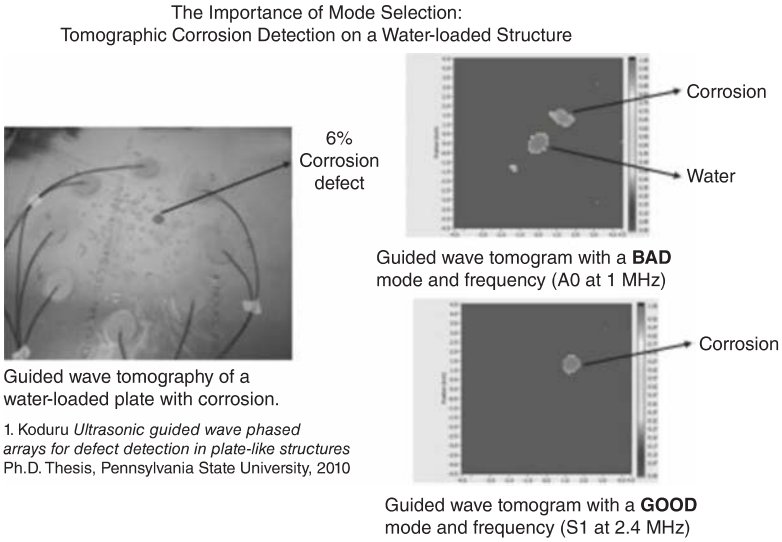

Figure 13-37 Use of an annular array transducer with a bad and good wave structure selection.

13.7 Phased Array for Plate

Phased array application is now going beyond medical and ultrasonic bulk wave phased arrays, to guided wave phased arrays for pipe, and now to guided wave phased arrays for plates. A simulation of a radar-like scan is simulated in Fig. 13-38 with static shot shown at seven positions. Proper sensor design is required to do this from a small circular array of sensors at the center of a plate. Keep in mind here that appropriate mode and frequency control is also necessary in order to optimize defect detection sensitivity, to scan a composite plate, and to overcome skew angle and group velocity variation in the plate. Multiple scans might be necessary. A sample result is presented in Fig. 13-39. Some of the challenges in moving this method forward are outlined in Table 13-10.

Phased array possibilities for an anisotropic plate are much more complex compared to an isotropic plate. The dispersion curve becomes a function of direction and skew angles can lead to missed portions of a structure. Multimode and frequency sensors are often required for complete evaluation of a structure. See Fig. 13-40 for a description of the situation. The directional dependence of the wave velocities and energy distributions of guided waves in multilayer anisotropic composite plates sometimes make it impossible to steer the guided wave beam into a certain direction with a phased array. An example of failure is shown to the left, by choosing guided wave modes and frequencies that are insensitive to wave launching directions in the composite plates; successful beam steering can be achieved for any direction, good example to the right.

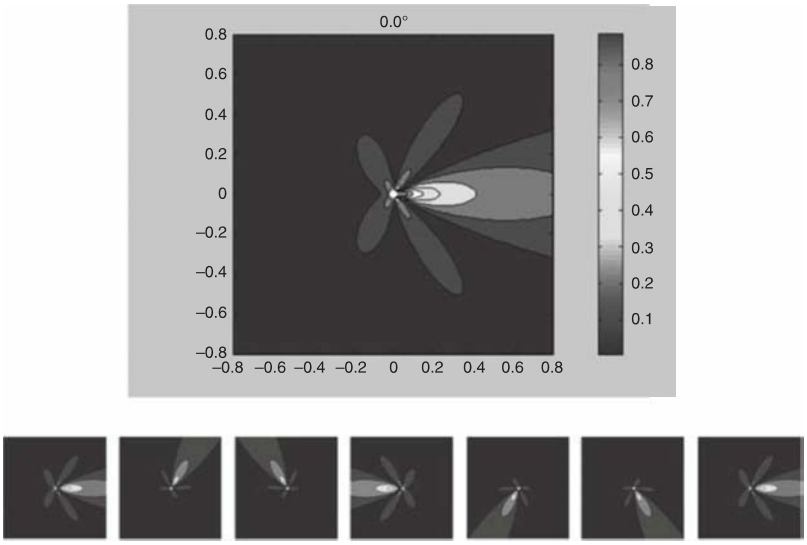

Figure 13-38 Ultrasonic guided wave beam steering concept using phased arrays. *Notes:* Guided wave beam can be steered into different directions by applying phase delays to the elements of an array, circular array example.

Product Description: Phased array guided wave inspection of plate-like structures. From a single probe position, a guided wave beam is steered throughout the structure via time delay control of elements within an array.
Competition: Point by point bulk wave inspection
Advantage: Allow 100% coverage, ability to look at hidden structures, rapid screening possible
Product Availability: Under Development

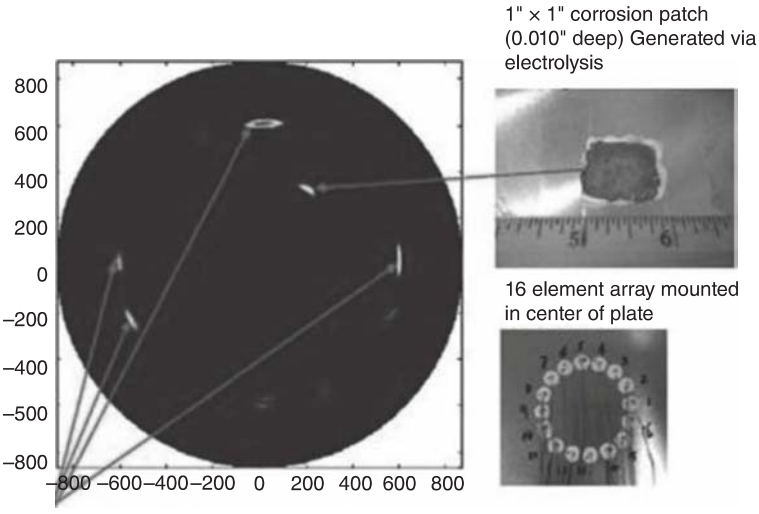

Figure 13-39 Phased array guided wave inspection for plate.

Technical Challenges	Potential Solution
• Multimodes application environment	• Guided wave transducer design and mode tuning to achieve single mode excitation and detection
• Guided wave dispersion	• Wave number/frequency domain beam steering
• Skew effects in anisotropic plates	• Select a guide wave mode and frequency that is insensitive to the material anisotropy

Table 13-10 Guided Wave Phased Array Technical Challenges and Solutions

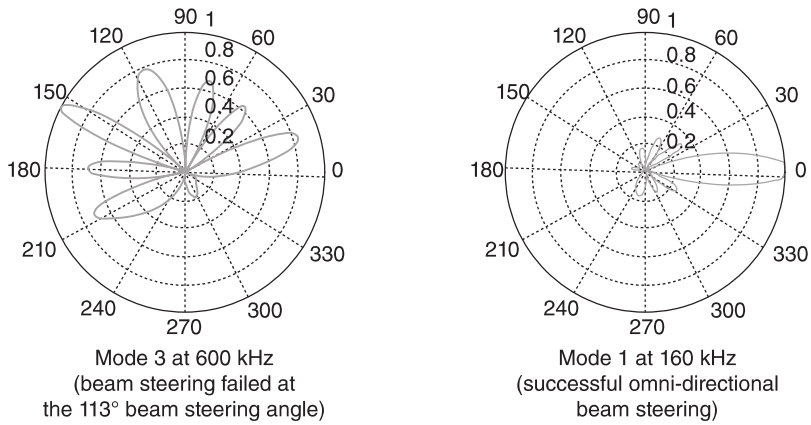

Figure 13-40 Phased array for multilayer anisotropic composite plates.

13.8 Ultrasonic Vibrations

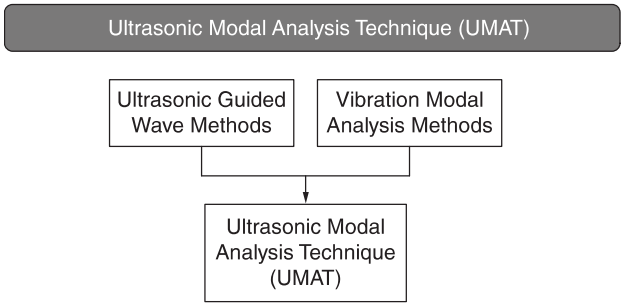

A new ultrasonic guided wave method to provide a robust signature of a structure has recently been introduced. This technique bridges the gap from transient high frequency guided wave analysis to more traditional low frequency ultrasonic modal analysis. The characteristics of the methods are presented in Table 13-11. An interesting result is shown in Fig. 13-41. The high frequency ultrasonic resonances and modal pattern or ODS depends on the ultrasonic loading function. Sensitivity optimization is possible

	Defect Detection Size	Sender Positions	Speed
Ultrasonic Guided Wave	Very small ✓	Many ×	Slow ×
Vibration Modal Analysis	Large ×	One ✓	Fast ✓
UMAT	Small to intermediate ✓	One ✓	Fast ✓

✓ good news, × bad news.

TABLE 13-11 Method Comparisons

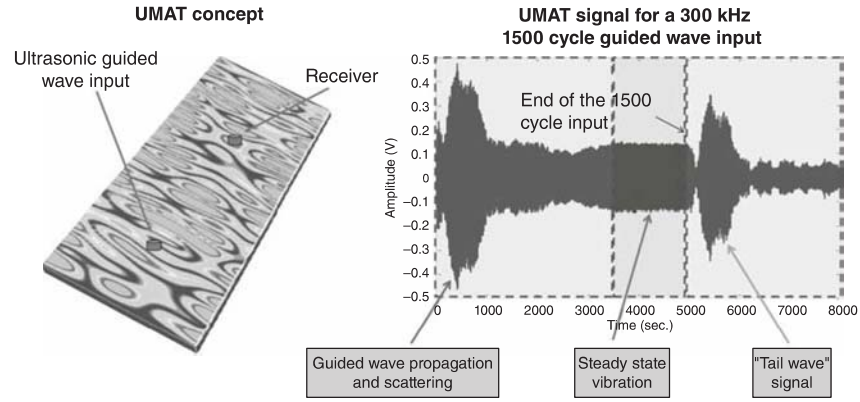

FIGURE 13-41 The importance of mode selection in the ultrasonic vibration concept.

here, again, by selecting the proper mode and frequency for the phase velocity dispersion curve space. This approach is particularly useful in manufacturing hundreds of a complex shaped part and follow-up later, in an in-service environment. Structural and boundary condition variability poses serious challenges to date for this method but some specific applications are working out quite well.

13.9 Advantages and Limitations

13.9.1 Advantages of Ultrasonic Guided Wave Inspection

1. Provides rapid screening for in-service degradation (long-range inspection)—potential to achieve hundreds of feet (meters) of inspection area.
2. Capable of detecting internal and external metal loss.
3. Reduced time and cost to gain access.

4. Insulated line can be inspected with minimal insulation removal.
5. Corrosion under supports can be examined without a need for lifting.
6. Inspection at elevated locations with minimal need for scaffolding, and inspection of road crossings and buried pipes.
7. Data can be fully recorded.
8. Fully automated data collection protocols.

13.9.2 Limitations of Ultrasonic Guided Wave Inspection

1. Interpretation of data is highly operator dependent.
2. Difficult to find small pitting conditions.
3. Not very effective at inspecting areas close to accessories.
4. Requires a detailed, qualified procedure

13.10 Concluding Remarks

Great breakthroughs on the use of ultrasonic guided waves in NDT and SHM have taken place in the last two decades. The advances were made possible because of increased understanding, interpretation of results, and tremendous leaps forward in computational power and efficiency. Very few investigators were involved from 1985 to 2000 as indicated in literature survey work, but since 2000 the work and interest have exploded. What follows in the concluding remarks is a brief outline of a few successes and challenges associated with practical application of ultrasonic guided waves.

Ultrasonic guided waves for aircraft and composite material inspections have come a long way in the past decade or so. Many successes have come about but many challenges remain, some of which are outlined below. The same is true for pipeline inspection.

Successes in guided waves, in general, over the past decade, are listed in Table 13-12, in composite materials in Table 13-13, in aircraft applications in Table 13-14, and in pipeline inspection in Table 13-15. The topics speak for themselves.

• Computational developments and understanding basic principles
• Phased array and focusing developments in plates and pipes (animations and practice)
• Demonstration of optimal mode and frequency selections for penetration power, fluid loading influences, and defect detection sensitivities

Table 13-12 Successes—Guided Waves in General

• Understanding guided wave behavior in anisotropic media (slowness profiles and skew angle influence)
• Development of ultrasonic guided wave tomographic imaging methods
• Comb sensor designs for optimal mode and frequency selection (linear comb and annular arrays)
• Implementation of time-delay comb-type transducers for phased array composite plate inspection

Table 13-13 Successes—Composite Materials

- Demonstration of feasibility studies in lap splice, tear strap, skin to core delamination, corrosion detection, and other applications
- Introduction of ultrasonic modal analysis testing (linking guided waves to modal vibration analysis)
- Guided wave ice detection and deicing studies initiated

Table 13-14 Successes—Aircraft Applications

- Understanding of both axisymmetric and non-axisymmetric modes
- Achieving excellent penetration power with special sensors, focusing, and mode and frequency choices
- Handling fluid loading with torsional modes
- Defect sizing accomplishments to less than 5 percent cross-sectional area
- Reduced false alarm calls in inspection due to focusing for confirmation
- Circumferential location and length of defect estimations with focusing
- Testing of pipe under insulation, coatings, and/or soil

Table 13-15 Successes—Pipe Inspection

Finally, although many promising methods are evolving into promising inspection tools, numerous challenges remain. Many of the challenges are focused on technology transfer work tasks to a realistic practical environment. Challenges are listed in Table 13-16 for guided waves in general, in Table 13-17 for composite materials, in Table 13-18 for aircraft applications, and in Table 13-19 for pipeline inspection. The topics are self explanatory and can be used to define future work efforts.

- Long numerical solution computation times often necessary with FEM (especially for high frequency, and solutions at long distances from the actuator)
- Modeling accuracy is critically dependent on accurate input parameters (especially for anisotropic and viscoelastic properties, interface conditions, and defect characteristics)
- Signal interpretations often difficult (due to multimode propagation and mode conversion, along with special test structure geometric features)
- Mode and frequency selection for optimal penetration power and defect detection sensitivity
- Low-frequency limitation for thick structures
- Equipment cost and reliability
- Sensor robustness to environmental situations like temperature and humidity
- Sensor robustness to high stress, mechanical vibrations, shock, and radiation
- Adhesive bonding challenges for mounting sensors and sustainability
- Sensor type and development for achieving the desired guided wave mode and frequency (especially considering source influence, side lobes, and multimode generation potential)
- Guided wave propagation in structures with variations in cross-sectional areas and thicknesses
- Development of regulatory codes
- Educational level and inspector training
- Lack of realistic mock-up tests specimens for training and test development

Table 13-16 Challenges—Guided Waves in General

- Dealing with complex anisotropy and wave velocity and skew angle as a function of direction
- Viscoelastic influences
- Penetration power due to anisotropy, viscoelasticity, and inhomogeneity
- Optimal mode and frequency selection and appropriate transducer designs
- Differentiating critical composite damage such as delamination defects from structural variability during fabrication (including minor fiber misalignments, ply-drops, inaccurate fiber volume fraction, and so on)
- Guided wave inspection of composites with unknown material properties

Table 13-17 Challenges—Composite Materials

- Sensor and instrumentation weight considerations
- Cabling and wireless potential and energy harvesting
- Adhesive bonding inspection reliability (especially kissing bonds)
- Robustness of guided wave sensors under in-flight conditions
- High temperature environment possibilities
- Many wave scattering sources such as rivets, fasteners, stiffeners, and joints
- Influences of aircraft paint and embedded metallic mesh in composite airframes for lightning protection

Table 13-18 Challenges—Aircraft Applications

- Penetration power distances for plastic pipe and coated and buried steel pipe
- Tees, elbows, bends, and number of elbows and inspection beyond elbows
- Quantification in defect location, characterization, sizing, especially depth determination
- Inspection reliability and false alarms (due to multimode propagation, mode conversions, and so many pipe features like welds, branches, etc.)
- Reducers, expanders, unknown layout drawings, cased pipes, and sleeves
- Inspection time for a complete real-time focusing scan of a pipe
- Temperature effects on coating
- Improved axial and lateral resolution
- Reduction of dead zone

Table 13-19 Challenges—Pipe Inspection

New directions point to NDE and SHM with inexpensive distributive sensor networks and sparse arrays for a line of sight analysis, tomography, phased array work, and ultrasonic vibrations. Besides defect detection and location analysis for screening, new work also points to more detailed quantitative characterization analysis. Integration with wireless and energy harvesting technologies are underway. Emphasis on lightweight easy-to-use are of great interest and are being developed by several manufacturers.

Acknowledgments

Thanks are given to my M.S. and Ph.D. students over the years, as well as all of the employees at FBS, Inc. for their contributions to the field of ultrasonic guided waves. Cooperation has been a fun and rewarding experience. Thanks also to all of my sponsors over the years and many worldwide friends and colleagues in ultrasonics.

Note: Portions of this chapter are taken from Rose [2011], Workman et al. [2007], and Rose [2010a].

References

Achenbach, J.D., *Wave Propagation in Elastic Solids*, Elsevier Science, Amsterdam, 1973.

Achenbach, J.D., *Reciprocity in Elastodynamics*, Cambridge University Press Cambridge, United Kingdom, 2003.

Auld, B.A., *Acoustic Fields and Waves in Solids*, John Wiley and Sons, 1973, Hoboken, NJ (Reprinted R.E. Krieger Publ. Co., Malabar, Florida, 1990).

Bartoli, I., Marzani, A., Lanza di Scalea, F., and Viola, E., "Modeling wave propagation in damped waveguides of arbitrary cross-section," *Journal of Sound and Vibration*, 295(3–5), 685–707, August 22, 2006.

Breon, L.K. Van Velsor, J.K., and Rose, J.L., "Guided wave damage detection tomography for structural health monitoring in critical zones of pipelines," *Materials Evaluation*, 65, 1215–1219, 2007.

Cantrell, J.H., and Yost, W.T., "Nonlinear ultrasonic characterization of fatigue microstructures," *International Journal of Fatigue*, 23(1), 487–490, 2001.

Chimenti, D.E., and Nayfeh, A.H., "Experimental ultrasonic reflection and guided wave propagation in fibrous composite laminates," *American Society of Mechanical Engineers, Applied Mechanics Division, AMD*, 90, 29–37, 1988.

Datta, S.K., and Shah, A.H., *Elastic Waves in Composite Media and Structures: With Applications to Ultrasonic Nondestructive Evaluation*, CRC Press, Boca Raton, FL, 2008.

Datta, S.K., Shah, A.H., and Karunasena, W., "Edge and layering effects in a multilayered composite plate," *Computers and Structures*, 37(2), 151–162, 1990.

Davies, J., and Cawley, P., "The application of synthetic focusing for imaging crack-like defects in pipelines using guided waves," *IEEE Transactions on Ultrasonics, Ferroelectrics, and Frequency Control*, 56(4), 759–771, 2009.

Demma, A., Cawley, P., and Lowe, M.J.S., "Mode conversion of longitudinal and torsional guided modes due to pipe bends," *AIP Conference Proceedings*, 557A, 172–179, 2001.

Ditri, J.J., and J.L. Rose, "Excitation of guided elastic wave modes in hollow cylinders by applied surface tractions," *Journal of Applied Physics*, 72(7), 2589–2597, 1992.

Fromme, P., and Sayir, M.B., "Detection of cracks at rivet holes using guided waves," *Ultrasonics*, 40(1–8), 199–203, May 2002.

Gao, H., and Rose, J.L., "Ice detection and classification on an aircraft wing with ultrasonic shear horizontal guided waves," *IEEE Transactions on Ultrasonics, Ferroelectrics, and Frequency Control*, 56(2), 334–344, 2009.

Gao, H., and Rose, J.L., "Goodness dispersion curves for ultrasonic guided wave based SHM: a sample problem in corrosion monitoring," *The Aeronautical Journal of the Royal Aeronautical Society*, 114, January 2010.

Gao, H., Shi, Y., and Rose, J.L., "Guided wave tomography on an aircraft wing with leave in place sensors," *Review of Progress in Quantitative Nondestructive Evaluation*, 760, 1788–1794, 2005.

Giurgiutiu, V., and Bao, J., "Embedded ultrasonic structural radar with piezoelectric wafer active sensors for the NDE of thin-wall structures," *ASME International Mechanical Engineering Congress and Exposition, Proceedings*, 31–38, 2002.

Graff, K.F., *Wave Motion in Elastic Solid*, Oxford University Press, New York, NY, 1975.

Grewal, D.S., "Improved ultrasonic testing of railroad rail for transverse discontinuities in the rail head using higher order Rayleigh (M21) waves," *Materials Evaluation*, 54, 983–986, 1996.

Gunawan, A., and Hirose, S., "Boundary element analysis of guided waves in a bar with an arbitrary crosssection," *Engineering Analysis with Boundary Elements*, 29(10), 913–924, October 2005.

Hall, J.S., and Michaels, J.E., "Computational efficiency of ultrasonic guided wave imaging algorithms," *IEEE Transactions on Ultrasonics, Ferroelectrics, and Frequency Control*, 58(1), 244–248, January 2011.

Hayashi, T., Kawashima, K., Sun, Z., and Rose, J.L., "Analysis of flexural mode focusing by a semianalytical finite element method," *Journal of Acoustical Society of America*, 113, 1241–1248, 2002.

Hayashi, T., and Murase, M., "Defect imaging with guided waves in a pipe," *The Journal of the Acoustical Society of America*, 117, 2134–2140, 2005.

Hayashi, T., Song, W., and Rose, J.L., "Guided wave dispersion curves for a bar with an arbitrary crosssection, a rod and rail example," *Ultrasonics*, 41(3), 175–183, May 2003.

Hinders, M.K., Malyarenko, E.V., and McKeon, J.C.P., "Ultrasonic Lamb wave tomographic scanning," *Proceedings of SPIE—The International Society for Optical Engineering*, 3586, 279–291, 1999.

Hosten, B., and Castaings, M., "Finite elements methods for modeling the guided waves propagation in structures with weak interfaces," *Journal of the Acoustical Society of America*, 117(3), 1108–1113, March 2005.

Ing, R.K., and Fink, M., "Time-reversed Lamb waves," *IEEE Transactions on Ultrasonics, Ferroelectrics and Frequency Control*, 45(4), 1032–1043, July 1998.

Kim, Y.Y., Park, C.I., Cho, S.H., and Man, S.W., "Torsional wave experiments with a new magnetostrictive transducer configuration," *Journal of the Acoustical Society of America*, 117 (6), 3459–3468, June 2005.

Kwun, H., and Dynes, C., "Long-range guided wave inspection of pipe using the magnetostrictive sensor technology—Feasibility of defect characterization," *Proceedings of SPIE—The International Society for Optical Engineering*, 3398, 28–34, 1998.

Lee, C.Y., Rose, J.L., and Cho, Y., "A guided wave approach to defect detection under shelling in rail," *NDT & E International*, 42(3), 174–180, April 2009.

Li, J., and Rose, J.L., "Excitation and propagation of non-axisymmetric guided waves in a hollow cylinder," *Journal of the Acoustical Society of America*, 109(2), 457–464, 2001a.

Li, J., and Rose, J.L., "Implementing guided wave mode control by use of a phased transducer array," *Ultrasonics, Ferroelectrics & Frequency Control*, 48(3), 761–768, May 2001b.

Li, J., and Rose, J.L., "Angular-profile tuning of guided waves in hollow cylinders using a circumferential phased array," *IEEE Transactions on Ultrasonics, Ferroelectrics and Frequency Control*, 49(12), 1720–1729, 2002.

Ma, J., Lowe, M.J.S., and Simonetti, F., "Feasibility study of sludge and blockage detection inside pipes using guided torsional waves," *Measurement Science and Technology*, 18(8), 2629–2641, August 1, 2007.

Mal, A.K., Xu, P., and Bar-Cohen, Y., "Ultrasonic nondestructive evaluation of adhesive bonds," *American Society of Mechanical Engineers, Materials Division (Publication) MD*, 9, 85–89, 1988.

Michaels, J.E., Cobb, A.C., and Michaels, T.E., "A comparison of feature-based classifiers for ultrasonic structural health monitoring," *Proceedings of SPIE–The International Society for Optical Engineering*, 5394, 363–374, 2004.

Mu, J., and Rose, J.L., "Long range pipe imaging with a guided wave focal scan," *Materials Evaluation*, 66(6), 663–666, 2008a.

Mu, J., and Rose, J.L., "Guided wave propagation and mode differentiation in hollow cylinders with viscoelastic coatings," *Journal of the Acoustical Society of America*, 124(2), 866–874, 2008b.

Mu, J., Zhang, L., and Rose, J.L., "Pipe inspection with guided wave synthetic focusing technique," *Materials Evaluation*, 68(10), 1171–1176, 2010.

Na, W., Kundu, T., and Ehsani, M.R., "Ultrasonic guided waves for steel bar concrete interface testing," *Materials Evaluation*, 60(3), 437–444, 2002.

Pavlakovic, B., Lowe, M., Alleyne, D., and Cawley, P., "DISPERSE: a general purpose program for creating dispersion curves," *Review of Progress in Quantitative Nondestructive Evaluation*, 1185–1192, 1997.

Pruell, C., Kim, J.-Y., Qu, J., and Jacobs, L.J., "A nonlinear-guided wave technique for evaluating plasticitydriven material damage in a metal plate," *NDT&E International*, 42(3), 199–203, April 2009.

Puthillath, P., and Rose, J.L., "Ultrasonic guided wave inspection of a titanium patch bonded to an aluminum aircraft skin," *International Journal of Adhesion and Adhesives*, 30, 566–573, 2010.

Raghavan, A., and Cesnik, C.E.S., "Modeling of piezoelectric-based Lamb wave generation and sensing for structural health monitoring," *Proceedings of SPIE,* 5391, 419–430, 2004.

Rizzo, P., Cammarata, M., Dutta, D., Sohn, H., and Harries, K., "An unsupervised learning algorithm for fatigue crack detection in waveguides," *Smart Materials and Structures*, 18(2), 025016 (11 pp.), February 2009.

Rokhlin, S.I., Chimenti, S.E., and Nagy, P.B., *Physical Ultrasonics of Composites*, Oxford University Press New York, NY CB2 8BS, United Kingdom, 2011.

Rose, J.L., "Guided waves successes and challenges for ultrasonic testing in NDT and SHM," *Materials Evaluation*, 68(5), 495–500, 2010a.

Rose, J.L., "The upcoming revolution in ultrasonic guided waves," *Proceedings of SPIE*, 7983, 798302 (2011); 10.1117/12.897025, [2011].

Rose, J. L., *Ultrasonic Waves in Solid Media*, Cambridge University Press, Cambridge, UK, 1999.

Rose, J.L., Ditri, J., and Pilarski, A., "Wave mechanics principles in acousto-ultrasonic NDE," *Journal of Acoustic Emission*, 12(1/2), 23–26, 1994.

Rose, J.L., Ditri, J.J., Pilarski, A., Rajana, K.M., and Carr, F.T., A guided wave inspection technique for nuclear steam generator tubing," *NDT&E International,* 27(6), 307–310, 1993.

Rose, J.L., and Mudge, P.J., "Flexural Mode Focusing in Pipe," *8th European Conference on Nondestructive Testing*, Barcelona, Spain, June 17–21, 2002.

Rose, J.L., Sun, Zongqi, Mudge, Peter J., and Avioli, Michael J., "Guided wave flexural mode tuning and focusing for pipe testing," *Materials Evaluation*, 61(2), 162–167, February 2003.

Rose, J.L., Yan, F., and Zhu, Y., "Ultrasonic guided wave modal analysis technique (UMAT) for defect detection," *Proceedings of IMAC XVIII, Jacksonville*, FL, February 2010b.

Ruzzene, M., "Frequency wavenumber domain filtering for improved damage visualization," *Smart Materials and Structures*, 16(6), 2116–2129, 2007.

Salas, K.I., and Cesnik, C.E.S. "Clover: An alternative concept for damage interrogation in structural health monitoring systems," *Aeronautical Journal of the Royal Aeronautical Society*, 113(1144), 339–356, 2009.

Senesi, M., Xu, B., and Ruzzene, M., "Experimental characterization of periodic frequency-steerable arrays for structural health monitoring," *Smart Materials and Structures*, 19, 055026 (11 pp), April 2010.

Sun, Z., Zhang, L., Gavigan, B.J., Hayashi, T., and Rose, J.L., "Ultrasonic flexural torsional guided wave pipe inspection potential," *ASME Proceedings of Pressure Vessel and Piping Division Conference*, PVP 456, 29–34, 2003a.

Sun, Z., Zhang, L., and Rose, J.L., "Flexural longitudinal and torsional modes natural focusing phenomena in a pipe," *Proceedings of QNDE*, 23, 193–197, 2003b.

Thompson, R.B., Alers, G.A., and Tennison, M.A., "Application of direct electromagnetic lamb wave generation to gas pipeline inspection," *Conference*: *IEEE Ultrason Symp, Proc*, 91–94, October 4, 1972–October 7, 1972.

Van Velsor, J.K., Gao, H., and Rose, J.L., "Guided-wave tomographic imaging of defects in pipe using a probabilistic reconstruction algorithm," *Insight: Non-Destructive Testing and Condition Monitoring*, 49(9), 532–537, 2007.

Van Velsor, J.K., Rose, J.L., and Nestleroth, J.B., "Enhanced coating disbound detection capabilities in pipe using circumferential shear horizontal guided waves," *Materials Evaluation*, 67 (10), 1179–1188, 2009.

Velichko, A., and Wilcox, P.D., "Post-processing of guided wave array data for high resolution pipe inspection," *Journal of the Acoustical Society of America*, 126(6), 2973–2982, 2009.

Venna, S., Lin, Y., and Botura, G., "Piezoelectric transducer actuated leading edge de-icing with simultaneous shear and impulse forces," *Journal of Aircraft*, 44(2), 509–515, 2007.

Wilcox, P.D., "A rapid signal processing technique to remove the effect of dispersion from guided wave signals," *IEEE Transactions on Ultrasonics, Ferroelectrics and Frequency Control*, 50(4), 419–427, April 2003a.

Wilcox, P.D., "Omni-directional guided wave transducer arrays for the rapid inspection of large areas of plate structures," *IEEE Transactions on Ultrasonics, Ferroelectrics and Frequency Corntrol*, 50(6), 699–709, 2003c.

Wilcox, P.D., Pavlakovic, B.N., Evans, M.J., Vine, K.A., Cawley, P., Lowe, M.J.S., and Alleyne, D.N., "Long Range Inspection of Rail Using Guided Waves" in Review of Progress in Quantitative NDE, 22, pp. 236–243, 2003b.

Workman, Gary L., and Kishoni, Doron (eds.), Ultrasonic Testing, Volume 7 in *Nondestructive Testing Handbook*, 3rd ed. (J. Rose contribution), American Society for Nondestructive Testing, Columbus, OH, 2007.

Yan, F., Qi, X., Rose, J.L., and Weiland, H., "Ultrasonic guided wave mode and frequency selection for defect detection and characterization in a multilayer hybrid laminate," *Materials Evaluation*, 68(2), 169–175, 2010a.

Yan, F., and Rose, J.L., "Defect detection using a ultrasonic guided wave modal analysis technique (UMAT)," *Proceedings of SPIE*, Vol. 7650, 76500R, 2010c.

Yan, F., and Rose, J.L., "Guided wave phased array beam steering in composite plates," *Proceedings of SPIE* 6532:65320G, 2007.

Yan, F., and Rose, J.L., "Time delay comb transducers for aircraft inspection," *The Aeronautical Journal of the Royal Aeronautical Society*, 113(1144), 417–427, 2009.

Yan, F., Rose, J.L., and Royer, R.L., Jr., "Ultrasonic guided wave imaging techniques in structural health monitoring," *Journal of Intelligent Material Systems and Structures*, 21(3), 377–384, 2010b.

Zhu, Y., Palacios, J.L., Rose, J.L., and Smith, E.C., "De-icing of multilayer composite plates using ultrasonic guided waves," *Collection of Technical Papers - 49th AIAA/ASME/ASCE/AHS/ASC Structures, Structural Dynamics and Materials Conference*, 2008.

Zhu, W., and Rose, J.L., "Lamb wave generation and reception with time-delay periodic linear arrays: ABEM simulation and experimental study," *IEEE Transactions on Ultrasonics, Ferroelectrics and Frequency Control*, 46(3), 654–664, May 1999.

This page intentionally left blank

CHAPTER 14
Shearography Nondestructive Testing

14.1 History and Development

Since it was first introduced in 1986, the shearography nondestructive testing (NDT) technology has been providing large productivity increases in manufacturing and overhaul of metal and composite structures in aerospace, marine, and rail industries. A high-throughput optical inspection technique, shearography uses a common path, laser-based imaging interferometer to detect, measure, and locate anomalies by imaging submicroscopic changes to a test part surface when an appropriate stress is applied. The shearography camera inspects a full field at a time, rather than scanning a single-point sensor or an array of sensors as with phased array ultrasonic testing. It is non-contact (except for portable vacuum shearography), non-contaminating, and near real time. While laser light is a non-penetrating radiation, shearography systems are capable of inspecting composite structures for both surface and subsurface discontinuities such as impact damage, disbonds, delaminations, near surface porosity, wrinkled fibers, fiber bridging, foreign objects (FOs), heat damage, and cracks.

Shearography is an evolutionary development from holographic interferometry first developed by Karl Stetson in 1964 [1]. Initial shearography techniques invented by Y. Y. Hung in 1982 [2] were further enhanced with the development of electronic phase detection by S. Nakadate [3] in 1988. Commercialization of electronic shearography NDT began in 1986 with the first integration of the technology into a major aircraft manufacturing program by J. Newman [4].

Shearography NDT methods are mature and can be highly effective solutions for a wide range of composite NDT applications. Common successful applications include metal and composite honeycomb, foam-core panels, bonded elastomers or cork, solid composite laminates, fiber-wound structures such as composite over-wrap pressure vessels (COPVs), solid-propellant rocket motors, and liquid-propellant rocket engines. Test objects ranging from less than 1 in. in width to very large composite structures have been successfully inspected. Figure 14-1 shows the composite (fiberglass/foam-core) wind fairings added to the entire span of the Bronx Whitestone Bridge in 2003 [5]. These foam-core panels were inspected during manufacturing and in situ using portable vacuum shearography.

(a)

(b)

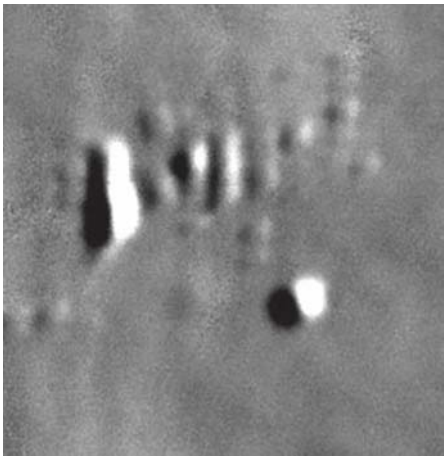

(c)

Figure 14-1 In 2003, triangular-shaped fiberglass and foam-core wind fairings, similar to those shown in (*b*), were added to stiffen and improve the wind aerodynamics of the Bronx Whitestone Bridge. Weighting a total of 890,000 lb, these 390 FRP structures were the largest composite project in the world at that time. All panels were inspected for disbonds and delamination using portable vacuum shearography equipment. In (*a*), is a shearography result with multiple disbonds in the 12 × 12-in. FOV of the instrument.

Benefits of shearography include very high throughput. Large production systems easily achieve throughput rates of 300 to 700 ft^2/h (27 to 65 m^2/h) compared to typically only 10 ft^2/h (0.93 m^2/h) with ultrasonic C-scan. In many cases shearography NDT methods are noncontact, ideal for space applications. Production shearography cameras do not require precision contour following and can inspect a structure at an offset angle, eliminating the costs associated with precision gantries such as required for UT C-scan systems. In addition, because many shearography NDT methods are noncontact composite structures manufactured with multiple cure cycles can be inspected in-process allowing repairs or scrapping of the part with the lowest possible cost implications. The technology lends itself to a wide range of configurations to meet the discontinuity detection and logistical requirements.

As with all NDT methods in use, a critical element is operator training and certification to recognized standards. Shearography NDT operators are trained and tested to the requirements of the American Society of Nondestructive Testing (ASNT) SNT-TC1A and CP105, National Aerospace Standard NAS410, or European Standard EN 4179. Shearography operator training courses meeting these requirements are commercially available.

Shearography NDT is based on the phenomenon that when an object is subjected to a change in load, subsurface anomalies can produce slight local deformations on the surface (Figs. 14.2 and 14.3). These out-of-plane deformations may be as small as several nanometers (nm) but are easily imaged by a shearography camera. For example, when a carbon-fiber laminate panel is exposed to infrared radiation the change in temperature causes primarily in-plane thermal expansion. In a panel with a delamination, the laminate on the heated side of the panel expands more and sooner than the laminate on the cooler side of the panel away from the heat. This differential expansion coupled with the discontinuity boundary causes the material over the discontinuity to deform out of plane. A shearography camera is used to capture a reference image before the application of the thermal stress to the panel and then a second image as the heat is flowing through the laminate plies. These images are processed to produce an image of the delamination that can be measured and located on the part. In addition to thermal stress, the range of shearography techniques include pressure changes, vacuum stress, vibration stress using both sonic and ultrasonic signals, mechanical load changes, varying magnetic field loads, and microwave stress changes. Figure 14-2 shows the setup for shearography inspection of a COPV and in Fig. 14-3 an aircraft radome.

14.2 Theory and Principles of Operation

A shearography NDT system consists of a laser light source, a shearing image interferometer, an image processing computer, display monitor, and a means to provide a controlled and repeatable stress to the test object [2, 4, 6–13]. Shearography cameras are relatively resistant to environmental vibration and motion. Large production systems with 30-ft (9.14-m) gantry scanners have been built as well as portable systems for on-vehicle inspection. Shearography is relatively insensitive to test part bending or deformation due to the applied stress but still highly sensitive to local deformation caused by a discontinuity.

Shearography cameras are sensitive to changes in the distance from the object surface to the camera and in practice these *z*-axis surface deformations may be as small as 2 nm, depending on environmental noise. Test parts can be inspected with a few images

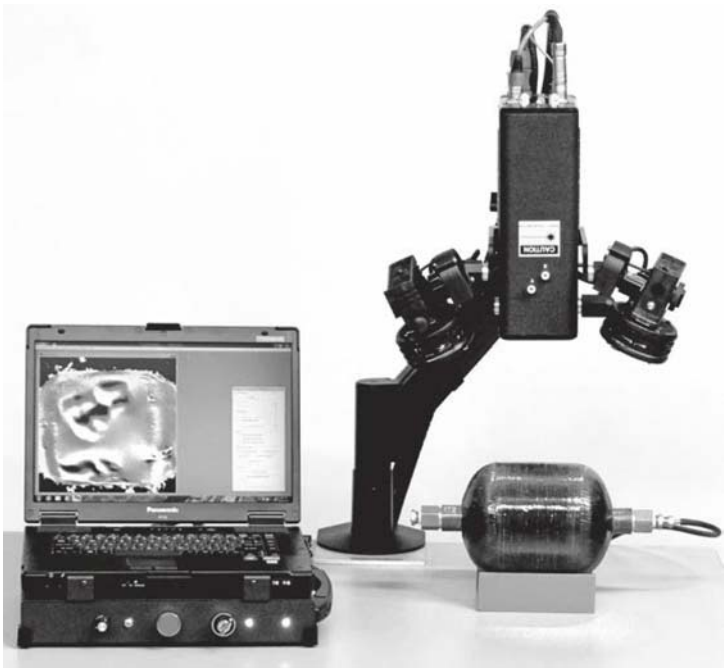

(a)

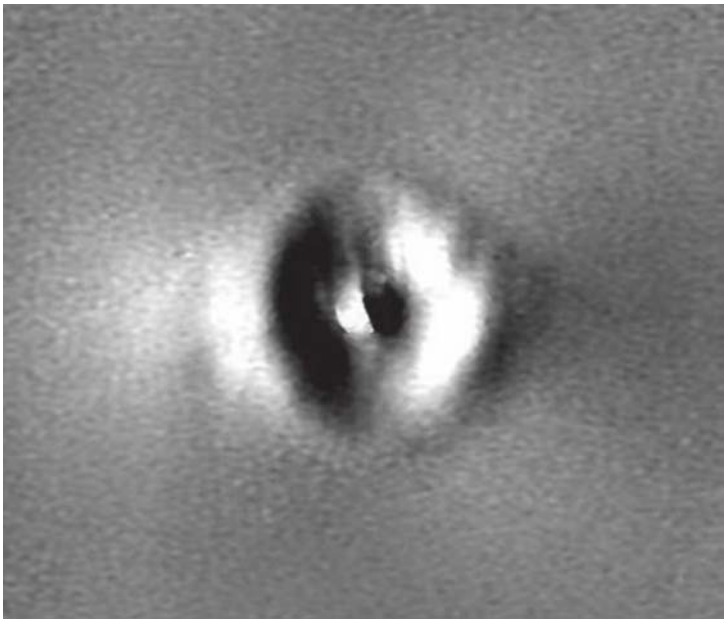

(b)

Figure 14-2 A shearography test setup (*a*) for a small carbon-fiber COPV is shown. The tank is rated for 7250 psi (50 MPa) using small pressure changes of only 5 psi (0.03 MPa) to image non-visible impact damage as shown in (*b*). The small impact strike is in the center of the circular delamination which measures 3.2 in. (81.3 cm) in diameter. No visual evidence of damage was seen on this COPV.

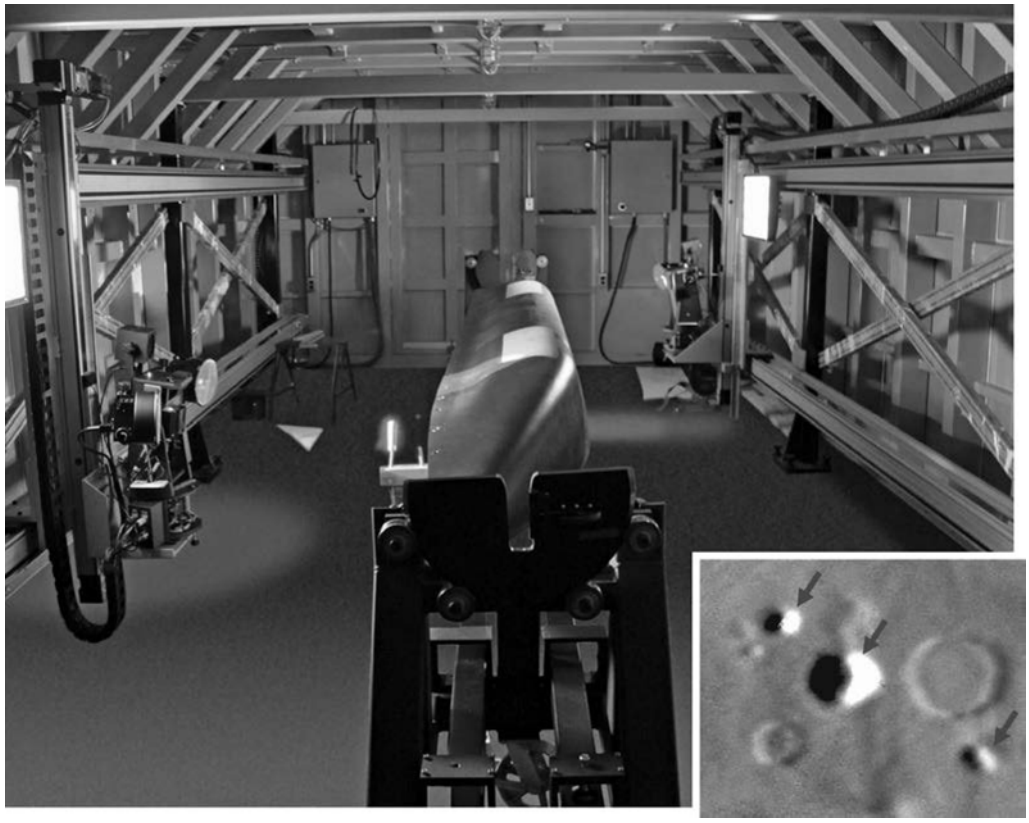

Figure 14-3 At left, an aircraft radome is shown undergoing shearography testing in a test chamber using a partial vacuum change from ambient to –2 psi (–0.014 MPa). Unlike older impedance bond testing methods routinely used for radomes, shearography can distinguish defects like impact damage and disbonds from repairs thus eliminating needless rework. The result at bottom right shows three indications of impact damage which appear as crater-like circles (arrows) with darker gray levels on the left and white on the right. Two repairs with the reverse-edge gray levels (referred to as phase) are also seen. The flat appearance of the repairs is due to the added stiffness of the epoxy repair reducing the deformation of the radome face sheet when the test was performed.

using a large field of view (FOV) camera lens setting, or for greater resolution many images with a smaller FOV can be recorded and automatically stitched together. The optimal FOV for a shearography test depends on the maximum allowable discontinuity size, camera resolution, laser illumination power, the ability to uniformly apply a stress change to the test part over the FOV, and background noise. Figure 14-4 shows a schematic diagram of a thermal shearography system that includes the laser and optical elements for test part illumination, an imaging shearing optical system consisting of a beam splitter with a two-axis tilting mirror, a second mirror with a piezoelectric phase stepper to translate the mirror in half wavelength steps at video frame rates and finally the CCD camera. The laser light is expanded through lenses to illuminate the test area on the panel. Light from point P1 is reflected from the panel surface, where it is well bonded to the core. Light from point P2 is reflected from the surface above a

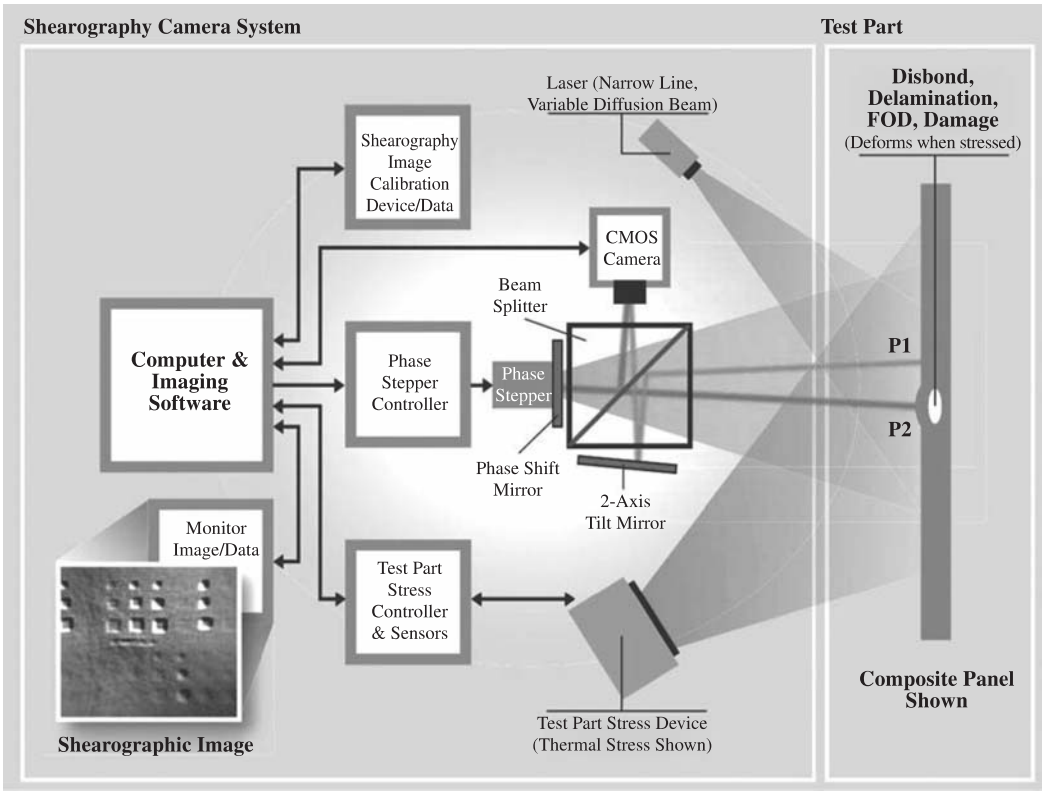

(a)

Figure 14-4 (*a*) Schematic diagram of a digital shearography camera and thermal stress system. The separation distance and direction, or shear vector, between the paired points P1 and P2 on the test part surface determine the camera sensitivity to surface deformation, and the light intensity detected by each pixel in the CMOS camera is determined by the complex addition of the light from these two points on the target. (*b*) An example of a shearography camera with all of the elements in (*a*). Instruments with this configuration are used on benchtop mounts, tripods, gantrys, or robots, depending on the application. All the shearography electro-optical components and the single-frequency laser are built into the sealed housing. Thermal stress is achieved with the 2 to 1-kW quartz thermal lamps.

skin-to-core disbond. If the panel is stressed with a small temperature change or a partial vacuum, the panel face sheet above the disbond will deform out-of-plane toward the shearography camera. This shorter distance traveled by light from point P2 causes a phase shift with respect to light from point P1. Light from both P1 and P2 are combined by the shearing interferometer at a single pixel in the CMOS array as depicted in Fig. 14-5.

The phase stepper applies a $\pi/2$ phase step to a mirror in the interferometer at video frame rates (typically 30 to 120 frames per second) to generate a phase map and subsequent quantitative determination of the deformation derivatives between two strain states [3, 4, 11, 14]. As the applied load on the test object is changed, two sets of phase-stepped images, (I1-I4) and (I5-I6), are captured and the phase calculation is

(b)

FIGURE 14-4 (*Continued*)

performed for each pixel in the image, using the following equation for the four-phase-step method:

$$\Delta(x, y) = \tan^{-1}[I_8(x, y) - I_6(x, y)/I_5(x, y) - I_7(x, y)] - \tan^{-1}[I_4(x, y) - I_2(x, y)/[I_1(x, y) - I_3(x, y)]$$

where I_1 through I_8 are eight sequentially phase-stepped captured images, described by:

$$I_1(x, y) = I'(x, y) + I''(x, y)\cos[\Phi(x, y)]$$
$$I_2(x, y) = I'(x, y) + I''(x, y)\cos[\Phi(x, y) + \pi/2]$$
$$I_3(x, y) = I'(x, y) + I''(x, y)\cos[\Phi(x, y) + \pi]$$
$$I_4(x, y) = I'(x, y) + I''(x, y)\cos[\Phi(x, y) + 3\pi/2]$$
$$I_5(x, y) = I'(x, y) + I''(x, y)\cos[\Phi(x, y) + \Delta(x, y)]$$
$$I_6(x, y) = I'(x, y) + I''(x, y)\cos[\Phi(x, y) + \Delta(x, y) + \pi/2]$$
$$I_7(x, y) = I'(x, y) + I''(x, y)\cos[\Phi(x, y) + \Delta(x, y) + \pi]$$
$$I_8(x, y) = I'(x, y) + I''(x, y)\cos[\Phi(x, y) + \Delta(x, y) + 3\pi/2]$$

where:
I' = bias intensity
I'' = modulation intensity
Φ = random phase variable due to reflection of the laser light from test object
Δ = quantity directly proportional to the differential displacement due to the test part deformation from the applied load change

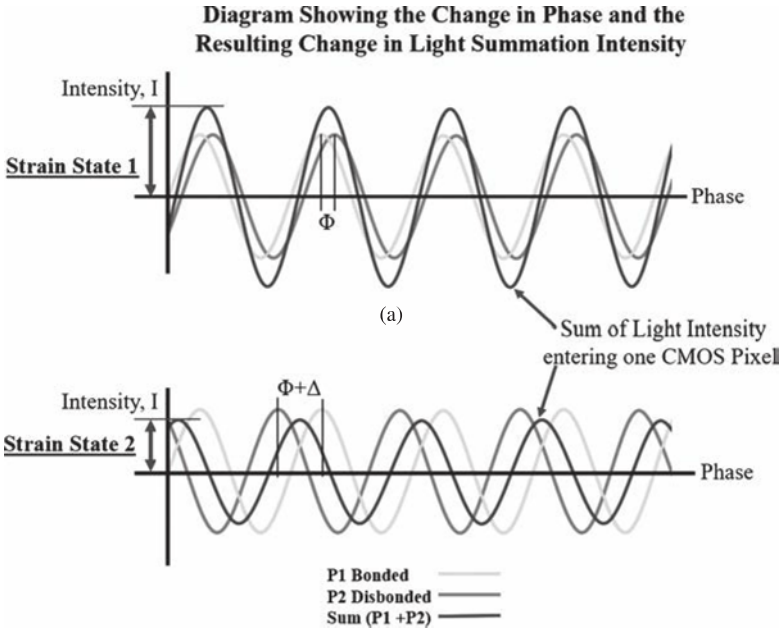

Figure 14-5 (*a*) shows how the coherent, single-frequency light, from adjacent points on the part, is combined in each pixel in the shearography camera. The random phase difference Φ results from the random surface roughness on a diffusely reflecting test part surface. Stressing the part causes a relative phase shift Δ between light from well-bonded homogeneous material and light from the surface above discontinuity or non-homogeneous material. In two dimensions, this is expressed as $\Delta(x, y)$. (*b*) shows a plot of the light intensity (I) at each pixel in the camera detector and how I changes due to a phase shift when the strain state changes and the light paths are reflected from areas on the test part with different compliance or stiffness caused by the presence of an anomaly.

The result of the phase calculation yields a wrapped phase map image that shows the surface deformation derivative resulting from the load change. A flat metal plate deformed with a point load and imaged with a shearography camera reveals the surface deformation, as shown in Fig. 14-6.

Shearography images also include quantitative calibration data for the image scale and the image offset or shear vector. These data are used to obtain accurate discontinuity dimensions D by subtracting the shear vector component from the measured dimension D_m. For example, if the shear vector, S_v, is in the horizontal (or 0°) direction with a shear of 0.5 in. (5 mm), the total horizontal uncorrected measured dimension D_m of any indication will be greater than S_v. The measured dimension D in the vertical direction, perpendicular to the direction of S_v, will equal the measured dimension D_m. For any measured dimension at any angle α to the shear vector D and be calculated a $D = (D_m - \cos \alpha)$. The calibration data is also used during calculation of the integrated shearogram to extract the z-axis deformation of the part surface anywhere in the field of view.

Finally, the calibration data can be combined with the stress data to measure discontinuity deformation rates as a function of the applied stress change. This technique

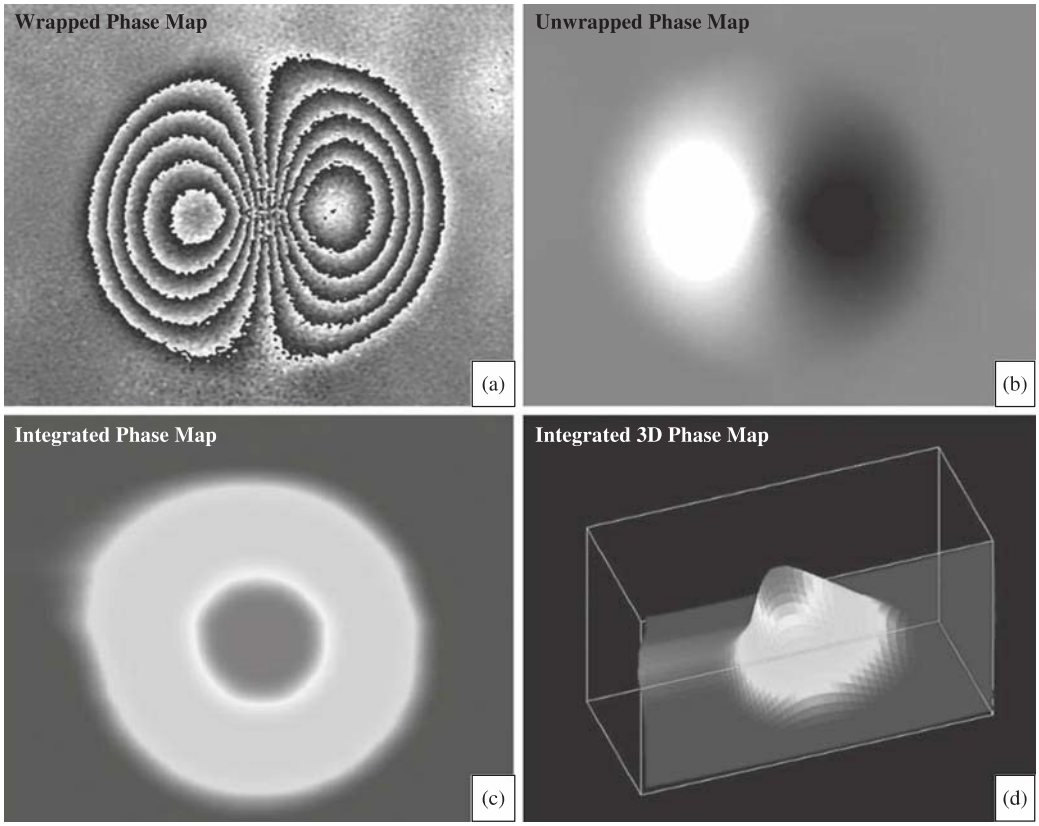

Figure 14-6 Shearography images. (*a*) Phase map of the deformation derivative. (*b*) Unwrapped phase map. (*c*) Integrated unwrapped phase map. (*d*) 3D representation of the plate deformation. Numerical values of deformation over the entire field of view can be exported for analysis and comparison to finite element models.

has been used for example to establish a model for grading impact damage to honeycomb distinguishing between crushed core and disbonds. Applications using thermal stress can us a noncontact remote temperature sensor to measure the test part temperature change and the resulting discontinuity thermal deformation.

Real-time phase maps and unwrapping algorithms can be performed at video frame rates and quantitative measurement of the *z*-axis deformation can be computed. For NDT, shearography images can provide details of surface damage and subsurface discontinuities and structural features. Figure 14-7 shows a vacuum stress shearogram of a 14×24-in. (36×61 cm) section of a metal spacecraft honeycomb radiator panel with face sheets 0.025 in. (0.63 mm) thick. The cells, disbonds, and voids are detected. Two shearograms were made in 14 s in a shearography test chamber with a pressure reduction of only 0.5 psi (3.4 kPa) below ambient air pressure. The metal face sheet over the honeycomb cells and discontinuities develop submicroscopic dimples as the air pressure in the test chamber is reduced. One indication in particular (large white arrow, left side) is a disbond on top of a coolant tube. This discontinuity was not detectable

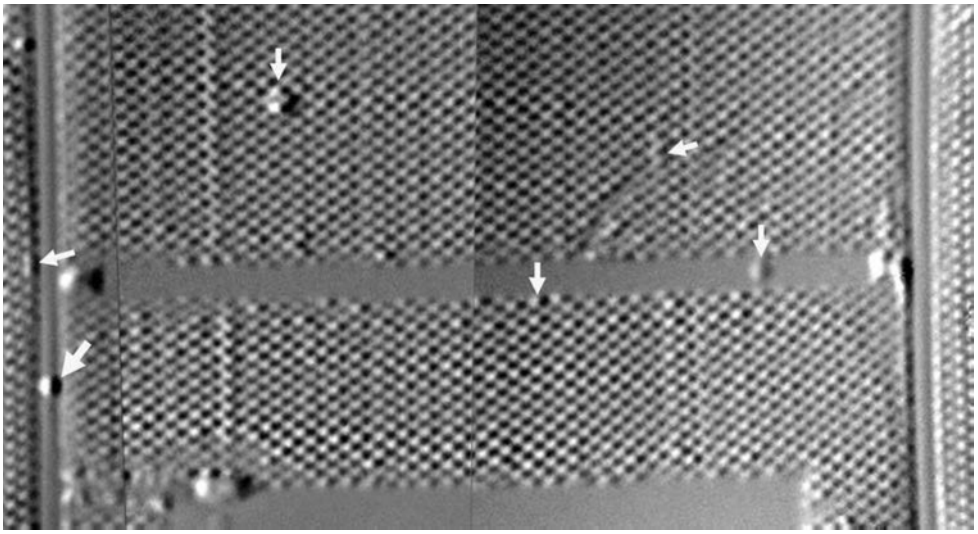

Figure 14-7 A shearogram of a 24 × 14 in. (61 × 35.6 cm) section of a honeycomb spacecraft radiator panel showing the honeycomb cells, disbonds, and embedded coolant tubes. A disbond is seen at near the left edge on top of an embedded coolant tube (large arrow). This disbond was not detected with ultrasonic C-scan.

with through-transmission ultrasonic NDT, due to the presence of the tube beneath it blocking the ultrasonic signal. In addition, shearography NDT was specified for this spacecraft program, and many like it, not only because of a high throughput that was 10 times greater than UT C-scan, but shearography does not use any liquid couplant required to induce uniform ultrasonic signals into the panel. With shearography so the test parts remain dry and uncontaminated. In addition, shearography NDT in many cases, is able to detect anomalies in areas with complex geometry or conditions that prevent the use of traditional NDT techniques.

14.3 Shearography Equipment and Accessories

Shearography cameras usually are built with integrated stressing equipment such as thermal or vacuum stress. The probability of detection (PoD) for each type of camera and stressing mechanism must be determined for the structures and discontinuity types expected for a given application. The development and production of accurate representative NDT standards is a part of every shearography NDT process. Shearography systems are divided into two main types: First, shearography cameras and accessory subsystems for scanning the test part and equipment for stressing the test part. The scanning equipment ranges from manually moved tripod, integrated pan/tilt mechanisms, robots to robotic x/y gantries. Stressing equipment can include thermal lamps, sound compression drivers, vacuum chambers as seen in Fig. 14-3, and ultrasonic exciters. Second, shearography cameras are available with integrated stressing equipment, such as the portable vacuum/thermal stress system shown in Fig. 14-8. Systems such as these are used for composite sandwich structures on composite launch vehicle fuel tanks, aircraft, naval ships, yachts, and even rail cars (Fig. 14-9).

(a)

(b)

Figure 14-8 (*a*) Several classes of composite naval vessels are built using a portable vacuum/thermal stress shearography NDT system throughout for the inspection of the FRP face sheet to foam-core bonds, as seen in (*b*). The disbond (*c*) measured 9×3.2 in. in size. The typical throughput for a portable vacuum shearography system is about 150 ft^2/h.

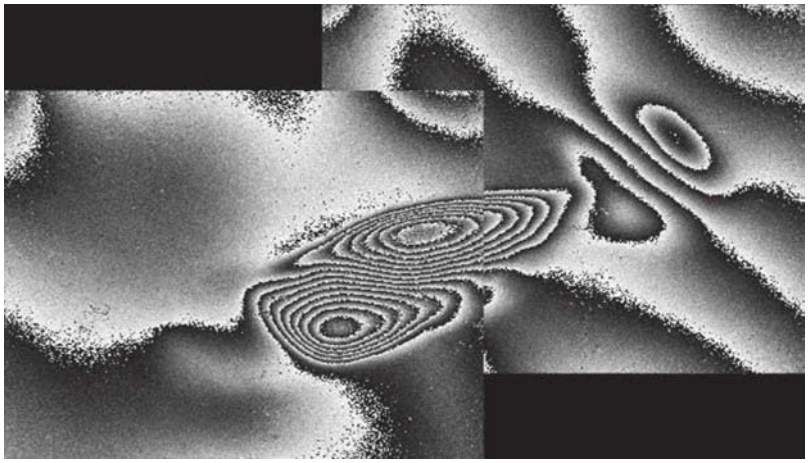

(c)

Figure 14-8 (*Continued*)

(a)

Figure 14-9 (*a*) A small thermal shearography camera is shown being used to inspect a mass transit rail car interior for disbonds. The fiberglass/Nomex® cored sandwich structure is easily inspected for face sheet to core disbonds as shown in (*b*). The camera includes tools for measuring size and area of indications.

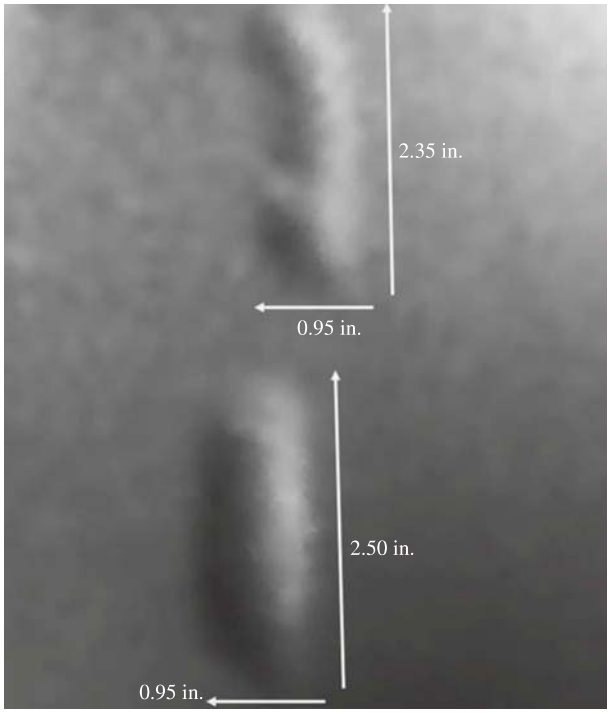

(b)

Figure 14-9 (*Continued*)

14.4 Applications and Techniques

Shearography NDT uses a wide range of stressing and load timing techniques to detect discontinuities in materials and structures. These stress techniques include heating or cooling the test part, vacuum, pressure, mechanical bending, sound, ultrasonic signals, and microwaves [15]. The applied load changes are typically very low, compared to normal operating conditions of the test piece. For example, composite over-wrapped pressure vessels (COPVs) are typically pressurized to 1/1000 of the nominal working pressure or less to detect cracks, impact damage, and fiber bridging [16]. Refer to Table 14-1 for stressing methods and applications.

14.4.1 Pressure Shearography

Pressure shearography has provided good results on a wide variety of pressure-containing structures, including COPVs (see Fig. 14-10), composite drive shafts, tubular struts, and solid-propellant rocket motors (see Fig. 14-11). Pressure shearography uses a gas to pressurize the test object to between 0.01 and 5 percent working pressure [16]. Anomalies that affect the hoop strain or create strain concentrations generate indications of the surface. Test articles are usually placed on a support frame, allowing part rotation. Pressure shearography proceeds by capturing reference images and a bias pressure, increasing the pressure to a test level and capturing

Method	Units	Range	Applications
Thermal	Degrees °F, °C Surface temperature change	1–30°F (–17 to –1°C)	*Carbon-fiber laminate panels:* Impact damage, delamination, wrinkled fibers, porosity, embedded foreign material, repairs, foreign objects (FO) *Sandwich panels—honeycomb, foam core:* Impact damage, skin-to-core disbond, damaged core, foam-foam disbonds, metal core-skin disbonds, repairs, kissing disbonds, skin delamination, water *Resin transfer molded composites:* Resin lean areas, porosity, damage *Engine stators, vanes, composite fan blades:* Erosion strip bond, voids, resin lean areas, damage, FO *Steel, aluminum, ceramics, composites:* Surface breaking or near surface breaking cracks *COPV with metal liners:* Disbonds at the liner/composite bond, fiber bridging
Partial vacuum	psi, kg/cm^2 pressure reduction change	–0.02 to –7.0 psid (–0.00141 to –0.49215 kg/cm^2)	*Elastomers:* Coatings, rubber and plastic components and structures, tires, solid rocket motor liners, rubber to substrate bond, cork to substrate bond: voids, disbonds *Sandwich panels—honeycomb, foam cores:* Such as radomes, aircraft control surfaces, flaps, air brakes, helicopter blades, turbine engine ducts, laminated wood structures: impact damage, voids, disbonds *COPV:* Fiber bridging, liner to composite wrap disbonds
Pressure	psi, kg/cm^2 pressure change	0.01 to 5,000+ psid (0.0007 to –351.5348 kg/cm^2)	*COPV and composite rocket motors:* Impact damage, composite cracks, broken fibers, fiber bridging, liner wrinkles, porosity *Pressure vessels and heat exchangers/radiators:* Metal pressure tanks, actively cooled liquid-propellant rocket engine thrust chambers, nozzles, exit cones, thrust ramps, piping, vented core honeycomb
Vibration	Air coupled 0.5–20 kHz; mechanically coupled 4.0–500 kHz	90–125 dB	*Foam rocket thermal protection systems:* Damage, disbonds, delamination, cracks *Light-weight honeycomb:* Spacecraft solar panels and structures *Metal honeycomb:* Face sheet to core disbonds *Brazed metallic bonded and plasma sprayed engine compressor seals:* Disbonds

Table 14-1 Shearography NDT Stressing Methods and Applications [17]

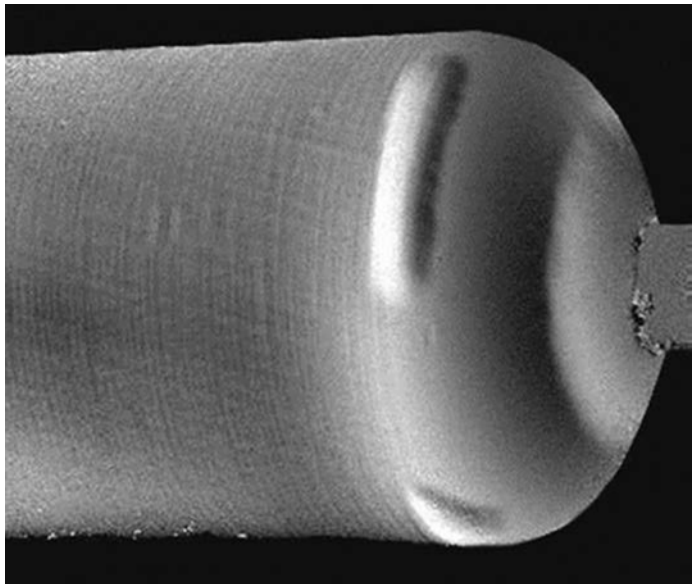

Figure 14-10 Shearography image of the end of a 6.3-in.-diameter (160-mm) COPV showing fiber bridging areas on the barrel transition area. With a maximum allowable working pressure of 8,560 psi (59 MPa), the shearography test pressure with the result shown above was made with only a 5.0-psi (0.034-MPa) pressure change.

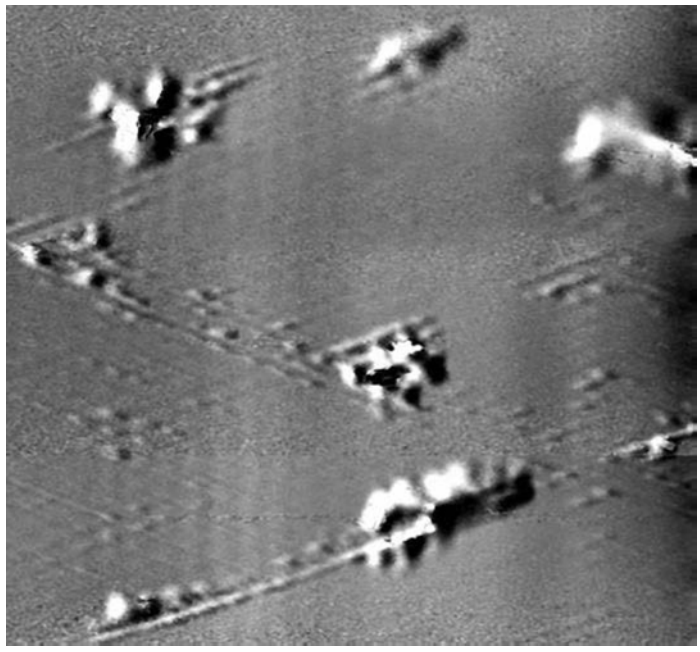

Figure 14-11 Illustrates a pressure shearography image of a composite rocket motor tube showing porosity, voids, and poor consolidation. The FOV on the tube is 10 in. (254 mm) axially and covers 120° circumferentially combining three 40° images.

the stressed data. The vessel can be vented to prepare for the next test. Shearography data can be taken both during pressurization and venting, if the phase of the data taken during venting is inverted to match that taken during pressurization.

Flight hardware, depending on contamination requirements, may require specific cleanliness precautions such as using ultrapure GN2 with oil-free valves, fittings, and piping. Each area on the tank is tested sequentially with the COPV rotated 30° to 45° after each section is completed. The end domes are also inspected at a 45° angle. The FOV on the tank is only as large as can be fully illuminated with the shear camera laser. Controlling the test pressure requires valves to pressurize and vent the test object. Commercial pressure shearography systems are available that allow rapid, preset pressurization and venting of the COPV and can set a minimum bias pressure to increase testing throughput and preload of the COPV.

Pressure shearography has also been used to image porosity and poor consolidation of composite tubes and pressure vessels [15]. The tensile loads on the fibers in the hoop and longitudinal directions on tank create strain concentrations at the site of porosity, voids, and poor consolidation.

Pressurizing the COPV increases the hoop strain on the aluminum liner and increases the compressive force on the Teflon insert between the liner and the composite over-wrap material. Pressure changes produce only a small strain change at the site of the insert, but a large strain change at the fiber bridging discontinuity as seen in Figs. 14-10 and 14-12a. Due to the slight insulating properties of the insert and delamination and fiber bridging discontinuities, the insert affects the thermal strain response of the COPV in several ways. First, the Teflon has a different thermal diffusivity and thermal expansion coefficient from the virgin structure. The result is a local high-strain state and a highly detectable shearography response as seen in Fig. 14-12b.

Representative NDT standards are critical to selecting the best technique, which may also involve multiple tests with different methods to capture all possible discontinuity types. Again, in the example of the COPV in Fig. 14-12, thermal stress is good for detecting liner to composite disbonds and foreign material (FO) as well as fiber bridging. For a COPV, pressure stress shearography is best for impact damage, cracks, and wrinkled or buckled liners, as shown in Fig. 14-13.

14.4.2 Partial Vacuum Shearography

Partial vacuum shearography can be accomplished in several ways. For portable testing, a vacuum window may be used consisting of a Lexan plate with edge seals and a variable, controllable vacuum blower. Often a small shear camera is built into a portable inspection head as shown in Fig. 14-14. Shearography inspection rates of 150 ft^2/h (13.9 m^2/h) are easily achieved. Honeycomb and foam-core aircraft control surfaces, rudder as shown in Fig. 14-14, stabilizers, flaps as shown in Figs. 14-15 and 14-16, and wing panels can be test in situ. Naval composites, yachts, railcars, and wind turbine blades are other composite structures tested extensively with portable vacuum shearography.

Partial vacuum stressing reduces the outside ambient air pressure on the test part. Internal disbonds or delaminations in the material contain small quantities of air and when the air pressure on the part surface is reduced, the test part surface at the location of the anomaly deforms. Critical for partial vacuum shearography is ensuring there are no leak paths allowing the rapid venting the entrapped gas in the discontinuity within the time frame of the data acquisition. Vented discontinuities will come to equilibrium

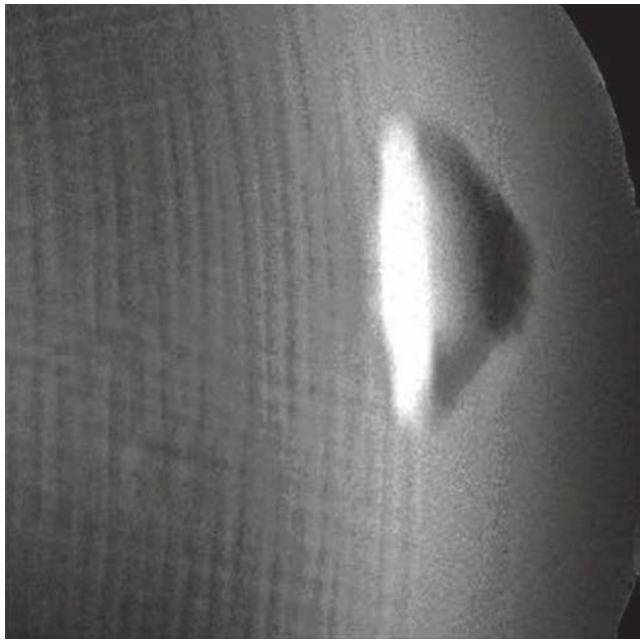

(a)

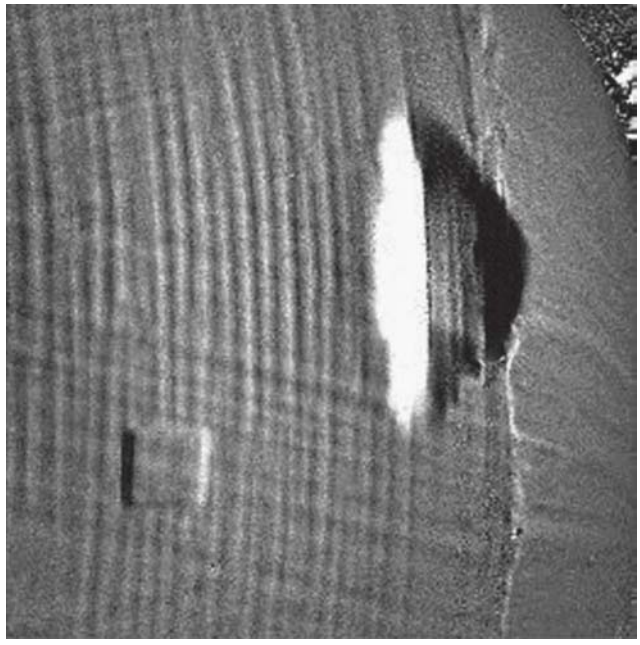

(b)

Figure 14-12 A 6.3-in.-diameter (16-cm) COPV tested with shearography methods. (*a*) Pressure shearography shows the fiber bridging discontinuity only; (*b*) thermal shearography reveals both fiber bridging and a square Teflon® insert between the 0.35-in.-thick (8.9-mm) composite and the aluminum tank liner.

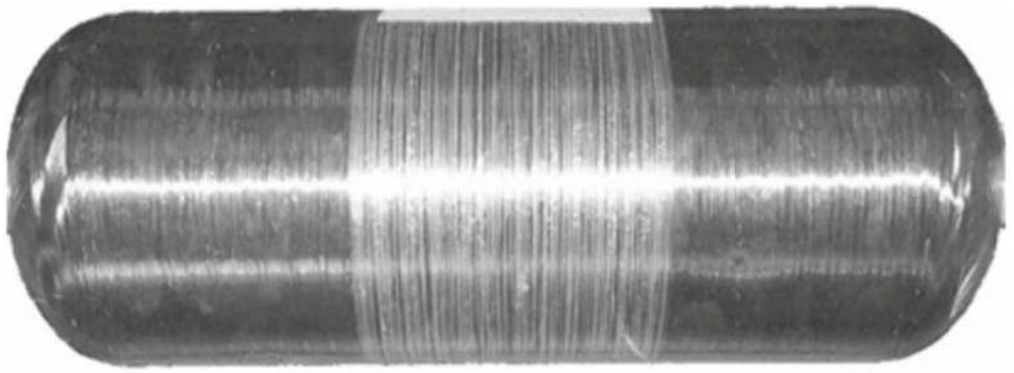

(a)

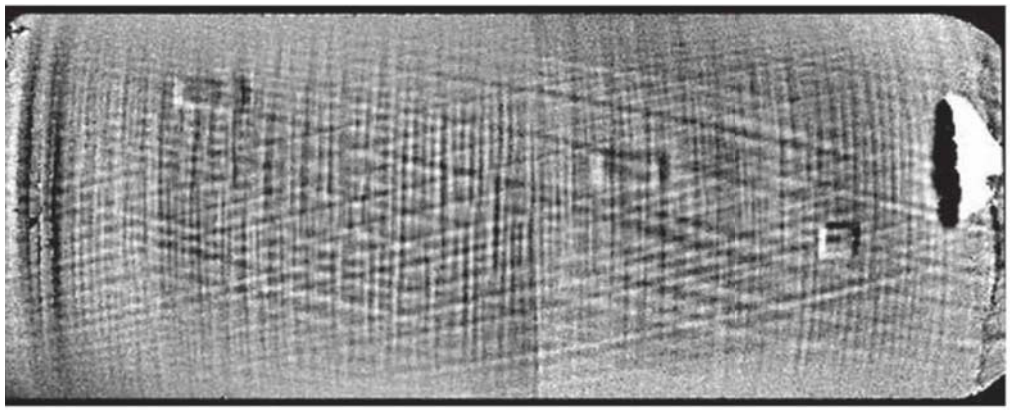

(b)

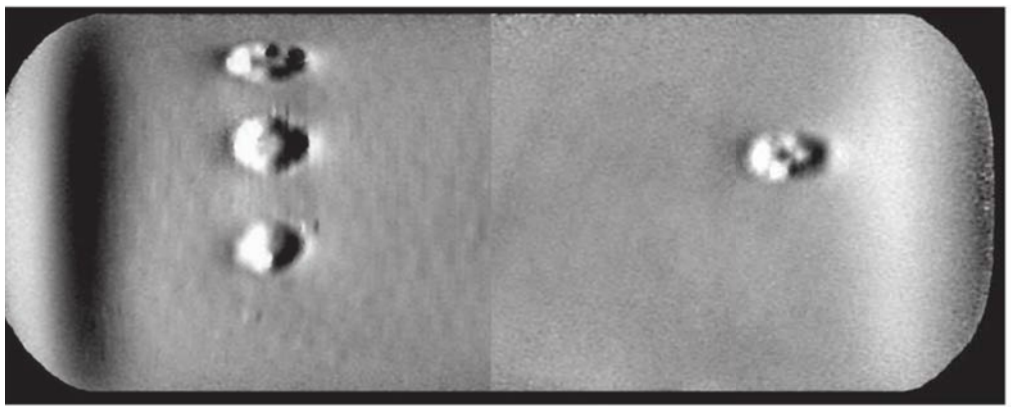

(c)

Figure 14-13 (*a*) A 6.3-in.-diameter carbon-fiber COPV is shown. This tank has a maximum operating pressure of 8,560 psi (59 MPa). (*b*) Shearography tests with thermal stress show three Teflon inserts placed on the aluminum liner then over-wrapped with the carbon-fiber wrap. (*c*) The shearography result with a pressure change of 2.5 psi (0.017 MPa). Non-visible impact damage is easily detected, producing very strong crater-like indications. These indications are areas of delamination and fracturing of the composite matrix.

(a)

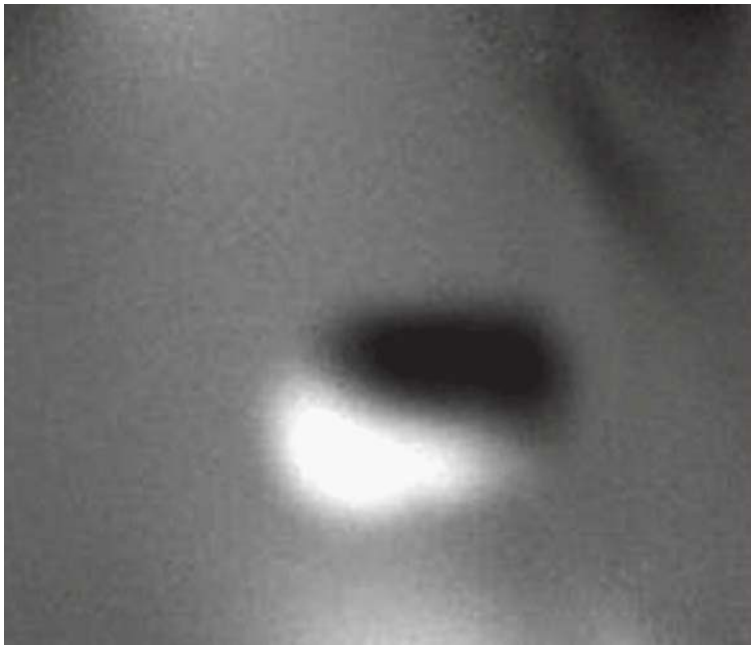

(b)

Figure 14-14 (*a*) An aircraft rudder inspection with a portable vacuum shearography system. (*b*) A shearography image is seen of disbond measuring 3.5 × 2.0 in. (8.9 × 5.1 cm).

Figure 14-15 A shearography camera is shown mounted on a large *x/y* scan gantry in a large vacuum test chamber. This system is used for shearography NDT of large honeycomb aircraft components. The air pressure inside this chamber can be reduced from ambient to –5 psi (–0.035 kg/cm^2) in less than 15 s, causing subsurface anomalies to produce surface deformations detected with a shearography camera. The shearography test results are automatically stitched, allowing both the indication measurement and location. Test part scan speeds of 400 ft^2/h are easily achieved by these systems. The author is standing at the back wall for scale.

with pressure changes allowing the surface deformation to relax and the shearography indications to disappear.

Several important characteristics of partial vacuum shearography NDT can be gleamed from the equation for calculation the displacement W of a circular disbond with a diameter D and depth H in an isotropic material with an elastic modulus E. A uniform partial vacuum is applied yielding a pressure change of P.

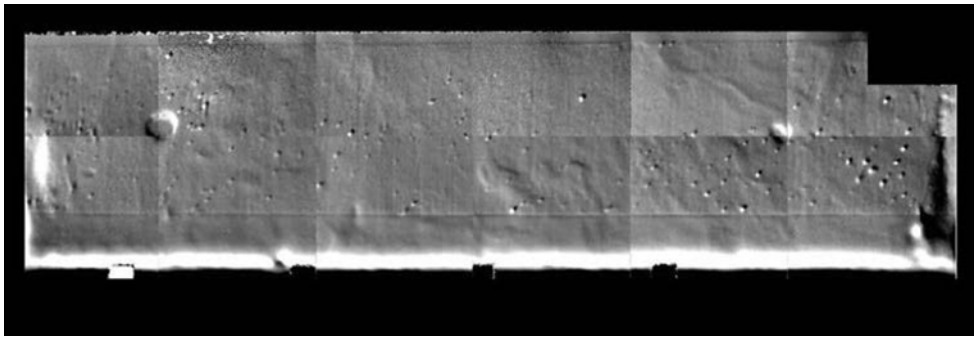

Figure 14-16 A 14-ft-long (304-cm) aircraft flap tested in a partial vacuum shearography chamber with automatic image stitching. Over 90 disbonds are detected requiring repair. This flap was inspected in less than 15 min including placement in the test chamber. Shearography NDT technology is providing large productivity increases in aerospace manufacturing and overhaul.

The *z*-axis displacement for the partial vacuum stressed disbond may be calculated as [16–20]:

$$W = k\left(\frac{PD^4}{EH^3}\right)$$

Notice first that the *z*-axis displacement increases with the 4th power of the disbond diameter D. For discontinuities at the same depth, doubling the diameter increases the displacement 16 times. As a result, small changes in the discontinuity diameter can have a large effect on the resulting displacement, which roughly corresponds to the signal strength and the signal-to-noise ratio. To double the displacement for given size disbond D_1 at the same depth, a disbond D_2 would have to be only 18.9 percent larger:

$$D_2 = D_1\sqrt[4]{2} = 1.189\,D_1$$

The following examples of vacuum shearograms illustrate some of the remarkable effects of this method for both metal and composite honeycomb. In Fig. 14-17, a metal honeycomb leading-edge flap that had been removed from an operational jet hours earlier has a large face sheet to core disbond the full width of the 18-in. FOV. In addition, a cracked core is seen, which is a very dangerous condition and a sign of imminent failure. In Fig. 14-18, a honeycomb test panel with carbon laminate face sheets and Nomex core is shown to have numerous programmed disbonds even on the ramp areas of the panel. Figure 14-19 shows a panel with imbedded foreign object debris (FOD). In this panel, shearogram detected all the FOD detected with through transmission C-scan.

14.4.3 Thermal Shearography

Thermal shearography has been applied successfully to a wide range of structures and material types, including solid laminates, metal or composite sandwich panels (limited to near side inspections only), COPV, and even for surface breaking fine crack detection in metal aircraft and nuclear reactor components.

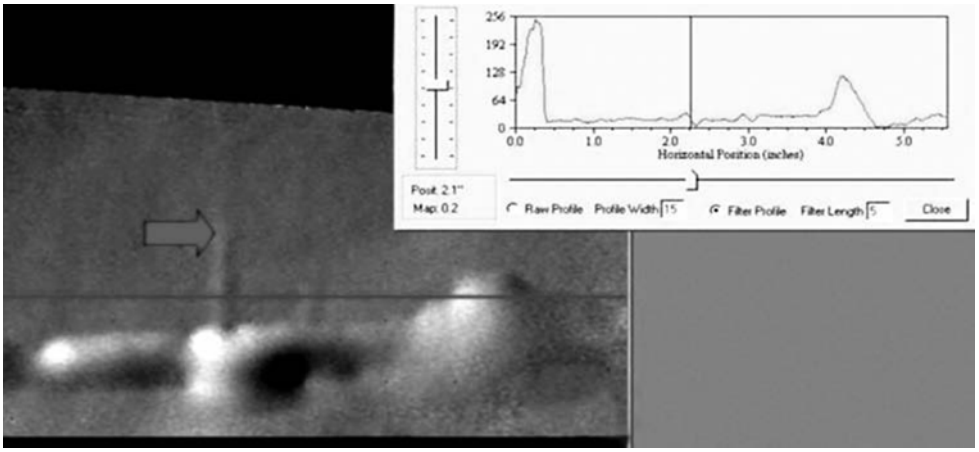

Figure 14-17 This shearogram shows a vacuum inspection of an aircraft leading-edge flap revealing a large honeycomb disbond. Repeated stress loading in operation is causing failure of the core adhesive bond (red arrow), a situation that could have led to structural failure. The full chord width of the flap is shown. The insert shows a line scan with the waveform of the signal at the failing core splice joint (black line) and at the disbond.

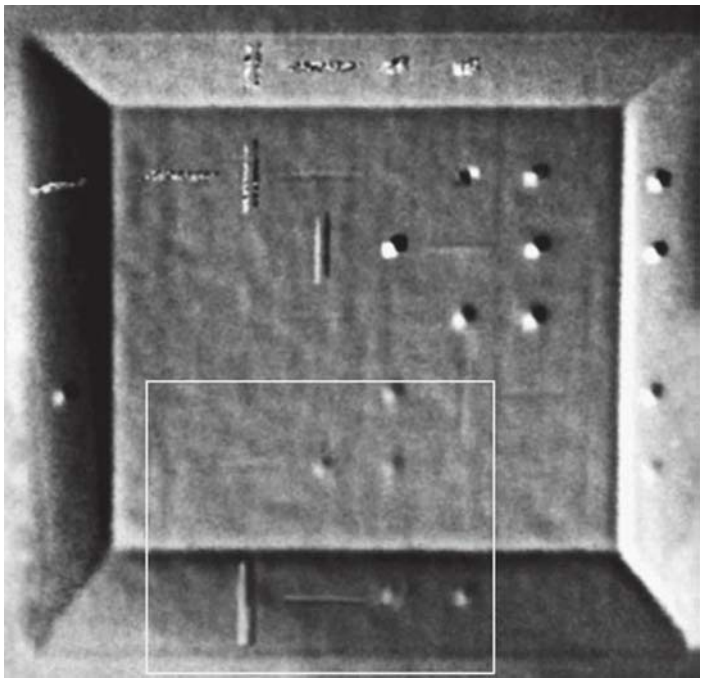

(a)

Figure 14-18 (*a*) A vacuum shearography image of a carbon-fiber sandwich panel with Nomex core measuring 14 × 14 in. (36 × 36 cm) inspected using a −1.0-psi (13.7-kPa) pressure reduction change. Indications are Teflon inserts at plies 4 and 6 as well as between the eighth ply and the adhesive on top of the core. (*b*) A close-up of the bottom edge ramp area.

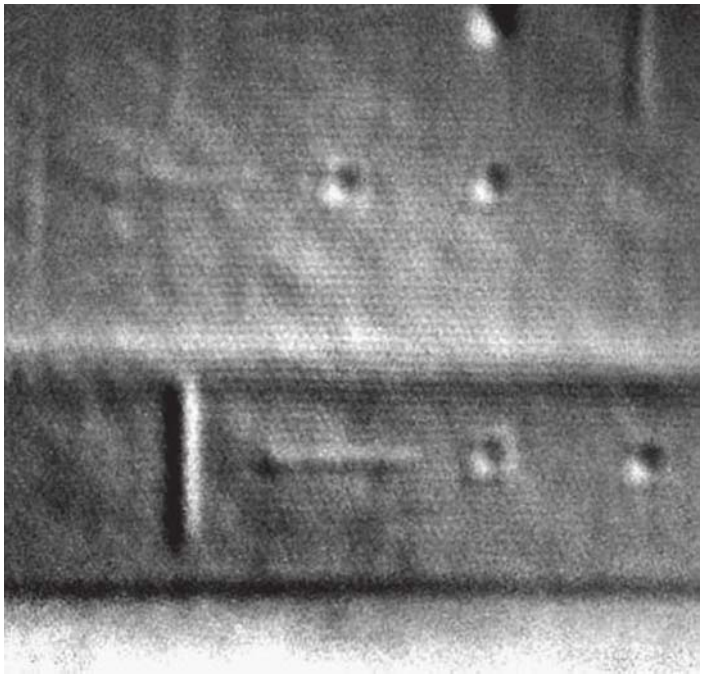

(b)

Figure 14-18 (*Continued*)

Unlike thermography which images surface temperature changes (or derivatives) over time, thermal shearography uses a temperature change to reveal local changes in the coefficient of thermal expansion (CTE) due to the presence of an anomaly. Thermal shearography is not affected by the test part emissivity and is equally able to inspect polished aluminum or painted surfaces without any surface preparation except to remove any grease or moisture.

For materials with a positive CTE, which includes most materials such as carbon laminate, aluminum, steel, and fiberglass, the test part surface is heated. For materials with a negative CTE, such as Kevlar, the component part must be tested by cooling the surface. Thermal stress is typically accomplished using radiant light with a high IR component such as shown in Fig. 14-20. These 1-kW quartz lamps with adjustable reflectors are mounted to the shearography camera and heat at distances up to 10 ft any target in the FOV of the shear camera.

Thermal shearography performed using hot air guns to heat the part is discouraged but it can produce adequate results in materials with a low thermal emissivity, such as polished aluminum. The user must be careful to heat the inspection area evenly. Manual heating of the test part with a hot air gun is also highly subjective and not quantifiable. For materials with a negative CTE, cooling the test part can be accomplished using compressed CO_2 or a vortex cold air gun, again though with the same limitations.

The thermal lamps are computer controlled from the shear camera software to provide consistent repeatable heating for each test. The reference images may be captured

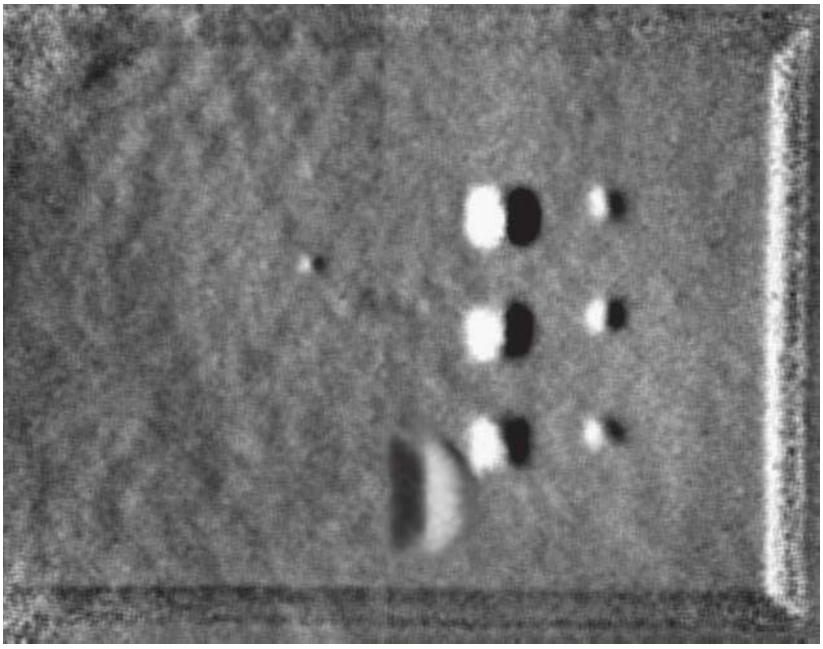

(a)

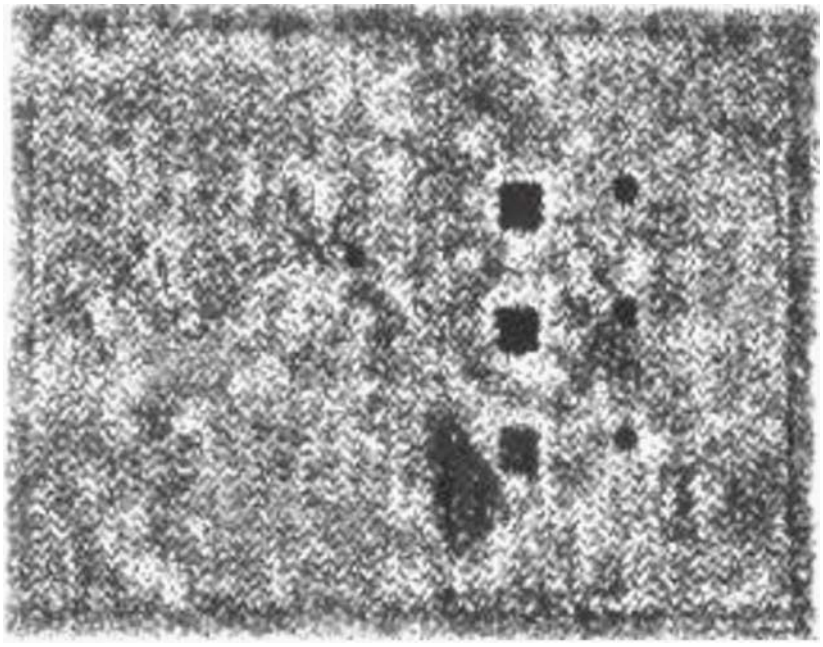

(b)

Figure 14-19 (*a*) FOD panel shearography result. A partial vacuum shearography test reveals various types of FOD including a razor blade, backing material, Kapton® , paper, and polyethylene. This 20 × 16-in. (51 × 41-cm) panel was inspected in two tests lasting 15 s. (*b*) Through-transmission UT result. An ultrasonic C-scan of this panel shows substantially identical results, with a considerably slower inspection rate and a lower signal-to-noise ratio.

(a)

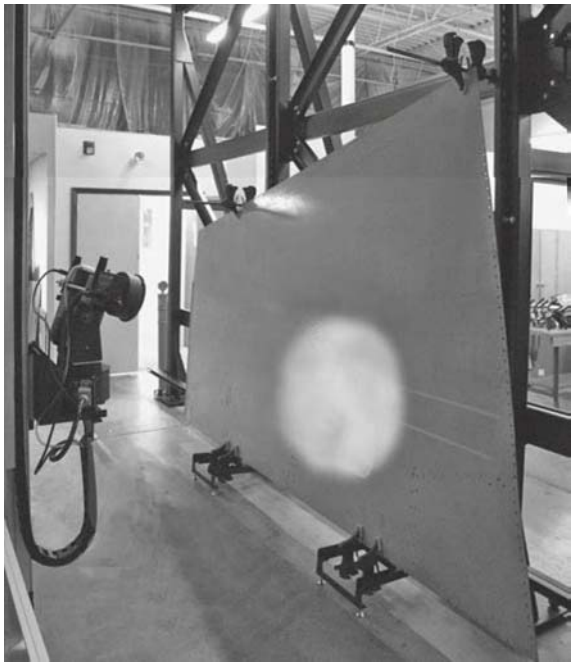

(b)

Figure 14-20 (*a*) A remote-controlled shearography camera with two 1-kW thermal lamps mounted on the camera to direct the IR energy wherever the camera is pointed, here an aircraft radome. (*b*) A thermal shearography camera on an automated gantry for scanning a large aluminum sandwich panel for a commercial aircraft.

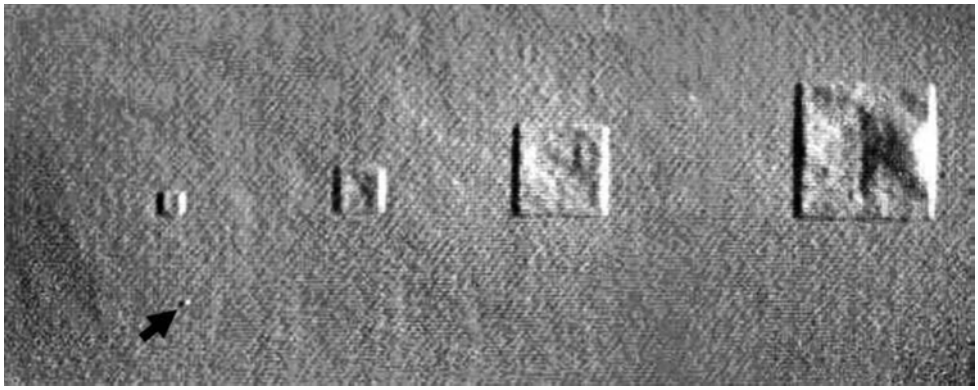

Figure 14-21 NDT standard panel with five-ply carbon-fiber face sheets and Nomex honeycomb manufactured with machined core and Teflon inserts in sizes starting with 0.25 in. (6.35 mm). A small natural discontinuity indication is seen lower left (arrow). The small shear vector, $S_v = 0.1$ in. at 0°, provides excellent detail and skin-to-core disbond sensitivity.

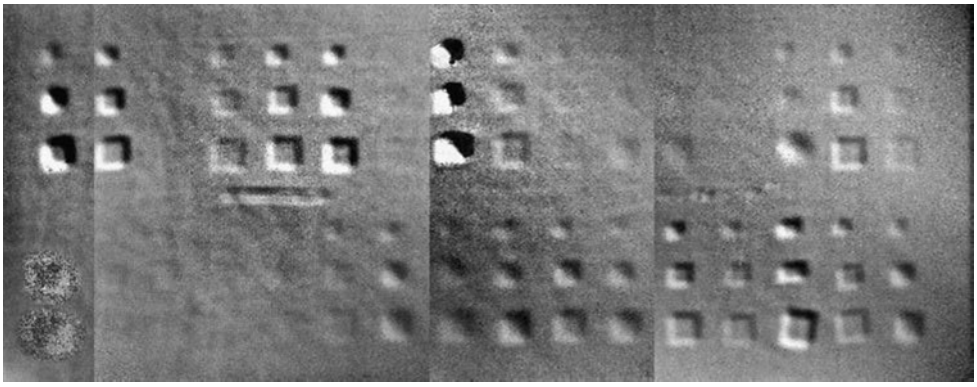

Figure 14-22 Four thermal shearograms stitched to image a 30-in.-long, 20-ply carbon-fiber laminate. Pieces of foreign material, peel ply, and Teflon were placed in the ply lay-up throughout the full thickness of the panel. The difference in the coefficient of thermal expansion for the FOD as compared to the carbon-fiber laminate produces the slight out of plane surface changes when thermally stressed allowing detection with the shearography camera.

either before [referred to as refresh before heat (RBH)] or after [referred to as refresh after heat (RAH)] the thermal stress is applied. Thermal stress parameters may be time-based or temperature-change-based using a remote sensor to measure the real-time test part surface temperature change during heating.

Thermal shearography can provide excellent disbond detection in sandwich panels. (As illustrated in Figs. 14-21 and 14-22). Defects typically detectable in sandwich panels with thermal shearography include face sheet to core disbonds, damaged core, disbonded core splice joints, crushed core, and impact damage. Defect sensitivity varies with the sandwich construction. Materials with high coefficients of thermal expansion C_t such as metallic and carbon-fiber laminate face sheets and metal cores yield the best

shearography results, often detecting disbonds on both near and far sides from one side. Figure14-23 is one such example of a thermal shearography test of NDT STD for a satellite dish antenna made with carbon laminate face sheets and aluminum core. Programmed disbonds on both sides are detected. Nomex and foam-core sandwich panels can be effectively inspected but only on a single side due to low thermal conductivity; for these materials, vacuum shearography is highly effective.

The detection of fiber wrinkles in composite structures can be extremely important and challenging for traditional NDT methods. Figure 14-24 shows an example of a very serious tooling induced fiber wrinkle in a large aircraft fuselage, detected with thermal shearography. Fiber wrinkles can often also occur at corners and curves. Being a noncontact NDT method, where contour following and being normal to the part surface is not a requirement, shearography is excellent for detecting wrinkled fibers.

Thermal shearography has been used successfully to inspect composite repairs, as shown in Fig. 14-25. Engineered repairs can contain porosity, disbonds, and FO, all of which have been detected. Impacts can leave no visible trace on a composite surface.

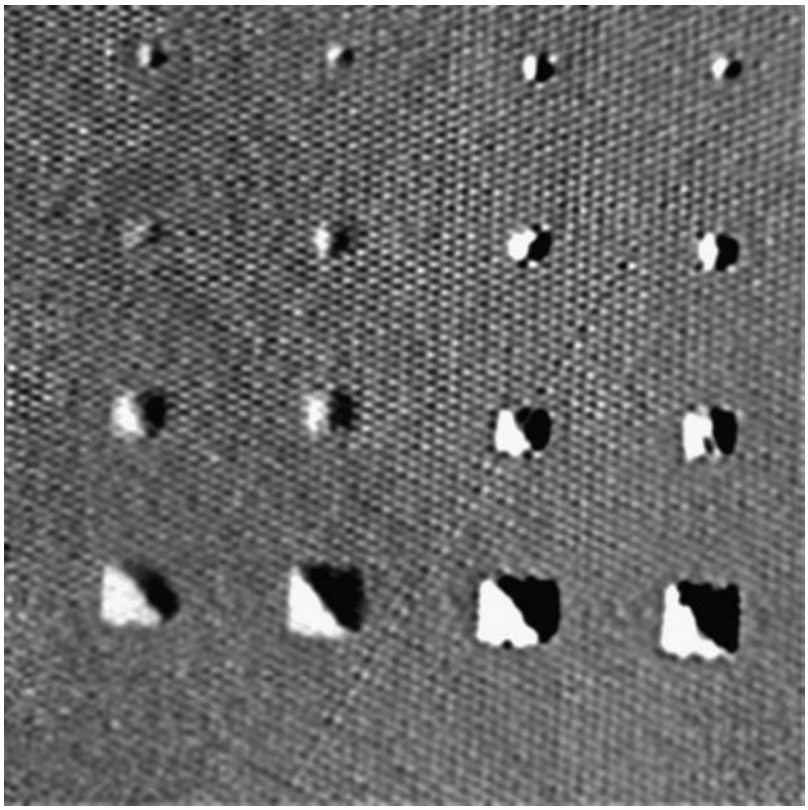

Figure 14-23 A thermal shearography image of a panel with thin carbon-fiber face sheets and aluminum honeycomb core. This NDT STD, measuring 16 × 16 in. (40 × 40 cm), was manufactured with Teflon inserts between the core and the adhesive to simulate disbonds in a spacecraft antenna. Eight near-side skin-to-core inserts are detected in the right side of the panel and eight far-side inserts on the left side.

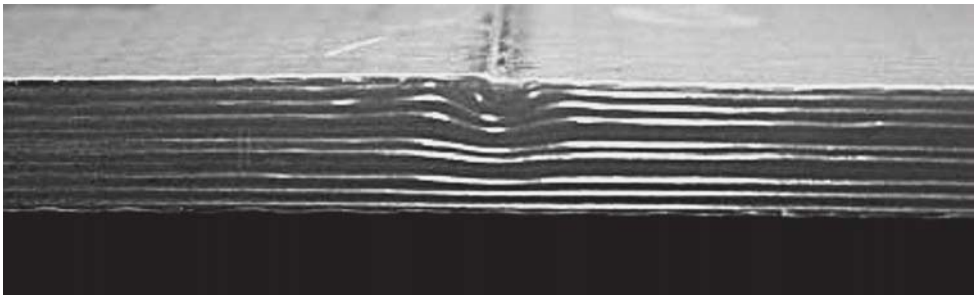

(a)

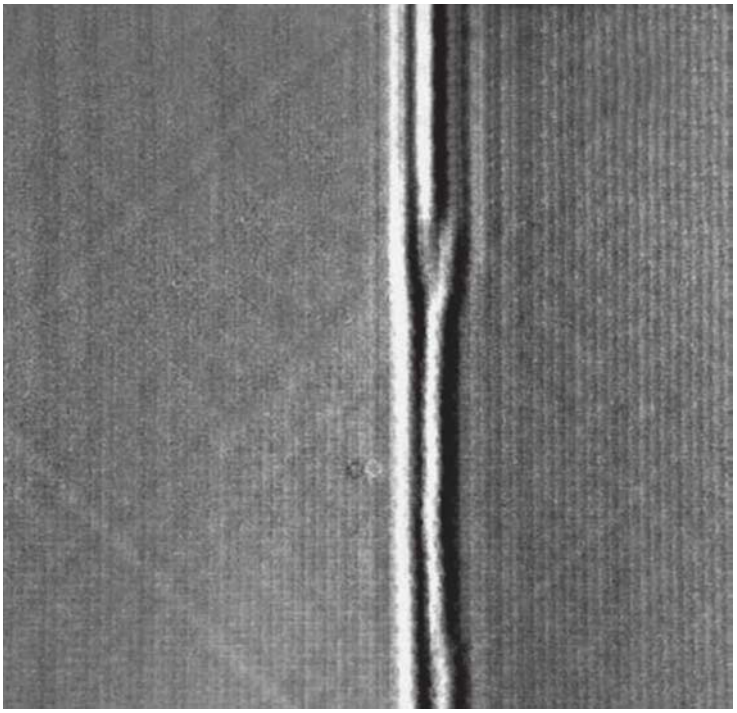

(b)

Figure 14-24 (*a*) Wrinkled fibers are seen in this photo of a section of a composite aircraft fuselage. The wrinkles run in an axial direction substantially weakening the ability of the fuselage to support pressurization loads. (*b*) The thermal shearography result taken from what would be the outside surface of the fuselage showing the wrinkle in the fibers running from top to bottom. The FOV is 12 × 12 in. (30.5 × 30.5 cm).

The thermal shearography provides outstanding sensitivity for impact damage to carbon-fiber laminates.

14.4.4 Vibration Shearography

Vibration shearography uses either an air coupled or a mechanically coupled ultrasonic source to induced vibrations into the test part in the frequency ranges for the resonance

(a)

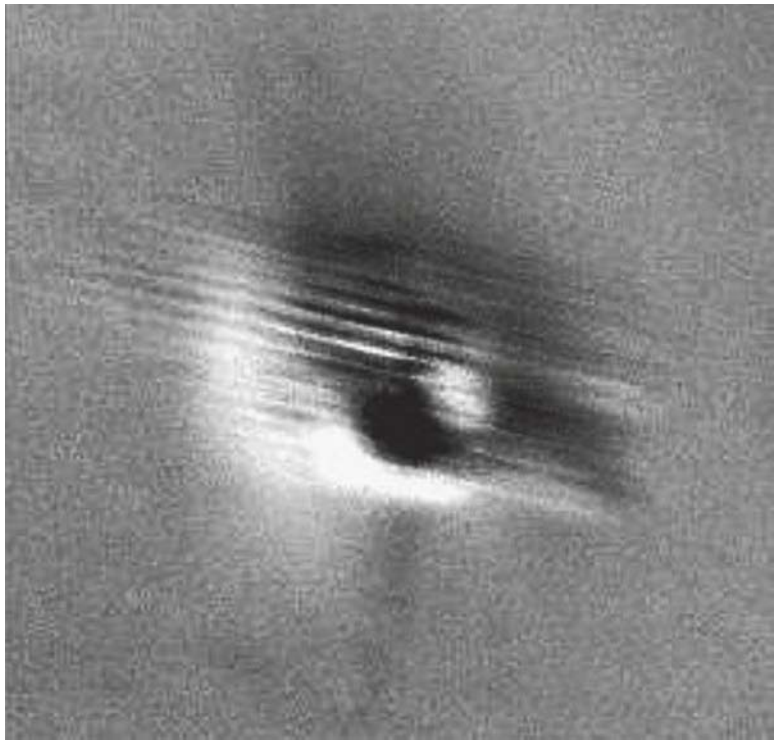

(b)

Figure 14-25 (*a*) A thermal shearography test of an 8-in.-diameter (203-mm) composite repair on an aircraft vertical stabilizer shows a large 1.5-in. disbond and areas of porosity. (*b*) Non-visible impact damage to a solid carbon laminate wing panel. The actual impact site appears like a crater with broken fibers and a deeper under-laying delamination.

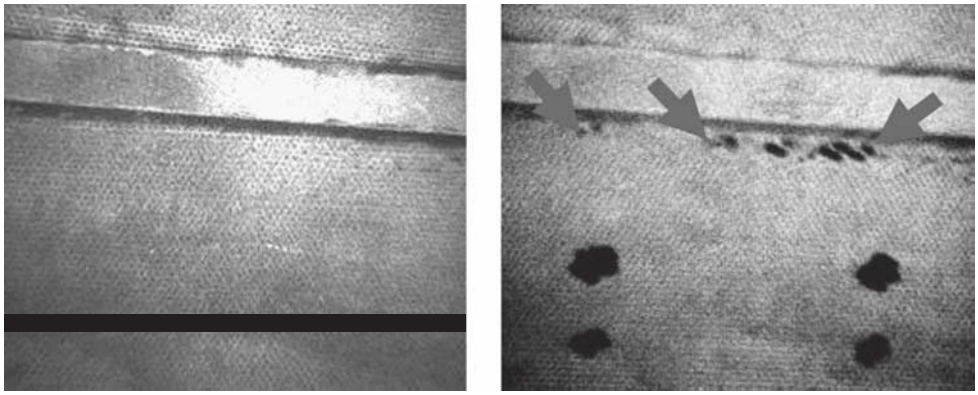

Figure 14-26 (*a*) A live image as seen through the shearography camera of a large aircraft engine inlet duct with perforated aluminum face sheets and metallic honeycomb. (*b*) The shearography results show natural disbonds (arrows) and four mill flat bottomed holes from the far side, measuring 0.5 and 0.8 in. in diameter. Testing is real time.

modes of anomalies. Air-coupled acoustic drive (ACAD) should be considered for light weight structures or insulation materials such as honeycomb with thin face sheets and foam insulation used for launch vehicle cryogenic fuel tanks. Mechanically coupled acoustic drive (MECAD) should be considered for metal to metal bonding, metal honeycomb and is especially good for structures with perforated face sheets such as aircraft engine inlet ducts such as shown in Fig. 14-26. Vibration shearography is fully real time and the system will operate continuously during data acquisition as the camera scans and briefly stops to acquire data.

Acoustic stress shearography (ACAD) testing is performed using a speaker with a directional horn. Production systems such as shown in Fig. 14-27 use an acoustic horn or waveguide to focus the acoustic energy over a 1-m^2 area for inspecting foam isolation of a launch vehicle cryogenic fuel tank. Power levels for ACAD typically produce acoustic pressure levels sometimes as high as 110 dB (decibels). Both ACAD and MECAD can produce sound levels well above safe exposure limits without hearing protection. Because of the very short inspection time required, acoustic shearography is ideal for large structures or launch vehicles. Production systems in current use are easily capable of an inspection rate of 1,500 ft^2/h.

14.5 Evaluation and Reporting of Test Results

The protocol for evaluating shearography images derives for the feasibility studies to determine the efficacy of the shearography stress method for a given application. Shearography instruments have a range of tools for measuring indication sizes, area, linear dimensions, *z*-axis deformation resulting from the stress change. These measurements compensate for the shear vector in every image (except image integration) and are used to accept or reject indications against the test part discontinuity accept/reject criteria.

(a)

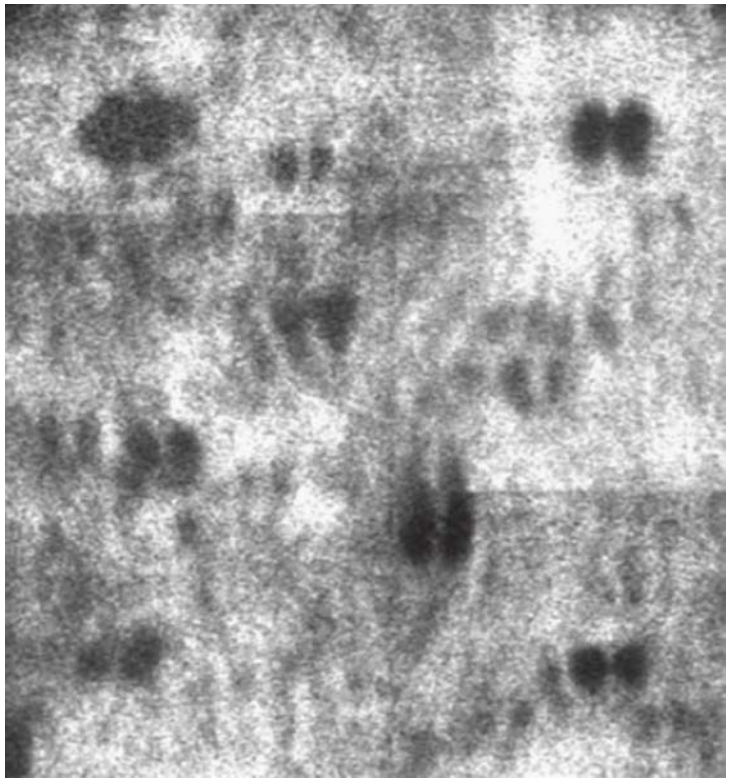

(b)

Figure 14-27 (*a*) An acoustic shearography system testing foam insulation on a large cryogenic rocket fuel tank. (*b*) A typical shearography test result. The black areas are foam to substrate disbonds. The FOV is 3×3 ft, with a test time of only 60 ms.

Shearography test reports include detailed description and photographs of the test setup and the shearography procedure. Also included are a listing of the test parameters including the shear vector, range to target, stress levels and rates, and data acquisition timing. Shearography test images of NDT STD(s) before and after every test run, images of all indications with dimensions. Secondary supplemental testing with UT is sometimes used for depth, where applicable.

14.6 Advantages and Limitations

The advantages of shearography NDT of conventional methods include high through-put. The time required to gather the raw data is typically determined by the time required to induce the load change be it thermal flow in a carbon-fiber laminate or pressurization of a rocket engine thrust chamber. The data processing is generally accomplished in less than 60 to 200 ms. A second advantage is no requirement for part contour following. Tilted test part surfaces can be inspected, greatly reducing the cost of a scanning shearography system. Third, shearography methods can employ many different test part stress methods often several in the same test. This diversity of techniques often leads to a positive NDT solution. Shearography can test a number of materials such as bond cork and foam that are extremely difficult for conventional NDT methods. Finally, shearography techniques and interpretation tend to be simpler than other NDT methods. For example, in NAS 410 the recommended training hours for level 2 shearography is 60 h and for ultrasonic testing is 80 h.

Limitations of the shearography method include reduced discontinuity sensitivity at depth. The deeper the flaw is from the surface the larger it must be to be detected. Extensive testing of matrix NDT STDs for common solid laminates have proven detection of 0.25-in.-diameter void through 15 plies. Imaging black glossy curved surfaces can be challenging. The use of penetrant developer to increase the surface reflectivity can help, if allowed. Finally, shearography images can be degraded by environmental vibration and noise.

14.7 Laser Safety

Laser shearography NDT systems utilize laser light to illuminate the surface of a test article being inspected. The laser provides a convenient source of monochromatic-coherent light that makes the implementation of shearography NDT possible. With the exception of extremely low powered laser systems, virtually all laser products pose some form of hazard [20]. The most common hazards associated with lasers come from the direct exposure of the eyes and skin. Within the United States, laser systems are classified in accordance with the regulations set forth by the Center for Devices and Radiological Health (CDRH) division of the Food and Drug Administration (FDA). Additional federal, state, and local regulations may also apply to further regulate the use of a laser product for a given application. Many of these secondary regulations are based on classification data provided by the American National Standards Institute (ANSI) [15, 16]. In the European community, laser system standards are overseen primarily by the International Electrotechnical Commission (IEC) and the British Standards Institution (BSI).

14.8 Glossary of Key Terms

Coherent Light Source A light source that converts electrical energy to a coherent beam of light.

Composite Material A substance consisting of two or more materials, insoluble in one another, which are combined to form a useful engineering material possessing certain properties not possessed by the constituents.

Composite Component A finished part containing composite material(s) that is in its end use application configuration, and which has undergone processing, fabrication, and assembly to the extent specified by the drawing, purchase order, or contract.

Displacement Derivatives ($\partial w/\partial x$) Rate of spatial displacement change, where w is the surface displacement and x is the surface coordinates.

Filament Wound Pressure Vessel An inner shell over-wrapped with composite layers that form a *composite shell*. The inner shell or liner may consist of an impervious metallic or nonmetallic material. The vessel may be cylindrical or spherical and will have at least one penetration with valve attachments for introducing and holding pressurized liquids or gases. Also referred to as a composite over-wrapped pressure vessel of COPV.

Shear Vector The image separation direction angle and distance formed in an imaging shearing interferometer used for NDT. Shear vector is expressed as the angle from the x axis and distance between identical points in each image in inches or mm.

Shearogram The speckle pattern observed in laser shearography where a displacement derivative is detected.

Stress The stress change resulting from the application of an engineered force applied to the test object during shearography inspection. Stress most frequently used are vacuum, pressure, heat, mechanical and acoustic vibration in the sonic or ultrasonic ranges, magnetic fields, electric fields, microwave or mechanical load(s).

References

1. Stetson, K. A., 50 Years of holographic interferometry, *SPIE Optics and Measurement Conference Proceedings*, Vol. 9442, 2014.
2. Hung, Y. Y., "Shearography: A new optical method for strain measurement and nondestructive testing," *Optical Engineering*, Vol. 21, No. 3, pp. 391–395, 1982.
3. Nakadata, S., "Phase detection of equidistant fringes for highly sensitive optical sensing," *Journal of the Optical Society of America A*, Vol. 5, No. 8, pp. 1265–1269, 1988.
4. Newman, J. W., "Laser Testing: Shearography & Holography," P.O. Moore, editor, *The Nondestructive Testing Overview*, Columbus Ohio, American Society for Nondestructive Testing, 2012.
5. "New York's Bronx-Whitestone Bridge Span to Feature 390 Composite Wind Fairings," NetComposites, http://netcomposites.com/news/2003/october/22/new-york-s-bronx-whitestone-bridge-span-to-feature-390-composite-wind-fairings/, 2003.

6. Caufield, H. J. and Lu, S., *Applications of Holography*, New York, NY, Wiley-Interscience, 1970.
7. Chatters, T., Pouet, B., and Krishnaswamy, S., "Shearography With Synchronized Pressure Stressing," D. O. Thompson and D. E. Chimenti, editors, *Review of Progress in Quantitative NDE*, La Jolla, CA, Plenum Press, pp. 19–426, 1992.
8. Deaton, J. B., Jr. and Rogowhi, R. S., "Optimization of Image Shearing Parameters in Electronic Shearography for Nondestructive Evaluation," D. O. Thompson and D. E. Chimenti, editors, *NDE: An Answer for an Aging World*, Columbus OH, American Society for Nondestructive Testing, pp. 204–206, 1994.
9. Gryzagoridis, J., Oliver, G., and Findeis, D., "Modal frequency versus shearography in detecting and locating voids/delaminations in sandwich composites," *Insight*, Vol. 55, No. 5, pp. 249–252, 2013.
10. Post, D., "Optical Interference for Deformation Measurements—Classical Holographic and Moire' Interferometry," W. W. Stinchcomb, editor, *Mechanics of Nondestructive Testing*, New York, NY, Plenum Press, 1980.
11. Spicer, J. B., Champion, J. L., Osiander, R., and Spicer, J. W. M., "Time Resolved Shearography and Thermographic NDE Methods for Graphite Epoxy/Honeycomb Composites," *Materials Evaluation*, Vol. 54, No. 10, pp. 1210–1213, 1996.
12. Vest, V. M., *Holographic Interferometry*, New York NY, John Wiley, 1979.
13. Gryzagoridis, J., "Laser based nondestructive inspection techniques," *Journal of Nondestructive Evaluation*, Vol. 31, No. 4, pp. 295–302, 2012.
14. "Standard Practice for Shearography of Polymer Matrix Composites and Sandwich Core Materials in Aerospace Applications," American Society for Testing and Materials, ASTM E2581-14, web page: https://www.astm.org/Standards/E2581.htm.
15. "Standard Guide for Nondestructive Testing of the Composite Overwraps in Filament Wound Pressure Vessels Used in Aerospace Applications," American Society for Testing and Materials, ASTM E2981, 2015, web page: https://www.astm.org/Standards/E2981.htm.
16. Timoshenko, S. P. and Goodier, A. N., *Theory of Elasticity*, 3rd Edition, New York, McGraw-Hill Classic Textbook Reissue Series, 1970.
17. Newman, J. W., "Shearographic & Holographic Testing," R. H. Bossi, editor, *ASNT Industry Handbook Aerospace NDT*, Columbus Ohio, American Society for Nondestructive Testing, 2012, https://www.asnt.org/MajorSiteSections/Publications/NDT_Handbooks/Industry_Handbook_Aerospace.aspx.
18. Timoshenko, S. P. and Woinowsky-Krieger, S., *Theory of Plates and Shells*, 2nd Edition, New York, McGraw-Hill Book Company, 1959.
19. Prescott, J., *Applied Elasticity*, New York, Dover, 1946.
20. Sliney, D. H., Safety with Lasers and Other Optical Sources: A Comprehensive Handbook, New York, Springer Science, 1980.

APPENDIX

Basic Metric–U.S. Customary Conversions

To Convert	Into	Multiply by
Celsius	Fahrenheit	9/5 and add 32
Centimeters	Inches	0.3937
Cubic centimeters	Cubic inches	0.06102
Cubic meters	Cubic feet	35.31
Grams	Ounces	0.03527
Kilograms	Pounds	2.205
Kilometers	Miles	0.6214
Liters	Gallons (U.S.)	0.2642
Meters	Feet	3.281
Meters	Yards	1.094
Millimeters	Inches	0.0393
Square centimeters	Square inches	0.1550
Square kilometers	Square miles	0.3861
Square meters	Square feet	10.76
Square meters	Square yards	1.196

Metric to U.S. Customary

To Convert	Into	Multiply by
Cubic feet	Cubic meters	0.02832
Cubic inches	Cubic centimeters	16.39
Fahrenheit	Celsius	5/9 after subtracting 32
Feet	Meters	0.3048
Gallons (U.S.)	Liters	3.785

(*Continued*)

To Convert	Into	Multiply by
Inches	Millimeters	25.40
Inches	Centimeters	2.540
Miles	Kilometers	1.609
Ounces	Grams	28.35
Pounds	Kilograms	0.4536
Square feet	Square meters	0.0929
Square inches	Square centimeters	6.452
Square miles	Square kilometers	2.590
Square yards	Square meters	0.8361
Yards	Meters	0.9144

U.S. Customary to Metric

Index

Note: An *f* follows page numbers referencing figures; a *t*, tables; an *n*, notes.

A

A-scan:
  for PAUT, 631, 631*f*, 690
  for PEC, 481, 481*f*, 482*f*, 488, 489*f*
  for UT, 329–330, 329*f*, 330*f*, 348*f*, 387*f*, 410
a-Si. *See* Amorphous silicon X-ray detector
Abrahams, C., 293
Abrasive wear, 107
Absolute coil technique, 443–444, 443*f*, 473, 473*f*, 490
Absolute temperature scale, 499, 537
Absolute zero, 503, 537
Absorption, 231, 232*f*, 287, 319, 503
AC. *See* Alternating current
ACAD. *See* Acoustic stress shearography
ACCP. *See* ASNT Central Certification Program
Achenbach, J. D., 700
Acoustic emission testing (AE), 6*t*, 7*t*, 16
  advantages and limitations of, 581
  amplitude for, 548–549, 549*f*
  attenuation in, 555–557, 555*f*, 556*f*
  from crack face rubbing, 551, 552*f*
  displays for, 571*f*–579*f*, 572–579
  evaluation for, 579–580, 579*f*
  fatigue cracks from, 547–548, 547*f*
  glossary for, 582–584
  history of, 543
  instruments for, 564–572, 565*f*–572*f*
  Lamb wave in, 557, 558*f*, 559
  measurement for, 562–563, 563*f*, 564*f*
  from mechanical loading, 548–551, 549*f*, 550*f*
  overview of, 543–545, 544*f*
  sensors for, 544, 559–561, 561*f*
  signal-shaping chain and, 553–563, 553*f*, 555*f*, 556*f*, 558*f*–564*f*
  from stress, 545
  stress/strain curve for, 545, 546*f*
Acoustic impedance, 304, 412
Acoustic stress shearography (ACAD), 766, 767*f*
Adhesion, 163
Adhesive wear, 107
ADR. *See* Automated defect recognition
AE. *See* Acoustic emission testing
Aerospace, 522–523, 729*t*, 730*t*
AISI 304, 44
ALARA. *See* As low as reasonably achievable
Allotropic transformation, 43, 43*n*5, 50
Alpha iron, 40
Alternating current (AC), 183, 183*f*
  for electromagnetic yoke, 192–193, 192*f*, 208
  for ET, 417, 424–431, 425*f*, 426*f*, 428*f*–431*f*, 490
  influence of, 186
  for MT, 167, 195–196, 204, 217
American Industrial Radium and X-ray Society, 12, 17, 23, 227
American National Standards Institute (ANSI), 69, 93, 768
American Petroleum Institute (API), 93
American Society for Nondestructive Testing (ASNT), 12, 17, 23
  on ET, 417
  Level III certification by, 25–26
  Recommended Practice of, 69
  on shearography, 739
  on TIR, 497–498
American Society for Testing and Material (ASTM):
  on AE, 543
  E1417, 134
  E2446, 593
  E2597, 595
  standards of, 93, 611
  on TIR, 498
  on wire penetrameters, 253
American Society of Heating, Refrigeration, and Air Conditioning Engineers (ASHRAE), 498

American Society of Mechanical Engineers (ASME), 28
on AE, 543
Boiler and Pressure Vessel Code of, 69–70, 116
on DAC, 365
Rules for Inservice Inspection of Nuclear Power Plants of, 69
standards of, 93
American Welding Society (AWS), 69, 663–664, 664*f*
Structural Welding Code of, 116
Amorphous silicon X-ray detector (a-Si), 596, 596*f*, 617
Ampere, Andre-Marie, 167, 178
Amperes (amps), 184, 185, 205–208
Amplitude. *See also* Distance, amplitude
for AE, 544, 548–549, 549*f*, 562–563, 582, 583
impedance, 430, 431*f*
linearity, in UT, 361, 412
MAS, 393–396, 394*f*, 395*f*
maximum, 293–294
of sound waves, 322–323, 323*f*
UT and, 309, 410
Amplitude control linearity verification, 361
Amps (amperes), 184, 185, 205–208
ANDE-1. *See* ASME Nondestructive Examination and Quality Control and Certification Program
Angle beam, 365, 710*f*
pulse-echo techniques for, 372–373
transducers, 333, 334–335, 337*f*, 348, 349*f*, 350, 351, 351*f*, 410
for PAUT, 623
Angle of field, 77, 84, 89, 125
Angstrom, 74, 125, 163, 287
Angular resolution, 692
Anisotropy, 34, 34*n*5, 54
Annealing, 54
Annotation tools, 608
Anodes, 236, 287
ANSI. *See* American National Standards Institute
Aperture, 626–627, 628*f*, 629–630, 690
for borescope, 84
virtual, 647, 692
API. *See* American Petroleum Institute
Apodization, 690
Aqueous developer, 153*f*, 164
Arc strikes, 105
Area amplitude blocks, 364, 365*f*
Area amplitude response curve, 364, 410
Articulating fiberscope, 111
Artifacts, 54, 266, 269, 271, 287
As low as reasonably achievable (ALARA), 279
ASHRAE. *See* American Society of Heating, Refrigeration, and Air Conditioning Engineers
ASME. *See* American Society of Mechanical Engineers
ASME Nondestructive Examination and Quality Control and Certification Program (ANDE-1), 28
ASNT. *See* American Society for Nondestructive Testing
ASNT/ANSI-CP189, 26
ASNT Central Certification Program (ACCP), 27
Aspect ratio, 125
ASTM. *See* American Society for Testing and Material
Atoms, 417–418, 490
Attenuation:
AE and, 554, 555–557, 555*f*, 556*f*, 583
of sound waves, 316
TIR and, 518
ultrasonic guided wave inspection and, 707, 707*f*
UT and, 326–327, 370, 402, 410
Audible sound, 298
Auld, B. A., 700
Austenite iron, 40
AUT. *See* Automated ultrasonic testing
Automated defect recognition (ADR), 615–616, 616*f*
Automated ultrasonic testing (AUT), 672, 672*f*
AWS. *See* American Welding Society
Azimuthal scan, 690

B

B-scan:
for PAUT, 632–633, 633*f*, 638, 690
single value, 642, 690
for TOFD, 399, 399*f*–401*f*
for UT, 6*t*, 330, 331*f*, 399*f*, 410
Back reflection, 354, 370, 410
Back surface, 410
Back voltage, 435, 436*f*, 490
Background, 163, 168, 217, 518, 537, 741
thermal, 541
Bad pixels, 613, 617
Ball and plug valves, 111
Band-pass filters, 327–328, 510
Bandwidth, 327, 339, 340*f*
Bao, J., 712
Bartoli, I., 697
Basic spatial resolution (SRb), 617
BCC. *See* Body-centered-cubic
Beach marks, 50, 50*f*
Beam angle, 350–351, 626–627
Beam focusing, 627–628, 627*f*, 628*f*
Beam forming, 624–625, 625*f*, 690

Beam path distance, 357, 376–379, 377*f*, 378*f*
Beam profiles, 682–683
Beam sequencing, 630–631, 631*f*
Beam skew, 346
Beam spread, 320–322, 320*f*–322*f*, 351–353, 359, 390, 410
Beam steering, 628–630, 630*f*, 690, 698
Beaufort's wind scale, 525, 538
Bell, Alexander Graham, 322
Betz, Carl, 6*t*, 132, 133
Billet, 54, 677–678, 678*f*
Bit depth, 591–592
Black light, 133, 137–138, 138*f*, 163, 167, 188, 193, 194*f*, 211–212, 217
Blackbody, 505, 538
Blacksmiths, 4, 5*f*
Bleed-out, 149, 149*f*, 163
Blister, 37, 54
Blotting, 163
Blowhole, 54
Bly, James, 227
Bobbin-wound probes, 445, 445*f*
Body-centered-cubic (BCC), 40
Boiler Inspection Law, 8
Boilers, 115
  explosions of, 6–10, 8*f*, 9*f*, 69
Bolt hole probes, 446, 446*f*
Bond testing, 407, 697–698, 718–720, 719*f*, 720*f*
Borescope, 70, 70*f*, 71, 71*f*, 82–84, 83*f*, 125
  video, 84, 85*f*, 86
Boundary layer, 503, 538
Box demagnetizer, 189, 212*f*
Brady, Elliot, 134
Brazing, 46, 55, 97–98
Breon, L. K., 698
Bridge circuit, 443, 443*f*, 490
Brightness, 73, 74, 91, 125
British Standards Institution (BSI), 768
British thermal unit (Btu), 499, 538
Brittle cracking, 43–44, 55
Brittle fracture, 52–53, 52*f*, 53*f*
Broadband, 553–554
BS 2704, 362, 363
BSI. *See* British Standards Institution
Btu. *See* British thermal unit
Bubblers, 344, 345*f*, 410
Bulk waves, 708–709, 709*t*
Burmah castrol strips, 194, 195*f*
Burn-through, 104
Burned-in image, 125
Burning, 196, 217
Burr, 54, 55
Bursts, 55, 66*f*, 95, 548, 583
Butterfly valves, 111

C

C-scan:
  for PAUT, 636–638, 638*f*, 690, 691
  for PEC, 489*f*
  for shearography, 739, 746
  for UT, 6*t*, 330, 332*f*, 410
Calibration:
  for PAUT, 647–651, 648*f*–651*f*
    sensitivity of, 650–651, 651*f*, 691
    velocity and, 648, 648*f*, 649*f*
  for PEC, 482
  for shearography, 744–745
  time base:
    for compression waves, 353–356, 354*f*–356*f*
    for shear wave transducers, 356–357, 356*f*
  for TIR, 518, 519
    temperature and, 511
  for UT, 347–365
  for VT monitors, 90
Calibration blocks, for UT, 362–364, 363*f*, 364*f*
Calipers, 80, 81, 81*f*
Calorie, 499, 538
Calorimeter, 499
Cameras. *See also* Charge-coupled device
  fiber, 84, 85*f*, 122
  photographic, 120
  for shearography, 739–741, 742*f*
Canadian Certification System, 28
Cantrell, J. H., 698
Capillary action, 46, 55, 135–136, 135*f*
Carbon fiber reinforced plastic (CFRP), 672–673, 675*f*
Carbon-molybdenum steel, 41
Carrier, 144, 164
Carrier fluid, 200, 217
Cassette, 257, 287
Cast structure, 36, 55
Castaings, M., 698
Casting:
  cavities, 37
  discontinuities, 32, 34–41, 35*f*–38*f*, 40*f*, 41*f*
    RT for, 273–274, 275*f*–276*f*
  equilibrium phase diagrams for, 39–40, 40*f*
  fluorescent penetrant system for, 132, 133
  grains in, 34–35, 34*n*5
  primary-process discontinuities in, 96–97
  seams, 39
  shrinkage in, 55
  slags in, 33, 63*f*
Cathode ray tube (CRT), 90, 292–293, 296, 324–325, 600
Cavity radiator, 538
Cawley, P., 697
CCD. *See* Charge-coupled device

CCTV. *See* Closed-circuit television
CCU. *See* Central control unit
Center for Devices and Radiological Health (CDRH), 768
Central control MT technique, 198–199, 199*f*
Central control unit (CCU), 84, 87
Ceramics, 551
Certification, 22–28, 73
Certification Scheme for Welding and Inspection Personnel, 27–28
Certified Weld Inspector (CWI), 69, 116
Cesnik, C. E. S., 698
CFRP. *See* Carbon fiber reinforced plastic
Channel, 582, 583
Chaplets, 96–97, 274
Charge-coupled device (CCD), 71, 72*f*, 84–86, 125
  advantages and limitations of, 121
  cameras:
    advantages and limitations of, 122–123
    for nuclear reactor vessels, 114–115
    shearography and, 741
    for VT, 86–91, 87*f*, 88*f*, 91*f*
  cameras and, 84
  for TIR, 496, 538
Charpy test, 19, 19*f*, 55
Chatter, 55
Checks, 55
Chemical cleaning, 141
Chills, 96–97
Chimenti, D. E., 696, 697–698
Circumferential (circular) magnetization, 196–198, 198*f*, 205, 208, 217
Cladding, 471, 471*f*
Cleanliness, 74, 163*t*, 164
Cleavage, 44, 55
Clock voltage, 86
Closed-circuit television (CCTV), 114, 585, 587*f*, 588, 589
CloVER. *See* Composite long-range variable-length emitting radar
CMOS. *See* Complementary metal-oxide semiconductor
CNR. *See* Contrast-to-noise ratio
Code, 93, 125
Coefficient of convective heat transfer, 502
Coercive force, 174, 174*f*, 175, 176*f*
Cognizant Engineering Organization, 603
Coherent light source, 769
Cohesion, 164
Coil circuits, 439
Coil in air, 454, 490
Coil method, 198, 199*f*, 217
Coils:
  absolute coil technique, 443–444, 443*f*, 473, 473*f*, 490
  AC demagnetizing, for MT, 195–196
Coils (*Cont.*):
  cross-axis, 447–448, 447*f*, 490
  demagnetizing, 195–196, 217
  differential coil technique, 444, 444*f*, 473, 473*f*, 491
  empty, 454, 491
  encircling, 449–450, 449*f*, 450*f*, 473, 474*f*
  for ET, 438, 443–451, 443*f*–451*f*
  external reference, 444, 444*f*, 491
  ferromagnetic metals in, 179
  internal, 451, 451*f*, 452*f*, 473, 474*f*, 492
  for longitudinal magnetization, 207
  magnetization in, 179
  probe, 422, 493
  reflection, 448, 448*f*, 493
  shielded, 447, 447*f*, 493
  spinning, 450, 451*f*
  spring-loaded, 446, 446*f*
  surface, 445–449, 445*f*–449*f*, 494
Cold shut, 55, 59*t*, 97, 273
Cold working, 55
Collimator, 244, 287, 410
Color, 73, 91, 125
Color contrast coatings, 187, 188*f*, 201, 205
Columnar crystal structure, 55
Comb sensors, 728*t*
Comparative thermography, 512–515
Comparators, 81, 562
  penetrant blocks, 138–139, 159*f*, 165
Compensation distance amplitude, 411
Complementary metal-oxide semiconductor (CMOS), 595–596, 742, 742*f*
Composite long-range variable-length emitting radar (CloVER), 698
Composite over-wrap pressure vessels (COPVs), 737, 739, 740*f*, 751*f*, 757
Composite viewing, 287, 672–673
Composites, 548–551, 549*f*, 550*f*, 697–698, 728*t*, 730*t*
  shearography for, 737, 738*f*, 769
Compression waves, 298, 299*f*
  pulse-echo techniques for, 366–372, 368*f*–372*f*
  time base calibration for, 353–356, 354*f*–356*f*
  transducers, 347–350, 348*f*, 349*f*
  in UT, 293, 300
  velocity of, 302
Compton scattering, 231, 232*f*
Computed radiography (CR), 593–600, 594*f*–596*f*, 598*f*–599*f*, 613–614
Computed tomography (CT), 614, 614*f*, 615*f*
Concavity, 103, 104*f*, 272
Conductance, 419, 457, 457*f*, 490
  thermal, 500–501, 501*t*, 541
Conductivity, 171, 417, 418, 419, 437, 460–462, 461*f*, 490, 538
Conductors, 449, 490, 501, 538
Cone, 73*f*, 77, 125

Constant potential X-ray unit, 240, 288
Constituent, 39, 55
Constructive interference, 317
Contact angle, 141
Contact testing, 335, 411
Contaminants, 139, 164
Continuous casting, 39*n*6
Continuous emission, 583
Continuous MT techniques, 199–201, 204
Contrast, 73, 125
  ratio, 141, 164
  resolution, 591–592, 592*f*
  sensitivity, 254, 288
Contrast-to-noise ratio (CNR), 617
Convection, 501–503, 502*f*, 517–518, 526, 538, 540
Convexity, 272
Coolidge, William D., 227
COPVs. *See* Composite over-wrap pressure vessels
Corrosion, 18, 47–48, 47*f*, 55, 107–108, 125
  applications and techniques for, 109–115
  crevice, 56, 101, 108, 125
  depth indicators for, 81
  FAC, 485
  IGSCC, 48, 669–670, 670*f*
  PEC for, 485
  RVT for, 92
  SCC, 48, 49*f*, 53
  VT and, 91
Corrosion under fireproofing (CUF), 478, 486
Corrosion under insulation (CUI), 478, 486
Coulomb, Charles, 167
Counts, 562, 563*f*, 583
Couplant, 305, 402, 411
CR. *See* Computed radiography
Crack face rubbing, 551, 552*f*
Cracks, 41–42, 42*f*. *See also* Fatigue cracks
  brittle, 43–44, 55
  in casting, 35–36, 36*f*, 39
  crater, 55, 60*t*, 100, 105, 105*f*
  creep, 51, 51*f*, 55
  fluorescent penetrant system for, 132, 149, 150*f*
  in forging, 46–47, 46*f*, 95
  from geometric discontinuities, 53
  from grinding, 56
  HAZ, with welding, 100
  HIC, 44–45, 53, 670–671, 671*f*
  hot, 39, 57
  IGSCC, 48, 669–670, 670*f*
  in ingots, 94
  longitudinal, 100
  matrix, 548
  microcracks, 100
  microshrinkage, 57
  MT for, 209*f*, 211
  RT for, 271, 273
Cracks (*Cont.*):
  RVT for, 92
  SCC, 48, 49*f*, 53
  shearography for, 737
  solidification, 43
  stepwise, 670–671
  from stress, 546–547
  thermal energy in, 506
  thermal shearography for, 757
  transverse, 100
  with welding, 43, 65*f*, 66*f*, 100
Crater cracks, 55, 60*t*, 100, 105, 105*f*
Crazing, 51
Creep cracking, 51, 51*f*, 55
Creep voids, 51, 55
Crevice corrosion, 56, 101, 108, 125
Criscuolo, Edward, 227
Critical angle, 373, 411
Critical temperature, 52
Cross-axis coil, 447–448, 447*f*, 490
Cross-sectional B-scan, 632–633, 633*f*, 638, 690
CRT. *See* Cathode ray tube
CT. *See* Computed tomography
CUF. *See* Corrosion under fireproofing
CUI. *See* Corrosion under insulation
Curie, Jacques-Paul, 331–332
Curie, Marie, 6*t*, 228–230, 228*f*, 229*f*
Curie, Pierre, 6*t*, 228–230, 228*f*, 331–332
Curie temperature, 333, 334*t*
Current density, 433–434, 463, 463*f*
Current flow MT technique, 196, 197*f*
Current induction method, 217
CWI. *See* Certified Weld Inspector

D

DAC. *See* Distance amplitude correction
DAC curve, 358, 358*f*, 367*f*, 390, 411
Damping:
  search unit, 334, 411
  vibration, 112–113
Dark heat, 495
Data storage, 510, 635
Datta, S. K., 698, 700
Davies, J., 697
dB. *See* Decibels
DC. *See* Direct current
DDA. *See* Digital detector array
Dead zone, 350, 411
Decarburization, 56
Decibels (dB), 293, 322–323, 323*f*, 583
  controls, in UT, 411
Defects, 31, 56
  ADR for, 615–616, 616*f*
deForest, A. V., 6*t*, 12, 133

deForest, Taber, 132
Deicing, 698
Delamination, 48, 548, 737, 740*f*
Delay line, 401, 411
Delay sweep, 362, 411
Demagnetization, 188–189, 195–196, 212*f*, 217
Demagnetizing coils, 195–196, 217
Demma, A., 697
Dendrite, 36, 56, 402–403
Denomination, 361
Densitometer, 267–269, 267*f*, 288
Depth indicators, 81, 652–656, 652*f*–656*f*
Depth of field (DOF), 77, 78, 84, 125
Depth of focus, 125
Destructive interference, 318
Destructive testing, 17–21, 18*f*–20*f*
Detection/detectors, 508–509, 519, 582, 583
  a-Si, 596, 596*f*, 617
  flaw, 6*t*, 294, 296, 318, 513, 677
  Hall, 449
  media, 186–188, 187*f*, 188*f*
  QDE, 595
  threshold of, 3
Detectivity, 518, 519, 538
Developer, 136, 144, 148, 149*f*, 153*f*, 164, 265
Development time, 148–149, 164
Dewar, 508
DGS. *See* Distance, gain, size technique
Diamagnetic metals, 168, 171, 421–422
Diaphragm valves, 111
DICONDE. *See* Digital Communication Nondestructive Examination
Differential coil technique, 444, 444*f*, 473, 473*f*, 491
Diffraction. *See also* Time of flight diffraction
  effects, 316
  technique, 396–400
Digital Communication Nondestructive Examination (DICONDE), 592–593, 608
Digital detector array (DDA), 593–600, 594*f*–596*f*, 598*f*–599*f*, 613–614
Digital image, 591
  enhancement, 593, 617
Digital light processing (DLP), 90
Digital radiography, 585–618
  contrast resolution for, 591–592, 592*f*
  CR and DDA, 593–600, 594*f*–596*f*, 598*f*–599*f*, 613–614
  displays for, 597–600
  evolving technology for, 614–616, 614*f*–616*f*
  IQI for, 612–614
  measurement for, 606–609, 606*f*, 607*f*
  SNR for, 592, 592*f*
  software for, 600–602, 602*f*
  spatial resolution for, 591
  systems for, 600, 601*f*, 610–611, 611*f*, 612*f*
  tools for, 603–610, 603*f*–607*f*, 609*f*
Diopter, 78
Direct current (DC), 167, 182, 182*f*, 186, 204, 208, 217, 422, 491
Direct cursor measurement, 657–661, 657*f*–660*f*
Direct viewing, 78–82, 126
Discontinuities, 3. *See also specific types*
  AC for, 186
  with brazing, 97–98
  casting, 32, 34–41, 35*f*–38*f*, 40*f*, 41*f*
    RT for, 273–274, 275*f*–276*f*
  depth indicators for, 81
  ET for, 431–432, 432*f*, 463–468, 463*f*, 465*f*–468*f*
  geometric, 45, 53–54, 56, 272–273
  glossary for, 54–58
  guide for, 58, 59*t*–61*t*
  in ingots, 94–95
  MT for, 133, 179–182, 180*f*–182*f*, 210–211, 210*f*
  origins and classification of, 31–58, 59*t*–61*t*
  from plastic deformation, 46–47, 46*f*
  RT for, 252, 271–274
  shearography for, 737, 739
  with soldering, 97
  UT for, 292, 363, 370–372, 374*f*–375*f*, 406, 411
    sizing of, 390–400, 390*f*–400*f*
  VT for, 93–106, 98*f*, 99*f*, 102*f*–105*f*, 106*t*
  with welding, 32, 42–46, 42*f*, 44*f*, 45*f*, 58, 98–106, 98*f*, 99*f*, 102*f*–105*f*
  X-rays for, 132
DISPERSE, 697
Dispersion, 701–711, 702*f*–708*f*, 709*t*, 710*f*, 711*f*
Displacement derivatives, 769
Displays:
  for AE, 571*f*–579*f*, 572–579
  for digital radiography, 597–600
  for ET, 439
  for TIR, 508, 510
Distance:
  amplitude:
    blocks, 365, 365*f*, 366*f*
    compensation, 411
  angle beam, 365
  beam path, 357, 376–379, 377*f*, 378*f*
  for borescope, 84
  HD, 350, 391–393
  object to film, 254, 289
  for PAUT, 652–656
  for RT, 279
  SFD, 251, 257, 289
  skip, 352, 414
  for transducers, 347–348
  for VT, 77, 79
Distance, gain, size (DGS) technique, 293, 359–360, 360*f*, 663, 663*f*
Distance amplitude correction (DAC), 293, 357–359, 365, 411, 656
Distorted fields, 179

Ditching, 45, 45*f*
Ditri, J. J., 697, 710
DLP. *See* Digital light processing
Doane, F. B., 6*t*, 12, 132
Document attachment tool, 608
DOF. *See* Depth of field
Domains:
  for ET, 362, 420, 421*f*, 491
  magnetic, 170, 218
Doppler effect, 408, 411
Dose measurement tool, 608
Double wall exposure, 258, 260*f*
  double view technique, 261, 262*f*
Drain time, 164
Drake, H. C., 6*t*, 11–12
Drawing, 96
Dry continuous MT technique, 200
Dry particle technique, 200, 217
Dry powder technique, 151*f*, 153*f*, 164
Dry residual MT technique, 200
Drying oven, 162, 164
Drying time, 164
Dual search unit, 327, 412
Dual transducers, 339–341, 341*f*, 342*f*
Ductility, 46, 56
Dust-tight, 126
Duty cycle, 240, 288
Dwell time, 131, 146, 164
Dynamic range, 412, 518, 519

E

E-scan, 691
Eddy current testing (ET), 5, 6*t*, 7*t*, 15
  AC for, 417, 424–431, 425*f*, 426*f*, 428*f*–431*f*, 490
  advantages and limitations of, 476–477
  coils for, 438, 443–451, 443*f*–451*f*
  for discontinuities, 431–432, 432*f*, 463–468, 463*f*, 465*f*–468*f*
  equipment for, 438–453, 439*f*–453*f*
  glossary of, 490–494
  history and development of, 415–417
  impedance plane for, 430–431, 431*f*
    displays for, 454–475, 455*f*–458*f*, 461*f*–463*f*, 463*t*, 465*f*–475*f*
    instruments for, 440–441, 440*f*, 441*f*
  inductance for, 424–429, 426*f*, 428*f*, 492
  lift-off for, 438, 457–459, 458*f*, 492
  PEC, 478–490, 480*f*–485*f*, 487*f*–489*f*
  standards for, 451–453, 453*f*
  theory and principles of, 417–423, 418*f*–421*f*, 423*f*, 424*f*
  voltage for, 418, 435, 435*f*
  voltage plane for, 429–430, 429*f*, 430*f*
Eddy currents, 431–438, 433*f*, 491
Edge effect, 459–460, 459*f*
Editing tools, 608
Effective depth of penetration, 434, 464, 491
Eigenfunctions, 558
Electric current, 182–186, 182*f*–185*f*, 415, 490
  induction, 6*t*, 11–12
  magnetism from, 177–179, 178*f*, 179*f*
Electric resistive welded pipe (ERW), 676, 677*f*
Electricity, 417–420, 491
Electromagnetic acoustic transducer (EMAT), 338–339, 338*f*, 710
Electromagnetic field direction, 177–179, 178*f*
Electromagnetic induction, 415–416, 491
Electromagnetic radiation, 503, 504, 505*f*, 538
Electromagnetic spectrum, 495, 538
Electromagnetic yoke, 192–193, 192*f*, 196, 208
Electromagnetism, 422, 425, 491
Electromagnets, 420, 491
Electrons, 417–418, 491
Elongation, 18, 33–34, 33*f*, 48
EMAT. *See* Electromagnetic acoustic transducer
Emissivity, 505–507, 506*t*, 517, 538
Empty coil, 454, 491
Emulsification time, 136–137, 164
Emulsifiers, 143, 162
  hydrophilic, 152–154, 154*f*, 164
  lipophilic, 152–154, 153*f*, 165
EN 473, 27
Encircling coils, 449–450, 449*f*, 450*f*, 473, 474*f*
Encoding, 635–636
Endoscope, 70, 71, 126
Energy surveys, 535–536, 536*f*
Entrant surface, 412
Equilibrium phase diagrams, 39–40, 40*f*
Equivalent penetrameter sensitivity (EPS), 288, 610
Erdman, Donald C., 6*t*
Erosion, 91, 92, 107–115, 126
ERW. *See* Electric resistive welded pipe
ET. *See* Eddy current testing
Etchants, 141
Etching, 132, 165
European Standard EN 4179, 739
Evaluation:
  for AE, 579–580, 579*f*
  for MT, 209–213, 210*f*, 212*f*
  for PAUT, 652–664, 652*f*–664*f*
  for PT, 158–159, 159*f*, 165
  for RT, 269–274, 270*f*
  for shearography, 766–768, 767*f*
  for TIR, 520–521
  for UT, 403–405, 403*f*
Evaporograph, 495–496
Event, 565, 582, 583
Excessive reinforcement, 101, 103*f*, 272
Exfoliation, 56

Explosion-proof, intrinsically safe, purged and pressurized, 126
Exposure table, 244, 288
Exposure time, 279
Extensometers, 408
External reference coil, 444, 444*f*, 491
Extruding, 96
Eyes, 72–73, 73*f*, 76, 77–78, 270

F

FAC. *See* Flow-accelerated corrosion
Face-centered-cubic (FCC), 40
False indication, 165, 209–210, 269, 579
Family, 139, 165
Far field, 316, 320–322, 320*f*–322*f*, 412
Faraday, Michael, 6*t*, 15, 415
Faraday's law, 425
Farrow, C., 6*t*
Fast frequency analysis (FFA), 713–715, 715*f*
Fastener (doughnut) probe, 446, 446*f*
Fatigue cracks, 42, 49–51, 50*f*, 56, 108–109
  from AE, 547–548, 547*f*
  applications and techniques for, 109–115
  surface finish and, 54
Fatigue life, 18
FBH. *See* Flat-bottomed hole
FCAW. *See* Flux core arc welding
FCC. *See* Face-centered-cubic
FDA. *See* Food and Drug Administration
Federal Regulations, 69
Felicity effect, 550*f*, 583
FEM. *See* Finite elements method
Ferrite iron, 40
Ferritic steel, 43–44, 52
Ferromagnetic metals, 168, 173, 179, 217, 420, 421–422, 462
FFA. *See* Fast frequency analysis
Fiber bridging, 737
Fiber cameras, 84, 85*f*, 122
Fiber optics, 70–71, 71*f*, 83, 83*f*, 126
Fiberglass, 548–550, 549*f*, 550*f*, 738*f*
Field indicators, 189, 204
Field of view (FOV), 89, 518, 539, 738*f*, 741
Filament wound pressure vessel, 769
Fill factor, 459, 491
Fillets, 82, 103
Film badges, 279
Film-based records, 120–121, 121*t*
Film characteristic curve, 249, 250*f*
Film contrast, 288
Film density, 267–269, 267*f*, 268*t*
Film speed, 263, 288
Filters, 279, 288, 441, 510–512
  band-pass, 327–328, 510
  flame, 511
Finite elements method (FEM), 698, 712–723, 712*f*–724*f*
Finite source, 317
Fink, M., 696
Firestone, Floyd, 6*t*, 16, 293
First Law of Thermodynamics, 499, 539
Fish pole technique, 12, 14*f*, 240–241, 242*f*
FL. *See* Focal length
Flakes, 48, 56
Flame filters, 511
Flat-bottomed hole (FBH), 357, 360
Flaws:
  characterization, 412
  detectors, 6*t*, 294, 296, 318, 513, 677
Flow-accelerated corrosion (FAC), 485
Fluid level measurement, 407
Fluorescence, 201, 205, 217
Fluorescent penetrant system, 15, 15*f*, 132, 133, 136, 136*f*, 137*f*, 149, 150*f*, 154–156
Fluorescent screens, 258
Fluorometallic screens, 258
Fluoroscopic system, 585–588, 586*f*, 587*f*
Flux, 100, 126, 208, 217
Flux core arc welding (FCAW), 42
Flux density:
  coercive force and, 174, 174*f*
  for ET, 420, 421*f*, 491
  hysteresis and, 172–177, 172*f*–177*f*
  magnetizing force and, 175
  for MT, 170, 218
  polarity and, 174–175, 175*f*
  residual magnetism and, 175–177
Flux field, 434
  penetration, 218
Flux leakage testing, 477
Flux lines, 420
FMC. *See* Full matrix capture
Focal laws, 626, 630–631, 691
Focal length (FL), 89
Focal plane array (FPA), 496, 508–509
Focal spot, 288, 626
Focused transducers, 341–342, 343*f*
FOD. *See* Foreign object debris
Foerster, Friedreich, 416
Fog, 264, 265, 288
Folds, 46, 56, 95
Food and Drug Administration (FDA), 768
Foot-candle, 79, 126, 158, 165
Forced convection, 503, 539
Foreground, 516, 539
Foreign object debris (FOD), 757
Forging:
  discontinuities, 32, 46–47, 46*f*, 56
  folds, 95
  laps, 62*f*, 95

Fossil-fuel power plants, 92
Fourier analysis, 553
Fourier's law, 500, 539
FOV. *See* Field of view
Fovea centralis, 126
FPA. *See* Focal plane array
Fractures, 48, 56
Frame (in television), 126
Frequency:
  AE and, 544, 553–554, 583
  ET and, 437–438, 440, 461–462, 462*f*
  FFA, 713–715, 715*f*
  multi-frequency testing, 416, 441–442, 442*f*
  PAUT and, 623
  PRF, 325, 412
  of sound waves, 296
  ultrasonic guided wave inspection and, 703
  UT and, 327–328, 370, 412
Fretting, 54, 56, 107
Fromme, P., 696
FSH. *See* Full screen height
Full matrix capture (FMC), 683–690, 685*f*–689*f*
Full screen height (FSH), 322, 359–360, 361
Full skip techniques, 374–376
Full-wave rectified alternating current (FWAC), 183, 184*f*
Full-wave rectified current (FWDC), 168, 204, 218
Fusion zone, 45
FWAC. *See* Full-wave rectified alternating current
FWDC. *See* Full-wave rectified current

G

G-M. *See* Geiger-Mueller counters
Gain, 326–327, 357, 403, 440
  DGS, 293, 359–360, 360*f*, 663, 663*f*
  TVG, 656, 661–663, 661*f*–663*f*
Galling, 54
Galvanic corrosion, 108
Galvanized steel (GS), 486–488, 488*f*
Gamma iron, 40
Gamma radiography, 6*t*, 12, 239–240, 288
Gamma rays, 228–230, 228*f*, 229*f*, 240–244, 242*f*–244*f*
Gao, H., 698
Gas holes, 56
Gas metal arc welding (GMAW), 98–99, 99*f*
Gas porosity, 37, 37*f*, 44, 56, 59*t*
Gas tungsten arc welding (GTAW), 98–99, 99*f*, 100
Gas voids, 273
Gating, 328–329, 328*f*, 388, 388*f*
Gauss, 170, 208, 209*f*, 420, 492
Geiger-Mueller counters (G-M), 280
General Electric, 15
Generators, 92, 439
Geometric anisotropy, 34
Geometric discontinuities, 45, 53–54, 56, 272–273
Geometric distortion, 126
Geometric unsharpness, 254, 257, 288
Giurgiutiu, V., 712
Glare, 74
Glass filters, 511
Globe valves, 110
GMAW. *See* Gas metal arc welding
Gouges, 53, 56
Graff, K. F., 696, 700
Grain boundary, 34, 56
Graininess, 257, 288
Grains, 56
  brittle fracture and, 52
  in casting, 34–35
  corrosion and, 48
Grating lobes, 681, 682*f*, 691
Grewal, D. S., 697
Grinding cracks, 56
Grinding wear, 107
Gross porosity, 56
GS. *See* Galvanized steel
GTAW. *See* Gas tungsten arc welding
Guard sensors, 570–572, 570*f*, 583
Gunawan, A., 697

H

Half-life, 240, 288
Half skip techniques, 374–376
Half-value layer (HVL), 231–232, 288
Half-wave rectified alternating current (HWAC), 183, 184*f*
Half-wave rectified current (HWDC), 183, 204, 218
Hall, E. H., 449
Hall, J. S., 698
Hall detector, 449
Handheld Gauss meter, 208, 209*f*
Hangers, 112–113
Hardness testing, 18, 19, 20*f*
Hartford Steam Boiler Inspection and Insurance Company, 10, 10*f*
Hayashi, T., 697
HAZ. *See* Heat-affected zone
HD. *See* Horizontal distance
Heat-affected zone (HAZ), 43–45, 44*f*, 56, 100
Heat exchangers, 92, 115, 452*f*
Heat of fusion, 518, 539
Heat wave distortion, 75
Henry, Joseph, 416
Herschel, John, 6*t*, 16, 495–496
Herschel, William, 6*t*, 495
Hertz (Hz), 296, 519
HIC. *See* Hydrogen-induced cracking
High-pass filters, 328, 510

Hinders, M. K., 698
Hirose, S., 697
Hit, 562, 563*f*, 564–572, 582, 583
Hole-type penetrameter, 252, 253*f*
Holographic interferometry, 737
Hooke's law, 694
Horizontal (hum) bars, 126
Horizontal distance (HD), 350, 391–393
Horizontal linearity, 361–362
Horseshoe probe, 445, 445*f*, 492
Hosten, B., 698
Hot cracks, 39, 57
Hot tears, 39, 57, 96, 273
Hsu-Nielsen pencil lead break technique, 556*f*, 557
Hue, 73
Hughes, E. E., 6*t*, 15
Hung, Y. Y., 737
HVL. *See* Half-value layer
HWAC. *See* Half-wave rectified alternating current
HWDC. *See* Half-wave rectified current
Hydrogen embrittlement, 48, 52*f*, 53, 57, 407
Hydrogen-induced cracking (HIC), 44–45, 53, 670–671, 671*f*
Hydrophilic emulsifier, 152–154, 154*f*, 164
Hysteresis, 172–177, 172*f*–177*f*
Hysteresis loop, 175, 177, 177*f*, 218, 422–423, 423*f*
Hz. *See* Hertz

IACS. *See* International Annealed Copper Standard
ICBs. *See* Integrated circuit boards
IEC. *See* International Electrotechnical Commission
IFOV. *See* Instantaneous field of view
IGA. *See* Intergranular attack
IGSCC. *See* Intergranular stress corrosion cracking
IIW. *See* International Institute of Welding
Illumination Engineering Society, 74
Illuminators, 269–270, 270*f*
Image, 126
  in borescope, 84
  with CCD, 86
  definition, 254, 288
  digital, 591
    enhancement, 593, 617
  intensifier, 587–588, 587*f*, 588*f*
  latent, 264, 289, 593, 617
  orientation tool, 608
  recording, 89–91, 90*f*, 91*f*
  retained, 128
  in shearography, 743, 744, 745*f*
  in TIR, 507, 508
    averaging of, 515
Image quality indicator (IQI), 252–258, 253*f*, 255*t*, 256*f*, 256*t*, 258*f*, 496, 589, 612–614
  sensitivity of, 252, 289
Immersion rinse, 165
Immersion testing, 305, 385–386, 385*f*, 386*f*, 387*f*, 412
Impact damage, 737
Impact resistance, 18, 19, 19*f*
Impedance, 492
  acoustic, 304, 412
  amplitude, 430, 431*f*
  phase angle, 430, 431*f*
  plane, 430–431, 431*f*, 440–441, 440*f*, 441*f*
    displays, 454–475, 455*f*–458*f*, 461*f*–463*f*, 463*t*, 465*f*–475
    normalization of, 455–456, 456*f*
  of surface coil, 460
Import and export tools, 608
In-service inspection (ISI), 406
Inclusions, 39, 57, 273
  in casting, 96
  in ingots, 94
  RT for, 272
  TIR for, 516
  with welding, 100
Incomplete fusion, 57
Incomplete penetration, 42, 57, 103–104, 104*f*, 272
Indications:
  in AE, 579
  false, 165, 209–210, 269, 579
  for MT, 217
  nonrelevant, 165, 210
  relevant, 210, 351, 413
  in TIR, 515–516
  in UT, 400, 412
Indium antimonide (InSb), 518, 539
Inductance, 424–429, 426*f*, 428*f*, 492
Inductive reactance, 427, 436*f*, 492
Industrial Radiography, 6*t*, 23
Inertia, 297
Infrared radiation, 504
Ing, R. K., 696
Ingots, 94–95
Inherent discontinuities, 32, 57
Inhomogeneity, 34, 34*n*4, 39
Initial pulse, in UT, 293, 412
Inline inspection, PAUT for, 675–676, 676*f*
InSb. *See* Indium antimonide
Instantaneous field of view (IFOV), 539
Institute of Welding (IOW), 363, 464
Insufficient throat, 103
Insulator/insulation, 529, 539
  CUI and, 478, 486
Integrated circuit boards (ICBs), 521–522
Intensifying screen, 257, 289
Intensity drop technique, 293, 390–391
Intensity threshold, 73
Interface triggering, 388, 388*f*
Interference effects, 316

Intergranular attack (IGA), 48
Intergranular stress corrosion cracking (IGSCC), 48, 669–670, 670*f*
Interlaced scanning, 126
Internal coil, 451, 451*f*, 452*f*, 473, 474*f*, 492
Internal Vessel Visual Inspection (IVVI), 114
International Annealed Copper Standard (IACS), 419, 492
International Electrotechnical Commission (IEC), 768
International Institute of Welding (IIW), 362, 363, 363*f*
International Standards Organization (ISO), 27, 498
Interpass cleaning, 101
Inverse square law, 74, 74*f*
Investment casting, 39*n*6
Ionization chambers, 279
IOW. *See* Institute of Welding
IQI. *See* Image quality indicator
Iris, 72
Iron, 40–41, 41*f*
ISI. *See* In-service inspection
ISO. *See* International Standards Organization
Isotherms, 515–516, 539
Isotopes, 230, 289
IVVI. *See* Internal Vessel Visual Inspection

J

Jaeger test, 73
Job-task-analysis (JTA), 28

K

Kaiser, Joseph, 6*t*, 16, 543
Kaiser effect, 550*f*, 583
Ketos ring, 203, 203*f*
kHz. *See* Kilohertz
Kilocalories, 499, 539
Kilohertz (kHz), 558, 583
Kim, Y. Y., 697, 698
Kinetic energy, 231, 289
Kirchhoff's law, 505, 539
Knee in the curve, 549, 549*f*
Knerr, H. C., 6*t*
Kwun, H., 697

L

Lack of fusion, 43, 57, 64*f*, 101, 272
Lack of penetration, 46, 67*f*
Lamb, Horace, 557
Lamb wave, 300, 383*f*, 384, 384*f*, 412, 557, 558*f*, 559, 698, 708
Lamellar tearing, 34, 57
Laminations, 57, 62*f*, 96, 370, 372, 373*f*, 516–517
Laps, 46, 57, 62*f*, 95
Lasers, 339, 710, 737, 741, 768
Latent energy, 500, 539
Latent heat of fusion, 500, 539
Latent heat of vaporization, 539
Latent image, 264, 289, 593, 617
Lateral resolution, 627, 692
Law of similarity, 474–475
LCDs. *See* Liquid crystal displays
LDA. *See* Linear diode array
Lead metaniobate (PMN), 333
Lead screens, 257, 258*f*
Lead zirconate (PZT), 333, 698
Leakage fields, 179–182, 181*f*, 182*f*, 210, 210*f*
Leaks, 551
LEDs. *See* Light-emitting diodes
Lee, C. Y., 697, 718
Left-hand rule, 178, 178*f*
Lenses:
  for borescope, 84
  as magnifiers, 78, 79*f*
  for TIR, 509
Lenz, Heinrich, 416
Lenz's law, 416, 492
Lester, Horace H., 6*t*, 10–11, 11*f*, 227
Leveling, 603, 603*f*
Li, J., 697, 698, 712
Lift-off, 438, 457–459, 458*f*, 482, 492
Light, 74–77, 145
  black light, 133, 137–138, 138*f*, 163, 167, 188, 193, 194*f*, 211–212, 217
  DLP, 90
  intensity, 587
    meters, 138
  sources of:
    for borescopes, 82–83
    for CCD cameras, 86–87
    for CCD tank cameras, 89
    coherent, 769
    for fiber cameras, 84
    for VT, 79
  ultraviolet, 167, 219
Light-emitting diodes (LEDs), 84, 138
Line pair test pattern, 591*f*, 617
Line pairs per millimeter, 618
Line scanners, 508
Linear accelerators, 238
Linear diode array (LDA), 596, 597
Linear scan, 633, 634*f*, 691
Linking, 635
Lipophilic emulsifier, 152–154, 153*f*, 165
Liquid crystal displays (LCDs), 90, 294, 296, 508, 510, 600
Liquid film developer, 164
Liquid flow rate, 408
Location:
  for AE, 544, 565–572, 567*f*–572*f*, 584
  marker, for RT, 289

Locus, 460, 492
Long-waves, 507, 518, 539
Longitudinal cracks, 100
Longitudinal magnetization, 190–191, 190*f*, 198, 207, 208, 218
Longitudinal wave, 300, 412
Low-pass filters, 328, 510
Lumen, 79, 127

M

Ma, J., 697
Macroshrinkage, 57
Magnaflux Corporation, 11–12, 13*f*, 132–133
Magnetic domains, 170, 218
Magnetic field, 169–170, 169*f*, 435–437, 492
  detection, 6*t*, 11–12
Magnetic flow MT technique, 196, 197*f*
Magnetic flux, 170, 179–182, 181*f*, 182*f*, 435, 436*f*, 492
  left-hand rule for, 178, 178*f*
  right-hand rule for, 178
Magnetic footprint, 482–483
Magnetic forces, 169
Magnetic particle inspection, 209, 218
Magnetic particle testing (MT), 5, 6*t*, 7*t*, 12, 13*f*
  advantages and limitations of, 215–216
  amps for, 184, 185, 205–208
  applications for, 213–215
  for cracks, 209*f*, 211
  demagnetization for, 188–189, 217
  depth limitations for, 211
  detection media for, 186–188, 187*f*, 188*f*
  for discontinuities, 133, 179–182, 180*f*–182*f*, 210–211, 210*f*
  equipment and accessories for, 189–195, 190*f*–195*f*
  evaluation for, 209–213, 210*f*, 212*f*
  glossary for, 217–219
  history and development of, 167–168
  for leakage fields, 179–182, 181*f*, 182*f*, 210, 210*f*
  oil and whiting technique and, 132
  portable units for, 191, 191*f*, 192*f*, 205
  QC for, 202–204, 202*f*–204*f*
  reporting results of, 211–213
  stationary units for, 189–191, 190*f*, 205
  techniques for, 196–204, 197*f*–199*f*, 202*f*–204*f*
  theory and principles of, 168–189, 169*f*, 171*f*–185*f*, 187*f*, 188*f*
  variables for, 204–209, 209*f*
Magnetic poles, 169, 218
  for ET, 462, 493
Magnetic writing, 209, 218
Magnetism, 167, 169–179, 169*f*, 171*f*–179*f*, 218, 420–422, 421*f*, 422*f*, 492
  electromagnetism, 422, 425, 491
  residual, 174, 175–177, 219, 423
Magnetization, 173, 177, 179, 181–182
  circumferential, 196–198, 198*f*, 205, 208, 217
  longitudinal, 190–191, 190*f*, 198, 207, 208, 218
Magnetizing force, 170, 173, 175–177, 218, 422
Magnetograph, 169*f*, 170, 171*f*
Magnifier:
  for CCD tank cameras, 89
  for digital radiography, 604, 605*f*
  in optical comparators, 81
  for RT, 270
  for VT, 78–79, 79*f*
Mal, A. K., 697
Manganese, 34
Manipulator, 388
Martensite, 43–44, 50, 52
MAS. *See* Maximum amplitude system
Material density, 233, 289
Materials Evaluation, 23
Matrix cracking, 548
Maximum amplitude, 293–294
Maximum amplitude system (MAS), 393–396, 394*f*, 395*f*
Maxwell, 420
MECAD. *See* Mechanically coupled acoustic drive
Mechanical fatigue, 109
Mechanical loading, 548–551, 549*f*, 550*f*
Mechanically coupled acoustic drive (MECAD), 766
Mehl, Robert F., 6*t*, 12
Mercury vapor lamp, 193, 218
Metallic glass, 34*n*3
Metallurgical notch, 57, 61*t*
Michaels, J. E., 698
Micro-bolometers, 519
Micro-power gas discharge (MPXL), 138
Microcracks, 100
Microfissure, 57
Microfocus X-ray systems, 588–589, 589*f*, 590*f*
Micrometers, 80
Microprocessor-based ET, 416
Microscopes, 78
Microsegregates, 57
Microshrinkage, 57
Mid-waves, 507, 518, 539
MIL-I-6866, 134
MIL-I-8474, 132
Milliamperes, 236, 289
Milliroentgens, 279
MILSTD-410E, 26
Misalignment, 101
Mismatches, 82
Misrun, 97, 273
Mode, 374, 383, 413
Mode conversion, 293, 309–316, 311*f*–315*f*, 413
Modulation analysis, 478
Modulus of elasticity, 299, 302

Modulus of rigidity, 299–300, 302
Monitors, 90, 90*f*, 124
MPXL. *See* Micro-power gas discharge
MT. *See* Magnetic particle testing
Mu, J., 697
Mudge, P. J., 697, 712
Multi-frequency testing, 416, 441–442, 442*f*
Multigroup inspection, 645, 691
Multiple back reflections, 355, 413
Mutual induction, 427, 428*f*

N

Na, W., 698
Nagy, P. B., 696
Nakadate, S., 737
Nanometer, 74
NAS 410, 26
National Electrical Manufacturers Association (NEMA), 613
National Fire Protection Association (NFPA), 498, 524
Natural convection, 503, 540
Navier's equation, 694, 703
NAVSEA 250-1500-1, 26–27
NDE. *See* Nondestructive evaluation; Nondestructive examination
NDI. *See* Nondestructive inspection
NDT. *See* Nondestructive testing
Near field, 316, 318, 320–322, 320*f*–322*f*, 413
NEMA. *See* National Electrical Manufacturers Association
Newman, J., 737
Newton, Isaac, 73
Newton's law of cooling, 502, 540
NFPA. *See* National Fire Protection Association
90° probe, 445, 446*f*
Noise. *See also* Signal-to-noise ratio
  AE and, 552–553, 584
  CNR, 617
  shearography and, 741
  in UT, 320, 413
Nominal pipe size (NPS), 87
Non-uniformity correction (NUC), 519
Nonaqueous developer, 144, 164
Nondestructive evaluation (NDE), 1
Nondestructive examination (NDE), 1
Nondestructive inspection (NDI), 1
Nondestructive testing (NDT). *See also specific techniques*
  benefits of, 21
  certification for, 22–28
  codes and standards for, 3
  concerns with, 3
  conditions for, 21–22
  defined, 1–2
Nondestructive testing (NDT) (*Cont.*):
  versus destructive testing, 17–21, 18*f*–20*f*
  history of, 3–17, 4*f*, 5*f*, 6*t*, 8*f*–17*f*
  limitations of, 21
  methods of, 5, 7*t*
  performance requirements for, 69–70
  SHM and, 709–710, 709*t*
Nonmetallic inclusion, 57
Nonrelevant indication, 165, 210
Normal incidence, 388
Normalization:
  for ET, 460, 492–493
  of impedance plane for ET, 455–456, 456*f*
  for ultrasonic guided wave inspection, 704*f*
  in UT, 386
Notches, 45, 53, 57, 61*t*
NPS. *See* Nominal pipe size
NUC. *See* Non-uniformity correction
Nuclear power:
  CCD cameras for, 114–115
  PAUT for, 621–622
  RVT for, 92
  thermal shearography for, 757
Nucleus, 417, 493
Null method, 516

O

Object, 72–73, 73*f*, 75, 127
  to film distance, 254, 289
  ratio, 73
O'Connor, Donald, 227
OCTG. *See* Oil country tubular goods
Oersted, Hans Christian, 167, 415
Offset method for shear waves, 389–390, 389*f*
Ohm's law, 430, 493
Oil and whiting technique, 6*t*, 15, 131–132
Oil country tubular goods (OCTG), 676
One-line scan, 636–638, 638*f*, 691
Optical comparators, 81
Oscillation, 298
Over-emulsification, 165
Over-removal, 148, 165
Overlap, 101, 103*f*
Overreinforcement, 101, 103*f*, 272

P

Pair production, 231, 232*f*
Pan, 88–89, 88*f*
Pan, tilt, and zoom (PTZ), 123
Pancake probe, 446, 446*f*
Paramagnetic metals, 168, 171, 421–422
Parametric inputs, 584
Partial discharge, 552
Partial vacuum shearography, 750*t*, 752–757, 753*f*–759*f*

Particle mobility, 200, 218
Particles, 187, 187*f*, 205
Passive plane, 623*f*, 692
PAUT. *See* Phased array ultrasonic testing
Pavlakovic, B., 697
PCBs. *See* Printed circuit boards
PDPs. *See* Plasma display panels
PE. *See* Post-emulsification
PEC. *See* Pulsed eddy current
Pencil probe, 445, 446*f*
Penetrameter, 252–254, 253*f*, 255*t*, 256*t*, 261
  EPS for, 288, 610
Penetrant, 141–142
  application of, 146, 147*f*
  comparator block, 138–139, 159*f*, 165
  post-emulsifiable, 136–137, 152–154, 153*f*, 156–157, 165
  removal of, 148, 148*f*
  solvent-removable, 152–154, 154*f*, 157–158, 165
  visible, 134, 156–158, 165
  water-removable, 150–152, 151*f*, 156, 165
Penetrant testing (PT), 5, 6*t*, 7*t*, 15, 15*f*
  advantages and limitations of, 162–163
  applications for, 160
  capillary action in, 135–136, 135*f*
  early techniques, 133–134
  equipment for, 136–139, 136*f*–138*f*
    checks of, 162, 163*f*
  evaluation for, 158–159, 159*f*, 165
  glossary for, 163–166
  history and development of, 131–134
  materials for, 139–144, 140*f*, 142*f*
  procedures for, 144–150, 146*f*–150*f*
  QC for, 160–162
  techniques and variables of, 150–158, 151*f*, 151*t*, 153*f*–155*f*
  theory and principles of, 135–136
Penetration depth, 413, 437, 438*f*
Perception, 76
Peripheral vision, 127
Permanent magnets, 193, 193*f*, 420–421, 493
Permeability:
  ET and, 417, 421, 422–423, 437, 493
  in magnetism, 170–171, 171*f*, 218
Personnel Certification in Nondestructive Testing, 28
Personnel protective equipment (PPE), 525
PEV. *See* Pyro electric vidicon
Phase change, 540
Phase diagram-binary, 39, 58
Phase diagrams, 39, 57
Phase lag, 457, 457*f*, 463, 463*f*
Phase stepper, 742–743
Phase transformation, 552
Phased array probe, 621, 627–628, 627*f*, 628*f*, 691
Phased array ultrasonic testing (PAUT):
  A-scan for, 631, 631*f*, 690
  applications for, 664–680, 665*f*–672*f*, 674*f*–679*f*
  AWS on, 663–664, 664*f*
  B-scan for, 632–633, 633*f*, 638, 690
  beam angle in, 626–627
  beam forming for, 624–625, 625*f*, 690
  beam sequencing for, 630–631, 631*f*
  beam steering for, 628–630, 630*f*, 690
  benefits of, 680–681
  billet in, 677–678, 678*f*
  C-scan for, 636–638, 638*f*, 690, 691
  calibration for, 647–651, 648*f*–651*f*
  combined image display for, 638–639, 639*f*
  composite viewing in, 672–673
  cross-sectional B-scan for, 632–633, 633*f*, 638, 690
  DGS for, 663, 663*f*
  evaluation for, 652–664, 652*f*–664*f*
  FMC and, 683–690, 685*f*–689*f*
  focal laws for, 626, 630–631, 691
  glossary for, 690–692
  for HIC, 670–671, 671*f*
  history and development of, 619–622, 620*f*, 621*f*
  for IGSCC, 669–670, 670*f*
  imaging modes for, 631–639, 632*f*–640*f*
  for inline inspection, 675–676, 676*f*
  instruments for, 640–646, 641*f*, 643*f*, 644*f*
    setup of, 646–647, 646*f*
  limitations of, 681–683, 682*f*
  linear scan for, 633, 634*f*, 691
  multigroup inspection for, 645, 691
  one-line scan for, 636–638, 638*f*, 691
  for piping, 676–678, 677*f*, 678*f*
  portable units for, 621–622, 621*f*
  for radius inspection, 673–674, 675*f*
  S-scan for, 633–636, 635*f*, 636*f*, 692
    porosity in, 667, 667*f*
  sensitivity calibration for, 650–651, 651*f*, 691
  sizing methods for, 656–664, 657*f*–656*f*
  TFM and, 683–690, 685*f*–689*f*
  theory and principles of, 622–639, 622*f*–628*f*, 630*f*–640*f*
  transducers for, 342–344, 344*f*, 619, 622–623, 622*f*
  TVG for, 656, 661–663, 661*f*–663*f*
  velocity calibration for, 648, 648*f*, 649*f*
  wedge delay calibration for, 648–650, 650*f*, 691
  wedges for, 623–624, 624*f*
  for welding, 620*f*, 666–672, 666*f*–672*f*
Phasing, 620, 691
Photoelectric effect, 231
Photographic cameras, 120
Photographic techniques, 121–122
Photoluminescent glasses, 280
Photons, 240, 289
Photostimulable luminescence, 618

Photostimulable luminescent phosphor, 618
Pie gauge, 194, 194*f*
Piercing, 96
Piezoelectric effect, 291–292, 324, 331–333, 335, 337*f*
  shearography and, 741
  ultrasonic guided wave inspection and, 698, 710
Pipe supports, 112–113
Pipe techniques, for UT, 379–381, 379*f*–381*f*, 381*t*
Piping:
  PAUT for, 676–678, 677*f*, 678*f*
  RVT for, 92, 112
  ultrasonic guided wave inspection for, 697, 705–707, 705*f*, 706*f*, 715, 715*f*–718*f*
    challenges with, 730*t*
    successes with, 729*t*
Pitch, 296, 629, 692
Pitting, 47–48, 47*f*, 58, 80, 81
Pixels, 121, 127
  bad, 613
  CCD and, 86
  of CCD digital cameras, 91
  digital radiography and, 594, 618
  shearography and, 743
  TIR and, 514
  of VT monitors, 90
Plasma display panels (PDPs), 90
Plastic deformation, 46–47, 46*f*, 50
Plate, ultrasonic guided wire inspection for, 698, 724, 725*f*, 726*f*
Plate waves, 300
Plating, ET for, 471, 471*f*
PMN. *See* Lead metaniobate
Point source, 316–319, 316*f*–319*f*
Poisson's ratio, 302, 693
Polansky, Daniel, 227
Polarity:
  coercive force and, 175, 176*f*
  for ET, 420, 420*f*, 493
  flux density and, 174–175, 175*f*
  in magnetism, 169, 171
Poling process, 333
Polymers, 551
Polyvinylidene fluoride (PVDF), 335–338
Porosity:
  in casting, 36
  gas, 37, 37*f*, 44, 56, 59*t*
  gross, 56
  microshrinkage, 57
  in PAUT S-scan, 667, 667*f*
  RT for, 272, 273
  shearography for, 737
  shrinkage, in casting, 36
  surface, 36, 65*f*
  with welding, 100, 101
Portable units:
  for MT, 191, 191*f*, 192*f*, 205
  for PAUT, 621–622, 621*f*
  for X-rays, 227
Post-cleaning, 150, 165
Post-emulsifiable penetrant, 136–137, 152–154, 153*f*, 156–157, 165
Post-emulsification (PE), 134, 151*t*, 165
Post-weld heat treatment (PWHT), 43, 44
PPE. *See* Personnel protective equipment
Precleaning, 139, 146, 146*f*, 166
Present tools, 608
Preservice inspection (PSI), 406
Pressure shearography, 749–752, 750*t*, 751*f*
PRF. *See* Pulse repetition frequency
Primary processing discontinuities, 32, 58, 95–97
Primary radiation, 257, 289
Printed circuit boards (PCBs), 514
Printing tool, 608
Probe, 445, 446, 446*f*, 492
  coil, 422, 493
  index, 350, 351
  for PEC, 483–485, 483*f*, 484*f*
  phased array, 621, 627–628, 627*f*, 628*f*, 691
Prods, 200, 208, 218
PRR. *See* Pulse repetition rate
Pruell, C., 698
Pseudo color tool, 609
PSI. *See* Preservice inspection
PT. *See* Penetrant testing
PTZ. *See* Pan, tilt, and zoom
Pulse-active thermography, 516
Pulse-echo technique, 366–374, 368*f*–373*f*, 413
Pulse length, 334, 346, 413
Pulse repetition frequency (PRF), 325, 412
Pulse repetition rate (PRR), 325
Pulse width, 347
Pulsed eddy current (PEC), 478–490, 480*f*–485*f*, 487*f*–489*f*
  A-scan for, 481, 481*f*, 482*f*, 488, 489*f*
  C-scan for, 489*f*
Pulser, 324, 325, 327, 631
  voltage, 642
Pumps, 109–110
Puthillath, P., 698
PVDF. *See* Polyvinylidene fluoride
PWHT. *See* Post-weld heat treatment
Pyro electric vidicon (PEV), 496
PZT. *See* Lead zirconate

Q

QC. *See* Quality control
QDE. *See* Quantum detection efficiency

QF. *See* Quality factor
QQI. *See* Quantitative quality indicator
Qualitative thermography, 540
Quality assurance, 600
Quality control (QC), 160–162, 202–204, 202*f*–204*f*
Quality factor (QF), 279, 339
Quantitative quality indicator (QQI), 195, 195*f*
Quantitative thermography, 507, 520, 540
Quantum detection efficiency (QDE), 595
Quartz transducers, 6*t*
Quasi-steady-state heat flow, 499, 540

R

R-value, 501, 540
Radian, 424, 434
Radiation, 503–507, 506*t*, 540
  electromagnetic, 503, 504, 505*f*, 538
  infrared, 504
  primary, 257, 289
  secondary, 257, 289
Radiographic contrast, 254, 256*f*, 289
Radiographic definition, 254, 256*f*, 288
Radiographic density, 261, 288
Radiographic equivalence factors (REFs), 247–249, 249*t*
Radiographic film, 263–264
  processing of, 264–266, 264*f*, 265*f*
Radiographic quality levels (RQLs), 252, 254, 256*f*, 289
Radiographic sensitivity, 289
Radiographic testing (RT), 7*t*. *See also* Digital radiography; X-rays
  advantages and limitations of, 278
  applications for, 274–278
  for casting discontinuities, 273–274, 275*f*–276*f*
  for cracks, 271
  for discontinuities, 252, 271–274
  equipment and accessories for, 240–244, 241*f*–244*f*
  evaluation for, 269–274, 270*f*
  examples of, 280, 280*f*–287*f*
  film density in, 267–269, 267*f*, 268*t*
  gamma radiography, 6*t*, 12, 288
    principles of, 239–240
  for geometric discontinuities, 272–273
  glossary for, 287–290
  history and development of, 221–230, 222*f*–229*f*, 585–591, 586*f*–590*f*
  for inclusions, 272
  for incomplete penetration, 272
  for lack of fusion, 272
  for porosity, 272
  radiographic film for, 263–264
    processing of, 264–266, 264*f*, 265*f*
  techniques and procedures for, 258–269, 259*f*, 260*f*, 262*f*, 264*f*, 265*f*, 267*f*, 268*t*
  theory and principles of, 230–240, 232*f*, 233*t*, 234*f*, 237*f*, 238*t*, 239*t*
Radiographic testing (RT) (*Cont.*):
  variables of, 245–258, 246*f*, 248*f*, 249*t*, 250*f*, 253*f*, 255*t*, 256*f*, 256*t*, 258*f*
Radiometric, 499, 506, 518, 540
Radiosity, 504, 540
Radium, 6*t*
Radius inspection, 673–674, 675*f*
Raghavan, A., 698
RAH. *See* Refresh after heat
Rail, 697, 718, 719*f*
Range, 325–326, 413, 510
Raster, 127, 668
Rayleigh, Lord, 291
Rayleigh scattering, 231, 232*f*
Rayleigh wave, 300, 300*f*, 413, 557, 693, 704
RBH. *See* Refresh before heat
Real-time X-ray systems, 588, 588*f*
Reference block, 364, 413
Reference cursors, 636
Reference standard, 127
Reflectance of object, 75
Reflection, 127. *See also* Scatter
  attenuation from, 556
  coil, 448, 448*f*, 493
  in optical comparators, 81
  of sound waves, 303–305
  VT and, 75
Reflective mode conversion, 310–316, 311*f*–315*f*
Reflectivity, 74
Reflector, 342, 413, 654
Refraction, 308–309, 308*f*, 309*f*, 529
Refresh after heat (RAH), 762
Refresh before heat (RBH), 762
REFs. *See* Radiographic equivalence factors
Reject control, 329
Relevant indications, 210, 351, 413
Reluctance, 171–172, 218
REM. *See* Roentgen equivalent man
Remnant field, 174
Remote field eddy current testing, 477–478
Remote viewing, 82–89, 127
Remote visual inspection (RVI), 69, 71, 86
Remote visual testing (RVT), 92, 112
Representative quality indicator (RQI), 611, 618
Residential Energy Service Network (RESNET), 498
Residual magnetism, 174, 175–177, 219, 423
Residual MT techniques, 199–201, 204
Resistance, 58, 419, 493, 540
Resistivity, 418
RESNET. *See* Residential Energy Service Network
Resolution, 77, 127
  angular, 692
  with CCD, 86
    digital cameras, 91
  contrast, 591–592, 592*f*

Resolution (*Cont.*):
with ET, 437
with FPA, 508
lateral, 627, 692
SRb, 617
with TIR, 518
of transducers, 347–348, 349*f*
with UT, 402
of VT monitors, 90
Resolving power, 77, 128
Resonant transformer, 238
Restraints, 112–113
Retained image (image burn), 128
Retentivity, 174, 219
Retina, 72, 128
Right-hand rule, 178
Rise time, 559, 584
Rizzo, P., 696
RMS. *See* Root mean square
Robotic crawler tractors, 87, 88*f*, 110, 115
Rock-candy fracture, 52, 52*f*, 551
Rod, 73*f*, 77, 125, 128
Rod techniques, 379–381, 379*f*–381*f*, 381*t*
Roentgen, Wilhelm Conrad, 6*t*, 221–226, 222*f*
Roentgen equivalent man (REM), 279
Rokhlin, S. I., 696
Rolling, 95–96
Roof angle, 340
Roof moisture, 532–535, 532*f*
Room temperature vulcanizing (RTV), 212
Root mean square (RMS), 184, 185
Rose, J. L., 697, 698, 700, 708, 710
RQI. *See* Representative quality indicator
RQLs. *See* Radiographic quality levels
RT. *See* Radiographic testing
RTV. *See* Room temperature vulcanizing
Ruzzene, M., 698
RVI. *See* Remote visual inspection
RVT. *See* Remote visual testing

S

S-scan. *See* Sector scan
SAFEM, 697
Salas, K. I., 698
Saturation, 73, 172, 423, 423*f*
SAW. *See* Submerged arc welding
Saxby, S. H., 6*t*
Sayir, M. B., 696
Scabs, 39, 94, 96, 485
Scale pits, 46–47, 58
Scanning, 351, 413, 508
Scatter, 556, 614
of sound waves, 319–320
SCC. *See* Stress corrosion cracking
Scintillators and scintillating crystals, 595, 618
Scoring, 96
Scratches, 54, 58
Screen height linearity verification, 361
Seams, 39, 46, 64*f*
Search unit, 331, 413
damping, 334, 411
Second Law of Thermodynamics, 499, 540
Secondary processing discontinuities, 32, 58
Secondary radiation, 257, 289
Sector scan (S-scan), 633–636, 635*f*, 636*f*, 667, 667*f*, 692
Segregation, 31, 41, 58
Self-induction, 425–426, 426*f*, 493
Sensitivity:
for AE, 544
contrast, 254, 288
EPS, 288, 610
of ET, 437
IQI, 252, 289
of PAUT, 627–628
calibration for, 650–651, 651*f*, 691
thermal, 515, 518
of transducers, 346
in UT, 339, 414
Sensors:
for AE, 544, 559–561, 561*f*, 582, 584
comb, 728*t*
guard, 570–572, 570*f*, 583
Sequential viewing tool, 604
Service discontinuities, 32, 58, 106–109
Settling test, 202–203, 202*f*
SFD. *See* Source to film distance
Shape of object, 75
Shear vectors, 769
Shear waves:
PAUT and, 677
wedge for, 624
pulse-echo techniques for, 372–373
transducers:
angle beam and, 350, 351, 351*f*
time base calibration for, 356–357, 356*f*
ultrasonic guided wave inspection and, 694
UT and, 293, 294, 300, 300*f*, 333
velocity of, 302
Shearography:
ACAD, 766, 767*f*
advantages and limitations of, 768
applications and techniques for, 749–766, 750*t*, 751*f*, 753*f*–766*f*
C-scan for, 739, 746
calibration for, 744–745
cameras for, 739–741, 742*f*
for discontinuities, 737, 739
equipment and accessories for, 746, 747*f*–749*f*
glossary for, 769
history and development of, 737–739, 738*f*

Shearography (*Cont.*):
image in, 743, 744, 745*f*
partial vacuum, 750*t*, 752–757, 753*f*–759*f*
pressure, 749–752, 750*t*, 751*f*
theory and principles of, 739–746, 740*f*–746*f*
thermal, 750*t*, 757–764, 760*f*–765*f*
vibration, 750*t*, 764–766, 766*f*
Shield metal arc welding (SMAW), 42, 98, 98*f*
Shielded coil, 447, 447*f*, 493
Shielding, 279
Shim-type penetrameters, 252, 254, 255*t*, 256*t*
SHM. *See* Structural health monitoring
Shrinkage:
in casting, 35–39, 36*f*, 38*f*, 55
RT for, 273
Side lobes, 681, 692
Signal, 582, 584
Signal description, 584
Signal features, 582, 584
Signal-shaping chain, 553–563, 553*f*, 555*f*, 556*f*, 558*f*–564*f*
Signal-to-noise ratio (SNR), 327
in digital radiography, 592, 592*f*, 610, 618
in RT, 585, 589, 590*f*
Silk, M. G., 294, 397
Simple magnifier, 128
Single value B-Scan, 642, 690
Single wall exposure, 258, 259*f*
Sinusoid, 424, 425*f*, 493
SIS. *See* Specific industry sector
Size of object, 75
Skin effect, 186, 433, 493
Skip distance, 352, 414
Slags, 42, 58, 62*f*, 100
in castings, 33, 63*f*
RT for, 273
Slit response function (SRF), 540
Slugs, 96
SMAW. *See* Shield metal arc welding
Smith, Rebecca, 134
SMPTE. *See* Society of Motion Picture and Television Engineers
Snell's law, 308, 309*f*, 624
SNR. *See* Signal-to-noise ratio
SNT. *See* Society for Nondestructive Testing
SNT-TC-1A, 23–25, 69
Snubbers, 112–113
Society for Nondestructive Testing (SNT), 23
Society of Motion Picture and Television Engineers (SMPTE), 600
SOHIC. *See* Stress-oriented hydrogen-induced cracking
Sokolov, S. Y., 6*t*, 292
Solar glint, 526, 540
Soldering, 97
Solenoid, 494
Solidification cracks, 43
Solidification shrinkage, 35–39, 36*f*
Soluble developer, 164
Solvent-removable penetrant, 152–154, 154*f*, 157–158, 165
Solvents, 139
remover, 143–144, 154, 166
Sound path, 397, 414
Sound waves:
absorption of, 319
attenuation of, 316
beam characteristics of, 316–319, 316*f*–319*f*
beam spread of, 320–322, 320*f*–322*f*
diffraction effects of, 316
interference effects of, 316
mode conversion of, 309–316, 311*f*–315*f*
nature of, 295–296
PAUT and, 619
point source for, 316–319, 316*f*–319*f*
propagation modes for, 298–300, 299*f*, 300*f*
properties of, 301–324, 306*f*–307*f*
reflection of, 303–305
refraction of, 308–309, 308*f*, 309*f*
scatter of, 319–320
velocity of, 301–302
vibration and periodic motion of, 296–298, 296*f*–298*f*
wavelength of, 302–303
Source energy, for AE, 584
Source to film distance (SFD), 251, 257, 289
Sources:
for AE, 544–553, 582, 584
of light:
for borescopes, 82–83
for CCD cameras, 86–87
for CCD tank cameras, 89
coherent, 769
for fiber cameras, 84
for VT, 79
point, 316–319, 316*f*–319*f*
in RT, 261, 289
of ultrasonic guided wave inspection, 710, 710*f*, 711*f*
Span, 510, 540
Spatial resolution:
for DDA, 613
for digital radiography, 591
for RT, 587
for TIR, 508, 540
Spatter, 105
Specific activity, 240
Specific heat, 500, 540
Specific industry sector (SIS), 28
Specifications, 128
for VT, 93
for welding, 101

Sperry, Elmer, 6*t*, 11–12
Sperry Products, 16, 17*f*
Sperry Rail Service, 11, 12*f*
Spinning coils, 450, 451*f*
Split-screen tools, 604, 605*f*
Splits, 37, 47, 58
Spot radiometers, 507, 508, 540
Spot size, 507, 541
Spring-loaded surface coil, 446, 446*f*
Spring supports, 112–113
Sproule, D. O., 6*t*, 293
Squint angle, 340
Squirters, 344, 345*f*
SRb. *See* Basic spatial resolution
SRF. *See* Slit response function
Standard depth of penetration, 433–434, 494
Standards, 128
  of ASTM, 611
  for ET, 451–453, 453*f*
  for VT, 93
Starling, Becky, 134
Stationary units, 189–191, 190*f*, 205
Statistics tool, 609, 609*f*
Steady-state heat transfer, 514, 518, 541
Steam cleaning, 140
Steam traps, 530
Steel:
  AE for, 556
  carbon-molybdenum, 41
  elongation in, 33–34, 33*f*
  ferritic, 43–44
  GS, 486–488, 488*f*
  stringers in, 33–34, 33*f*
  ultrasonic guided wave inspection for, 704, 704*f*–706*f*, 705–707
  for UT, 335
Steering plane, 692
Stefan-Boltzmann constant, 503, 541
Stefan-Boltzmann law, 506, 541
Step wedge comparison film, 290
Stepwise cracking, 670–671
Stetson, Karl, 737
Stockman, Lloyd, 134
Stop bath, 265
Storage memory, 329
Storage tools, 609
Straight beam compression wave technique, 293, 348
Straightedge scale, 80
Stress:
  AE and, 545
  analyses, UT for, 407–408
  cracks from, 546–547
  in shearography, 746–747, 769
Stress corrosion cracking (SCC), 48, 49*f*, 53
  IGSCC, 48, 669–670, 670*f*
Stress-oriented hydrogen-induced cracking (SOHIC), 670–671
Stress/strain curve, 545, 546*f*
Stringers, 33–34, 33*f*, 58, 59*t*
Structural health monitoring (SHM), 695–696, 698, 709–710, 709*t*
Subject contrast, 290
Submerged arc welding (SAW), 42, 98, 98*f*
Subsonic vibrations, 296
Sultana (steamship), 9–10, 9*f*
Sun, Z., 697, 707
Supersonic Reflectoscope, 16
Suppression reject, 413
Surface coil, 445–449, 445*f*–449*f*, 460, 494
Surface condition:
  for light, 75
  for PT, 145
  for UT, 402
Surface finish, 54
Surface porosity, 36, 65*f*
Surface waves, 300, 300*f*
Suspension concentration test, 202
Sweep controls, 325–326
Swing check valves, 110
Switzer, Joseph, 15, 132
Switzer, Robert, 15, 132–133

T

TAM panel. *See* Testing and Monitoring panel
Tandem techniques, 382
Tanks:
  PT for, 136
  RVT for, 92
  TIR for, 530–532, 531*f*, 532*f*
  VT for, 113–115
Target, 236, 290, 517
Target to film distance (TFD), 251
Temperature:
  absolute scale for, 499, 537
  critical, 52
  Curie, 333, 334*t*
  light and, 75
  PT and, 145
  thermal energy and, 499
  TIR and, 524, 541
    calibration of, 511
  UT and, 401, 406–407
Templates, 82
Tenney, Gerald, 227
Tensile stress, 49
Tensile testing machine, 18*f*
Tesla, 170, 219, 420
Test panels, 138–139
Testing and Monitoring (TAM) panel, 138–139, 166

Texture, 34*n*5
of object, 75
TFD. *See* Target to film distance
TFM. *See* Total focusing method
Thermal background, 541
Thermal capacitance, 516, 541
Thermal conductivity, 500–501, 501*t*, 541
Thermal cycling, 50
Thermal diffusivity, 501, 517
Thermal energy, 499–500, 506
Thermal fatigue, 109
Thermal imaging, 16
Thermal infrared testing (TIR), 7*t*
advantages and limitations of, 537
applications for, 521–536, 524*f*, 526*f*, 527*f*, 528*t*, 529*f*–533*f*, 536*f*
equipment and accessories for, 507–512
evaluation for, 520–521
glossary for, 537–541
history and development of, 495–498, 497*f*
techniques for, 512–517, 513*f*, 515*f*
theory and principles of, 498–507, 501*t*, 502*f*, 505*f*, 506*t*
variables for, 517–520
Thermal mapping, 513–515, 514*f*
Thermal nondestructive evaluation (TNDE), 495
Thermal nondestructive testing (TNDT), 496, 501
Thermal resistance, 501, 541
Thermal sensitivity, 515, 518
Thermal shearography, 750*t*, 757–764, 760*f*–765*f*
Thermocouple, 495, 499
Thermodynamics, 501, 541
Thermographers, 500, 503, 504, 521, 524–525, 528, 537, 541
Thermography, 6*t*, 495, 498, 501, 507, 541
Thermoluminescent dosimeters (TLDs), 280
Thompson, R. B., 697
Three-phase current, 185, 185*f*, 512, 526–527
Threshold of detectability, 3
Through-thickness dimension, 293
Through-transmission technique, 381–382, 414, 448–449, 448*f*, 494
Thumbnail view tools, 604, 606*f*
Tilt, 88–89, 88*f*
Time:
for AE, 563
for RT, 279
threshold, 73
for transducers, 347
Time base calibration:
for compression waves, 353–356, 354*f*–356*f*
for shear wave transducers, 356–357, 356*f*
Time-base trigger module, 324
Time of flight diffraction (TOFD), 294, 300, 367
B-scan for, 399, 399*f*–401*f*
for discontinuity sizing, 397–400, 397*f*–400*f*
for PAUT, 635, 668, 669*f*
Time-varied gain (TVG), 656, 661–663, 661*f*–663*f*
Tip, 84, 128
diffraction signal, 293–294
TIR. *See* Thermal infrared testing
TLDs. *See* Thermoluminescent dosimeters
TNDE. *See* Thermal nondestructive evaluation
TNDT. *See* Thermal nondestructive testing
TOFD. *See* Time of flight diffraction
Tomography, 698, 720–721, 721*f*–724*f*
Total focusing method (TFM), 683–690, 685*f*–689*f*
Total Quality Management (TQM), 101
Toughness, 18
TQM. *See* Total Quality Management
Trace, 128
Transducers, 6*t*
for AE, 544
for PAUT, 342–344, 344*f*, 619, 622–623, 622*f*
shear wave, time base calibration for, 356–357, 356*f*
for ultrasonic guided wave inspection, 694–695, 698
for UT, 29, 296, 324, 330–346, 414
angle beam, 333, 334–335, 337*f*, 348, 349*f*, 350, 351, 351*f*, 410
bandwidth of, 327, 339, 340*f*
compression wave, 347–350, 348*f*, 349*f*
damping for, 334
dual, 339–341, 341*f*, 342*f*
EMAT, 338–339, 338*f*
focused, 341–342, 343*f*
frequency of, 327–328
phased array, 342–344, 344*f*
piezoelectric effect for, 335, 337*f*
problems with, 346
PVDF for, 335–338
tandem techniques for, 382
through-transmission technique for, 381–382, 414
wheel, 344–346
Transfer correction, 359
Transient transfer, 518, 541
Transmitted film density, 245, 290
Transverse cracks, 100
Tube current, 290
Turbines, 92
TVG. *See* Time-varied gain

U

Ultimate tensile strength, 18
Ultrasonic cleaning, 140, 140*f*
Ultrasonic flaw detector, 6*t*
Ultrasonic guided wave inspection, 693–730
advantages of, 727–728
angle beam and, 710*f*
attenuation and, 707, 707*f*

Ultrasonic guided wave inspection (*Cont.*):
bulk waves and, 708–709, 709*t*
challenges with, 729, 729*t*, 730*t*
dispersion and, 701–711, 702*f*–708*f*, 709*t*, 710*f*, 711*f*
FEM and, 698, 712–723, 712*f*–724*f*
fundamentals of, 699–701, 699*t*, 700*f*, 701*t*
limitations of, 728
literature survey on, 696–698, 699*f*
market forces on, 695–696
normalization for, 704*f*
for piping, 705–707, 705*f*, 706*f*
sources of, 710, 710*f*, 711*f*
for steel, 704, 704*f*–706*f*, 705–707
successes with, 728, 728*t*–729*t*
transducers for, 694, 698
Ultrasonic modal analysis technique (UMAT), 698, 726–727, 726*f*, 727*f*
Ultrasonic testing (UT), 6*t*, 7*t*, 16, 17*f*. *See also* Phased array ultrasonic testing; Sound waves
A-scan for, 329–330, 329*f*, 330*f*, 348*f*, 387*f*, 410
advantages and limitations of, 408–410
applications for, 405–408
attenuation and, 326–327, 370, 402, 410
B-scan for, 6*t*, 330, 331*f*, 399*f*, 410
C-scan for, 6*t*, 330, 332*f*, 410
calibration for, 347–365
calibration blocks for, 362–364, 363*f*, 364*f*
dendrite and, 402–403
for discontinuities, 292, 370–372, 374*f*–375*f*, 406
sizing of, 390–400, 390*f*–400*f*
economic factors for, 405
equipment for, 324–347, 324*f*, 326*f*, 328*f*–334*f*, 336*f*–338*f*, 340*f*–345*f*
evaluation for, 403–405, 403*f*
full skip techniques for, 374–376
gain and, 326–327, 403
gating in, 388, 388*f*
half skip techniques for, 374–376
history of, 291–294, 294*f*, 295*f*
immersion testing for, 385–386, 385*f*, 386*f*, 387*f*, 412
intensity drop technique in, 293, 390–391
interface triggering in, 388, 388*f*
Lamb wave in, 300, 383*f*, 384, 384*f*
for laminations, 96
lasers for, 339
manipulator in, 388
normalization in, 386
offset method for shear waves for, 389–390, 389*f*
PEC and, 478
pipe techniques for, 379–381, 379*f*–381*f*, 381*t*
reference block in, 364, 413
resolution and, 402
rod techniques for, 379–381, 379*f*–381*f*, 381*t*
surface condition for, 402
Ultrasonic testing (UT) (*Cont.*):
techniques for, 346–400
temperature and, 401, 406–407
theory and principles of, 295–323, 296*f*–300*f*, 306*t*–307*t*, 308*f*, 309*f*, 311*f*–321*f*, 323*f*
for thickness measurement, 405–406
transducers for, 29, 296, 324, 330–346, 414
angle beam, 333, 334–335, 337*f*, 348, 349*f*, 350, 351, 351*f*, 410
bandwidth of, 327, 339, 340*f*
compression wave, 347–350, 348*f*, 349*f*
damping for, 334
dual, 339–341, 341*f*, 342*f*
EMAT, 338–339, 338*f*
focused, 341–342, 343*f*
frequency of, 327–328
phased array, 342–344, 344*f*
piezoelectric effect for, 335, 337*f*
problems with, 346
PVDF for, 335–338
tandem techniques for, 382
through-transmission technique for, 381–382, 414
wheel, 344–346
variables for, 400–403
Ultrasonic vibrations, 296
Ultraviolet light, 167, 219
UMAT. *See* Ultrasonic modal analysis technique
Undercut, 45, 58, 82, 101, 102*f*, 272–273
Underfill, 101, 102*f*
Uniform corrosion, 108
Unity, 171
USAF Resolution Test Target, 90
UT. *See* Ultrasonic testing

V

Valves, 110–111
Van de Graaf generators, 238
Van Velsor, J. K., 698
Vapor degreasing, 139–140
Vee path, 414
Velichko, A., 697
Velocity:
of AE waves, 557–559
calibration, for PAUT, 648, 648*f*, 649*f*
of sound waves, 301–302
ultrasonic guided wave inspection and, 694–695, 703
UT and, 401
Venna, S., 698
Vernier caliper, 81
Vertical linearity, 361
Vessels, 113–115
Vibration dampers, 112–113
Vibration shearography, 750*t*, 764–766, 766*f*

Video, 128
Video borescopes, 84, 85*f*, 86, 122
Videoendoscopes, 71
Videoscope, 128
Virtual aperture, 647, 692
Viscosity, 141–142, 166
Visibility, 128
Visible penetrant, 134, 156–158, 165
Vision, 128
Visual acuity, 73, 128
Visual angle, 73, 76–77, 76*f*, 128
Visual field, 128
Visual perception, 128–129
Visual testing (VT), 2, 5, 7*t*, 69–124
  advantages and limitations of, 120–124
  applications of, 91–93
  CCD cameras for, 86–89, 87*f*
    digital, 90–91, 91*f*
    tank, 88–89, 88*f*
  codes for, 93
  defined, 129
  delivery systems for, 123–124
  direct visual aids for, 78–82, 79*f*–81*f*
  of discontinuities, 93–106, 98*f*, 99*f*, 102*f*–105*f*, 106*t*
  equipment and accessories for, 77–91
  evaluation and reports for, 115–120
  eyes for, 72–73, 73*f*, 77–78
  as first NDT method, 10
  human factors of, 75–77
  image recording for, 89–91, 90*f*, 91*f*
  light and, 74–77
  light sources for, 79
  magnifier for, 78–79, 79*f*
  measuring devices for, 80–82, 80*f*, 81*f*
  minimum angle for, 70, 70*f*
  monitors for, 90, 90*f*
    advantages and limitations of, 124
  remote visual aids for, 82–91, 83*f*, 85*f*, 87*f*, 88*f*, 90*f*, 91*f*
  specifications for, 93
  standards for, 93
  for tanks, 113–115
  theory and principles of, 72–77
  for vessels, 113–115
  for wear, 107
Voids, 31, 35, 58
  creep, 51, 55
  ET for, 463–464, 463*f*, 465*f*
  gas, 273
  in ingots, 94
Voltage:
  for AE, 544, 562
  back, 435, 436*f*, 490
  clock, 86
Voltage (*Cont.*):
  for ET, 418, 435, 435*f*, 494
  plane, 429–430, 429*f*, 430*f*
  pulser, 642
VT. *See* Visual testing

W

Waidelich, D. L., 479
Water and detergent cleaning, 140–141
Water path, 385–386, 414
Water-removable penetrant, 150–152, 151*f*, 156, 165
Water-rinsable PT, 133
Water-washable PT, 133
Waterproof, 92, 129
Watertight, 129
Watts, 183
Waveband response, 507–508
Wavelength, 302–303, 503
Weber, 219, 420
Weber, Wilhelm, 170
Wedge, 342, 343*f*, 350, 414
  drivers, 335
  for PAUT, 623–624, 624*f*
    delay calibration for, 648–650, 650*f*, 691
Welding. *See also specific topics*
  acceptance criteria for, 119–120
  cracks and, 42, 42*f*, 65*f*, 66*f*
  discontinuities with, 32, 42–46, 42*f*, 44*f*, 45*f*, 58, 98–106, 98*f*, 99*f*, 102*f*–105*f*
  ditching in, 45, 45*f*
  lack of penetration in, 46, 67*f*
  PAUT for, 620*f*, 666–672, 666*f*–672*f*
  slags in, 42, 63*f*
  specifications for, 101
  templates for, 82
Wenk, Samuel, 227
Wet continuous MT technique, 200–201
Wet residual MT technique, 201
Wetability, 141, 142*f*, 166
Wheel transducers, 344–346
Wilcox, P. D., 696, 697, 698
Wind-driven convection, 517–518
Windowing, 603, 604*f*
Wire penetrameter, 253, 255*t*, 256*t*
Wood, 551
Written Practice, 23

X

X-rays, 6*t*, 10–11, 11*f*, 14*f*, 585
  for discontinuities, 132
  discovery of, 221–222, 223*f*–227*f*
  equipment for, 240, 241*f*, 242*f*
  image intensifier for, 587–588, 587*f*, 588*f*
  microfocus systems for, 588–589, 589*f*, 590*f*

X-rays (*Cont.*):
portable units for, 227
real-time systems for, 588, 588*f*
resonant transformer for, 238

Y

Yan, F., 696, 698
Yield point, 18
Young, Thomas, 619–620
Young's modulus of elasticity, 299, 302

Z

Zero degree wedge, 623, 624, 624*f*
Zhu, W., 696
Zhu, Y., 698
Zones, 570–572, 571*f*, 572*f*, 584
dead, 350, 411
fusion, 45
HAZ, 43–45, 44*f*, 56, 100
Zoom, 88–89, 88*f*, 115
Zuschlag, Theo, 6*t*